UNIVERSIDAD DE CHILE
FACULTAD DE CIENCIAS FÍSICAS Y MATEMÁTICAS
DEPARTAMENTO DE INGENIERÍA ELÉCTRICA

MODELING OF SMALL PRODUCTIVE SOLAR PROCESSES AND THEIR INTEGRATION INTO AN ENERGY MANAGEMENT SYSTEM FOR A MICROGRID

TESIS PARA OPTAR AL GRADO DE DOCTOR EN
INGENIERÍA ELÉCTRICA

DANNY ALEXANDER ESPÍN SARZOSA

PROFESOR GUÍA:
RODRIGO PALMA BEHNKE

PROFESOR CO-GUÍA:
FELIPE VALENCIA ARROYAVE

MIEMBROS DE LA COMISIÓN:
PATRICIO MENDOZA ARAYA
LUIS VARGAS DÍAZ
CLAUDIO CAÑIZARES ESGUERRA
GUSTAVO VALVERDE MORA

SANTIAGO DE CHILE
2022

MODELAMIENTO DE LOS PROCESOS PRODUCTIVOS SOLARES DE PEQUEÑA ESCALA Y SU INTEGRACIÓN EN EL SISTEMA DE GESTIÓN DE ENERGÍA PARA UNA MICRO-RED

El uso productivo de la energía, especialmente de fuentes de energías limpias, mejora el desarrollo socioeconómico de las comunidades urbanas y rurales. Por lo tanto, la energía solar puede incluirse en los procesos productivos tradicionales realizados por las comunidades locales. Así, este nuevo tipo de procesos se definen como pequeños procesos productivos solares (SPSPs). El consumo eléctrico de los SPSP puede estar influenciado por variables climáticas externas. Además, los SPSPs suelen tener cargas dependientes de la tensión. Consecuentemente, el comportamiento eléctrico de estos SPSPs es complejo; por lo tanto, modelar su comportamiento es desafiante, ya que influye en el desempeño de la operación de una micro-red. Este trabajo propone una metodología para modelar y representar el complejo comportamiento eléctrico de los SPSPs a través de un modelo de carga ZIP multi-zona extendido (EMZ-ZIP). Este modelo captura la dependencia del voltaje y la influencia de las variables climáticas externas, y puede integrarse adecuadamente en un sistema de gestión de la energía (EMS). Los resultados muestran que la metodología propuesta i) captura adecuadamente la dependencia del voltaje de las cargas de los SPSPs, ii) captura la influencia que las variables climáticas externas pueden tener en el comportamiento energético de los SPSPs, iii) tiene un mejor desempeño en la estimación de los parámetros del modelo de carga propuesto, y iv) mejora el desempeño técnico-económico de la micro-red cuando el EMZ-ZIP se integra en el EMS.

MODELING OF SMALL PRODUCTIVE SOLAR PROCESSES AND THEIR INTEGRATION INTO AN ENERGY MANAGEMENT SYSTEM FOR A MICROGRID

The productive use of energy, especially from clean energy sources, improves the socio-economic development of urban and rural communities. Hence, solar energy can be included in the traditional productive processes performed by local communities. Thus, these this new kind of processes are defined as small productive solar processes (SPSPs). The electricity consumption of the SPSPs may be influenced by external weather variables. Furthermore, SPSPs generally have voltage-dependent loads. Consequently, the electrical behavior of such SPSPs is complex; hence, modeling their complicated behavior is challenging, as it influences the performance of microgrid operation. This work proposes a methodology to model and represent the complex electrical behavior of the SPSPs through an extended multi-zone ZIP load model (EMZ-ZIP). This model captures the voltage-dependency and the influence of external weather variables, and it can be properly integrated into an energy management system (EMS). The results show that the proposed methodology i) better captures the voltage-dependence of SPSPs loads, ii) captures the influence that external weather variables may have on the energetic behavior of the SPSPs, iii) has a better performance estimating the parameters of the proposed load model, and iv) improves the technical-economic performance of the microgrid when the EMZ-ZIP is embedded in the EMS.

"Keep your eyes on the stars, and your feet on the ground"

- Theodore Roosevelt

To my angels who take care of me from heaven,
and to my sisters Gissela and Jessenia.

Acknowledgements

There are many people who have supported me in various ways throughout my life to get to where I am today and accomplish this goal. It is very difficult to mention everyone, so if you are not included, please know that I am very grateful for your support. There are a few people who are very important in the success of this goal, and I hope I can mention them without making others feel left out.

First of all, I would like to express my gratitude to my PhD advisor Prof. Rodrigo Palma. As many people know, it is impressive how he knows and juggles different subjects. What is most inspiring is his wisdom and kindness. I enjoyed our time when he advised me on how to address research problems and other academic and non-academic issues, and I appreciated all his support, guidance, and patience in teaching me not only knowledge and skills to become a better researcher, but also how to be a better person.

I would also like to thank Dr. Felipe Valencia for all the time he spent supporting me and teaching me valuable lessons to steer my research in a fruitful direction. Felipe thank you for all the advice, discussions, and contributions to the development of my research. In addition, my sincere thanks to Dr. Patricio Mendoza for the valuable comments and suggestions.

I would like thank Diego Ortiz, my undergraduate professor, who motivated me to get involved in this wonderful world of research and supported me a lot in the beginning of my PhD studies. I would also like to thank Oscar Núñez for welcoming me when I first arrived in Chile and for his valuable suggestions for the development of my PhD.

I would like to thank my Ecuadorian friends, Alex V., Eve S., Jackie LL., Ricardo H., Andrés Ch., Daniel B., Luis S., Luis Miguel R., Mabel S., and Jhon I. for all the good times we shared and made this experience better. In addition, my sincere thanks to the people of the Energy Center of the FCFM, especially Paola, Myriam, Sandra, Yasmín and Fabián who with their good vibes generated a good working environment. Also, I would like to thank my friends from DIE and IEEE UChile Student Branch with whom I enjoyed spending time and sharing good moments.

My special thanks to Prof. Christian Rehtanz, Christoph Strunck and his family, and to the guys at ie^3 for their generous hospitality during my research stay at TU Dortmund, Germany.

I would like to express my gratitude to my PhD thesis committee for providing valuable comments and suggestions to improve the quality of this work.

To my beloved wife Ma. Mercedes for all her love, affection, patience, support and understanding throughout the long road we have traveled together. You achieved this goal with me!. Additionally, I would like to thank my parents, my sisters and all my family for all the support and love they have always given me from afar.

TABLE OF CONTENT

List of Tables

List of Figures

1 Introduction

1.1 Research Motivation

The Sustainable Development Goals (SDGs) promoted by the United Nations were conceived with the aim of working to eradicate poverty, to protect the planet and to improve the quality of life of people around the world. Thus, in 2015, the member countries of the United Nations approved the 17 goals for sustainable development [1]. Particularly, goal N° 7 focuses on access to affordable and nonpolluting energy. Such energy is key in the different activities that occur worldwide for example for industry, transportation, commerce, domestic activities, etc. [1]. Therefore, It is important to promote universal access to energy from renewable sources to create sustainable, inclusive, and resilient communities [1].

In this context, Chile, through its energy policy projected to 2050 based on 4 pillars, included energy as a driver of development and environmentally compatible energy [2]. Thus, Chile has recognized the importance of renewable energies, especially the solar energy potential in the northern part of the country [3]. Consequently, several large-scale solar projects, both photovoltaic and solar thermal, have been developed [4] and continue being developed [5]. Alternatively, at the small-scale level, recently the Solar Energy Research Center (SERC-Chile), has recently proposed the development and massive adoption of small-scale solar energy solutions for creating human capital and to promote the sustainable development of urban and rural communities in the region of Arica and Parinacota [6].

In addition, developments based on decentralized energy systems (DES) suggest a new vision on how energy is produced, delivered, and consumed [7]. DES are mainly based on non-conventional renewable energy (NCRE) technologies such as distributed generation (DG), electromobility, cogeneration, virtual generators, microgrids (MGs), smart grids, among others; they provide a clean and resilient option to achieve sustainable development goals [7]. Additionally, several NCRE technologies, mainly solar photovoltaic, have reached grid parity, i.e., they have reached competitive costs compared to traditional electricity systems [8].

Because of the reasons mentioned above, DES are increasingly being integrated into the conventional electricity system to take advantage of their benefits, among others, the ability to offer zero to low carbon emissions, to compensate for large capital investments for grid upgrades, to provide local energy independence and grid security, and to motivate cohesion and social capital. Therefore, it is expected that the conventional electrical system (see Figure 1.1(a)) will continue to evolve as by including DG and specific cases of MGs (see Figure 1.1(b)).
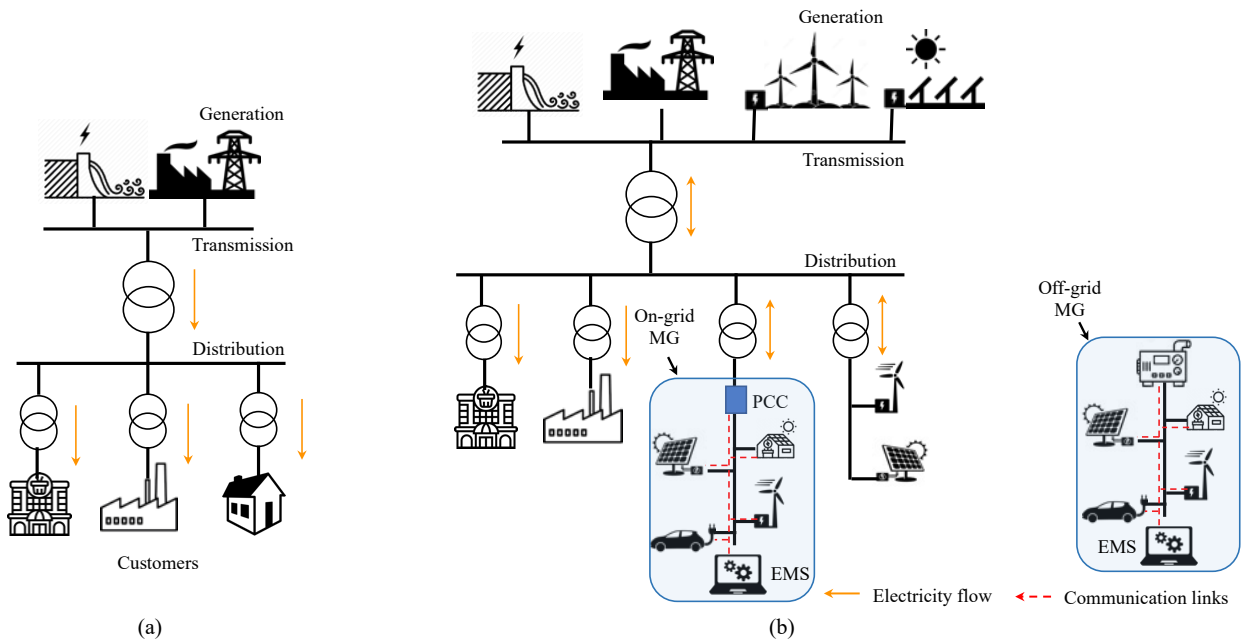
Figure 1.1 (a) Conventional electrical system, (b) current electrical system that includes DG and some specific cases of on-grid MGs and off-grid MGs

In this context, the advantages of MGs both on-grid and off-grid have caused them to be deployed in several parts of the world and an increasing trend is expected for their adoption in electrical systems in the future, as can be seen in Figure 1.2.
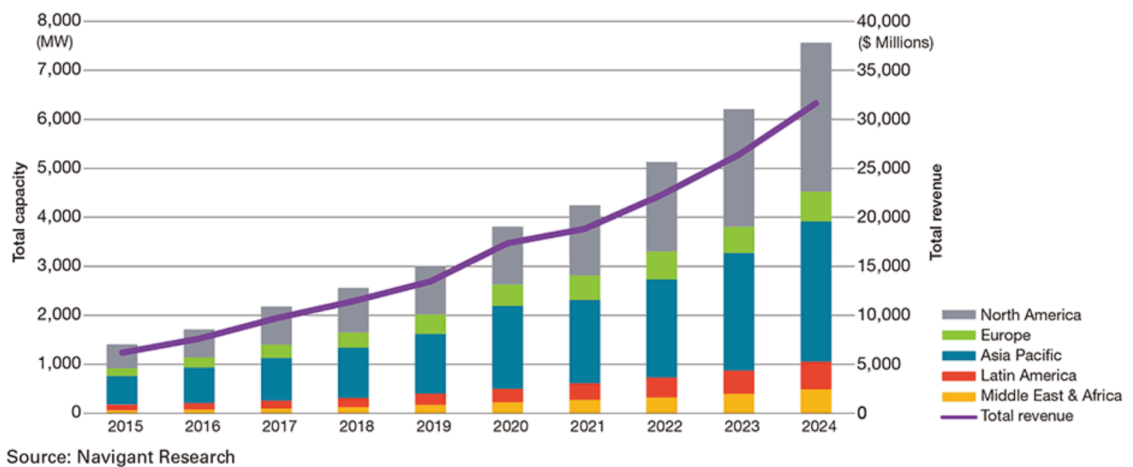
Figure 1.2 Evolution and projection of investments and installed capacity of MGs worldwide [9]

MGs will include more and more varied electrical loads, from small local applications to complex structures that will integrate different types of activities (domestic, industrial processes, etc.). In this sense, the operation of MGs will be more challenging, therefore, it is necessary to consider an energy management system (EMS) to ensure a cost-efficient and safe operation of MGs.

EMSs require adequate estimation tools to fulfill their purpose, i.e., generation and demand estimation. However, when having a combination of conventional electrical loads, production processes, etc., the modeling of the electrical demand, as reviewed in Section 1.2, will be an increasingly challenging task. Moreover, due to the alluded grid parity, future MGs will include technologies based mainly on solar energy [8] and it will lead to a massive adoption of different types of small productive solar processes (SPSPs) as it will be covered in Section 2.1, each one with its own characteristics and operation logic since it is a type of DES. This future scenario is exemplified in Figure 1.3. Generally speaking, SPSPs can be defined as small manufacturing industries that aim to increase income and productivity of people in, primarily rural communities.
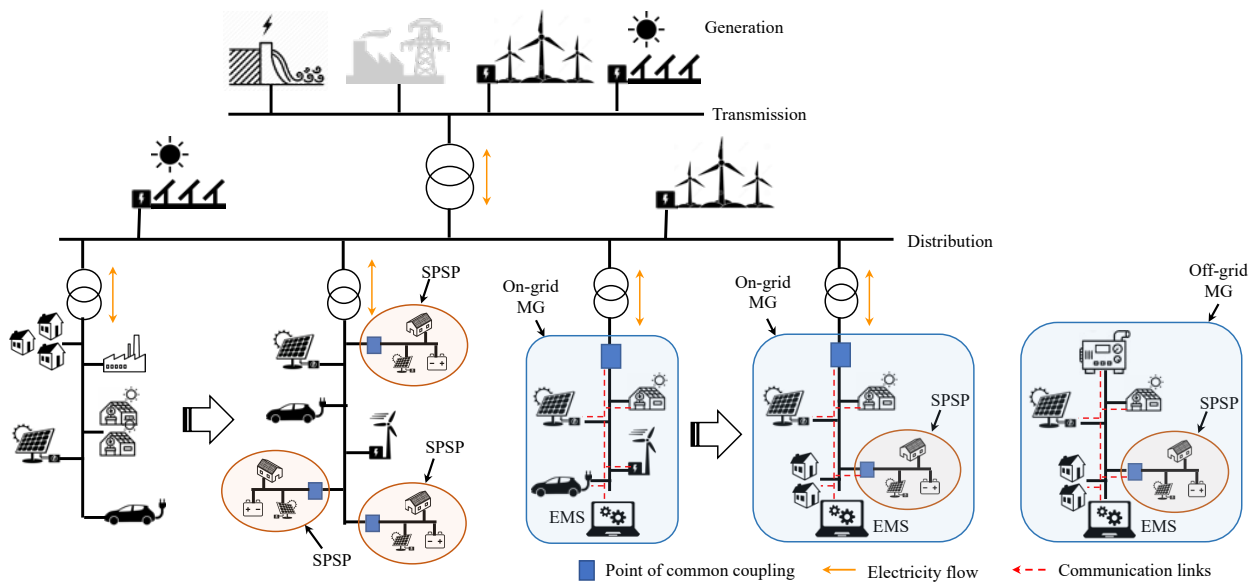
Figure 1.3 Future electrical system including several types of DES and some SPSPs

Consequently, MGs will not only consist of conventional electrical loads but also productive processes, with high levels of difficulty in their modeling since it requires capturing their complex electrical behavior. In this sense, it is challenging to achieve a complete understanding of each one of the processes. This is because the behavior of the processes is influenced by external weather variables, besides the production process of the SPSPs will be carried out inside facilities, mainly private, and to have a complete of the processes would require multiple measurement devices or control systems that in practice are not very feasible. Currently, the cost factor and private information are the main barrier.

In summary, the difficulty in fully understanding the electrical behavior and characteristics of small productive solar processes will lead to the appearance of new types of complexities that will cause the operation of MGs to face great challenges. It is the particular case of modeling and estimation of demand, since such estimation must meet certain criteria such as simplicity, and speed, among others. Further, as will be seen below, currently no methodologies propose

3

approaches to model the electrical consumption of small productive solar processes within MGs, so that they can be incorporated into EMSs to be operated efficiently.

1.2 Problem Statement

Electricity demand representation plays a key role in the operation of the MG. This is because the EMS makes decisions based on the expected electrical demand and available energy from distributed energy resources (DER), generally of NCRE type [10]. However, due to the diverse nature of conventional electrical loads and the appearance of new types of consumptions, i.e., SPSPs, the representation of electrical loads is a challenging task.

Regarding small productive processes, there are several works in the literature that consider this type of processes in MGs. For example, in [11], an EMS that manages the operation of a MG and considers a small copper mining process is proposed. In [12], the scheduling of units in a rural MG that includes residential loads, and an agricultural production process is presented. The authors in [13] present the design of the operation of a MG based mainly on solar energy to supply electric power in aquaculture processes for communities in southern Bangladesh. In [14], an EMS approach is proposed for a MG containing several DG units, residential loads, and production processes. In [15], the authors present an EMS to promote self-consumption in productive processes. Furthermore, they highlight the important feature that a typical industrial process contains electrical loads that are sensitive to voltage variations. However, in all the works mentioned above, the electrical loads of the productive processes are represented as constant power (CP), i.e., they do not consider the effect of voltage.

Concerning the representation of electricity consumption in MGs, one way to do this is to take advantage of the information available at the measurement points. From these measurement points, aggregated electricity consumption is obtained. Therefore, by combining the data measured at different points of the consumption centers in the network, it is possible to develop load representations that can be used by EMS to perform the economic operation of MG. For this purpose, the specialized literature presents different modeling approaches [16], [17].

Among available modeling approaches, those based on artificial intelligence (AI) [18]–[23], and those based on statistical models (e.g., ARMA, ARIMA, SARIMA models, among others) [24], [25] stand out. In both cases, the information collected from the measurement points is used to train the load representation models that are then used to calculate the expected electrical demand for the EMS. However, because the AI and statistical-based alternatives focus primarily on representing the aggregate power consumption profile, they generally do not directly consider the effect of voltage and external weather variables. The former is important to consider because, according to [15] production processes generally contain electrical loads sensitive to voltage

variations. In this sense, artificial neural networks (ANNs) may be used to represent complex loads considering the effect of external weather variables [26] and voltage variations. Nevertheless, it should be noted that this approach belongs to the black-box approaches [27], [28]; thus, its interpretability has been a challenging task [28]–[31]. Moreover, the ANN approach is useful when the model structure is hard to be mathematically represented and for systems that have already been developed [16].

The literature suggests using ZIP [16], [32]–[34] and exponential models [16], [35] as appealing alternatives to represent the electric loads considering the voltage effect. On the one hand, the exponential model proposes the representation of the electrical load based on the dependence of electrical consumption on voltage and an exponent representing the electrical consumption characteristic [36]. Alternatively, as it is widely known, the acronym ZIP refers to the characteristics of constant impedance "Z", constant current "I" and constant power "P" that all electrical loads exhibit [16], [37]. The ZIP model can represent the active and reactive power of a given electrical load as a function of either voltage, frequency, or both.

Recently, there has been a growing trend in the adoption of complex loads in electrical systems, such as electronic loads [38], electric vehicles [39], among others. These complex loads are generally connected to electrical networks through power converters. Consequently, to integrate the effects of such complex loads that are generally connected to electrical systems through power converters, ZIP models have been zoned (multi-zone) because conventional ZIP models did not adequately represent complex loads [38], [39]. In general, multi-zone models, combined with ZIP models developed for residential, commercial, and industrial loads [33], [34], are able to determine more accurately the behavior of electrical loads in power systems.

Despite the efforts made in describing the new characteristics of loads in power and distribution systems [38], [39], little attention has been paid to represent and analyze loads in MGs even more with the incorporation of complex electrical loads, i.e., SPSPs. Moreover, although there are recent studies of the incorporation of productive processes in MGs and this has been a trend in recent years [40], in most cases the effect of voltage on loads is not considered. Therefore, there is still a challenge in developing methodologies that allow better representation of the new complex consumption, that also consider the influence of voltage and that can be efficiently integrated in the EMSs for the operation of MGs. It is worth mentioning that, phase unbalances and disturbances are relevant and impactful in MGs [41]; however, the analysis of these types of conditions and the frequency dependence of the loads are beyond the scope of this work.

Based on the above, and considering Chile's pioneering experience in the development of the SPSPs [6], the interest of this work is focused on providing a methodology to develop sophisticated

mathematical models capable of capturing the complex behavior of the SPSPs electrical consumption and their sensitivity to voltage variations. Furthermore, these models can be efficiently incorporated into the EMS so that they can be coordinated with other electrical loads and energy sources present in a MG.

1.3 Hypotheses

Based on the aforementioned context and motivation, the hypotheses related with this work are:

1. SPSPs loads are sensitivity to voltage variations and can be modeled with sufficient accuracy for the purpose of energy management, without detailed information about their facilities, i.e., measurements of each equipment inside their processes.

2. The technical-economic performance of MG's EMS depends critically on the ability to model load consumption with high degree of complexity when SPSPs are considered as an integral part of such EMS's consumption.

1.4 Objectives

1.4.1 General Objective

The main objective of this thesis is:

To provide a model and a consumption estimation tool capable of representing and integrating the complex electrical behavior of the SPSPs into an EMS to enhance the technical-economic performance of future MGs.

1.4.2 Specific Objectives

To accomplish the general objective of this thesis, other issues related to the analysis shall also be addressed as listed below:

1. To develop a mathematical model that represents the complex electrical behavior of SPSPs and captures the influence of external weather variables and voltage variations.

2. To evaluate the performance of the proposed model and compare it with other methods for representing electricity consumption in MGs.

3. To efficiently integrate the developed model for SPSP behavior into an EMS optimization problem.

4. To evaluate the steady-state technical-economic performance of EMS and MG by including the developed model.

1.5 Contributions

This thesis proposes a novel methodology for modeling the SPSPs and integrating them into an EMS for the operation of an MG. In this context, the main contributions of this work are listed below:

- An approach to determine the zones at which specific devices of the SPSPs may be switched on is proposed. This is useful for both significantly decreasing the complexity of the parameter identification process, and for properly representing the sensitivity of SPSPs loads to voltage.

- An extended multi-zone ZIP load model (EMZ-ZIP) to represent the complex electrical behavior of SPSPs is developed by using a zoning procedure. The EMZ-ZIP considers the identified zones, the information of specific devices that belong to the SPSPs, and the voltage influence on SPSPs' load consumption.

- A procedure to identify the EMZ-ZIP load model parameters is proposed. This procedure deals with the non-convexity of the bilinear term of the flexible component of the EMZ-ZIP load model.

- A procedure to integrate the EMZ-ZIP load model into an EMS approach is proposed. The aim of this integration is that the proposed load model is embedded into an EMS formulation and that the resulting optimization problem is solved in an efficient way.

The aforementioned contributions are shared with the microgrids scientific community in the following published papers:

Journal papers

D. Espín-Sarzosa, R. Palma-Behnke, and F. Valencia, "Integration of Small Productive Processes into an Energy Management System for Microgrids", *IEEE Access,* vol. 10, pp. 69010-69030, 2022, doi: 10.1109/ACCESS.2022.3185656.

D. Espín-Sarzosa, R. Palma-Behnke, and F. Valencia, "Modeling of Small Productive Processes for the Operation of a Microgrid", *Energies*, vol. 14, no. 14, p. 4162, Jul. 2021, doi: 10.3390/en14144162.

D. Espín-Sarzosa, R. Palma-Behnke, and O. Núñez-Mata, "Energy Management Systems for Microgrids: Main Existing Trends in Centralized Control Architectures", *Energies*, vol. 13, no. 3, p. 547, Jan. 2020, doi: 10.3390/en13030547.

Conference papers

D. Espín-Sarzosa, R. Palma-Behnke, and F. Valencia, "Incorporation of Productive Solar Solutions for Communities into Microgrid Energy Management Systems", *ISES Solar World Congress*, 2019, pp. 1-11, doi: 10.18086/swc.2019.34.01.

Additionally, the author contributed to the following publications, that appeared as collaborations during the author's research stay at Institute of Energy Systems, Energy Efficiency and Energy Economics (ie[3]), Technical University Dortmund, Germany:

D. Sen Sarma, T. Warendorf, *D. Espín-Sarzosa*, F. Valencia-Arroyave, C. Rehtanz, J. Myrzik, and R. Palma-Behnke, "Multi-objective Energy Management for Modern Distribution Power Systems Considering Industrial Flexibility Mechanisms", *Sustainable Energy, Grids and Networks*, June 2022, https://doi.org/10.1016/j.segan.2022.100825.

C. Strunck, C. Rehtanz, *D. Espín-Sarzosa* and R. Palma-Behnke, "Control Possibilities for Community Microgrids Considering Small Production Processes and its Benefits to the Whole System", *2020 IEEE PES Transmission & Distribution Conference and Exhibition - Latin America (T&D LA)*, 2020, pp. 1-6, doi: 10.1109/TDLA47668.2020.9326150.

1.6 Thesis Outline

The remainder of this work is organized as follows. In Chapter 2, the theoretical background of the main topics treated in this work is presented. The proposed methodology for modeling the SPSPs, the integration into an EMS approach, the implementation aspects, and some feasible extensions of the proposed methodology are described in Chapter 3. The case study, the obtained results, their analysis, and discussion are presented in Chapter 4. Finally, the conclusions and future work of this thesis are discussed in Chapter 5.

2   Theoretical Background

This chapter presents the theoretical background of the main topics treated in this thesis. First, the concept and characteristics of the SPSPs are presented in Section 2.1. Second, several aspects and characteristics of EMSs for MGs are discussed in Section 2.2. Third, Section 2.3 describes different alternatives for representing loads in EMS in the context of MGs. Finally, Section 2.4 summarizes the most important concepts that are presented in this chapter and that are key to this thesis.

2.1   Small Productive Processes and Small Productive Solar Processes

2.1.1 Small Productive Processes worldwide

To contribute to eradicating poverty aligned with the SDGs, access to electricity primarily from clean energy sources is key to achieving SDGs. In this sense, the Human Development Index (HDI) has a direct correlation with electricity consumption per capita [42]. Figure 2.1 shows the correlation between the HDI and electricity consumption. As can be seen in Figure 2.1, the higher the energy consumption, the higher the HDI. For example, countries that have an annual electricity consumption per capita between approximately 5,000 to 8,000 (kWh/capita) have high human development. In contrast, countries with lower energy consumption have a low HDI.
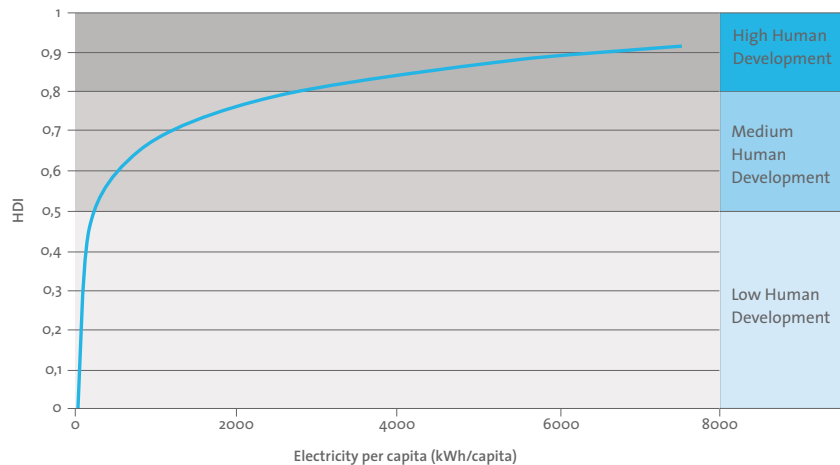
Figure 2.1 Correlation between energy consumption and The Human Development Index [42]

In this context, electricity has an impact on different aspects of society such as productivity, growth, and poverty. In [42], the authors present empirical evidence regarding the impact of electricity on several development outcomes. More concretely, Table 2.1 provides an overview of several studies about the nexus between electricity access and poverty reduction. In Table 2.1, one of the most important findings is that the authors in [43] concluded that in a developing country such as Tanzania, a 1% increase in the electrification rate may lift around 140,000 people out of poverty.

Table 2.1 Effects of electricity access on poverty [42]

Source	Country /Region	Data source/Sample size	Conclusion
[44]	China, India, Thailand	China: panel survey data of 1,143 households, field survey of 624 households India: survey of approx. 2,600 rural households. Thailand: survey of approx. 1,100 rural and urban households.	China: faster income growth among poor people with electrification than the non-electrified in the province of Shaanxi, no positive effect of electricity on poverty levels was found. India and Thailand: positive impact of electricity access on ownership of electric appliances by poor households but not on incomes was found.
[45]	Ethiopia	Survey of 800 households.	No significant effect of electrification on changes in household expenditure.
[43]	Tanzania	Household Budget Survey (HBS) of approx. 22,000 households; multi-stage, stratified sample.	1% increase in the electrification rate would lift approx. 140,000 people out of poverty.
[46]	India	Qualitative survey of 264 small businesses.	Low uptake of electricity for production of goods and services among low-income entrepreneurs was found. A substantial share of enterprises that have low incomes despite productive use of electricity was identified, but direction of causality not clear.

Considering that the most important objective of rural electrification is to achieve economic and social human development, supporting the productive use of energy (PUE) is generally justified as a direct measure for improving the development outcomes of total electricity access [47]. Besides, fostering the PUE can enhance the economic and financial sustainability of rural electrification programmes and projects [47].

Consequently, the PUE, especially in rural context, has become an important topic in recent years because it can contribute to the social and economic development of communities. The Deutsche Gesellschaft für Internationale Zusammenarbeit (GIZ) defines the PUE as *"agricultural, commercial, and industrial activities involving electricity services as a direct input to the production of goods or provision of services"* [48]. In developing countries, primarily in rural locations, typical examples of PUE can be found in agro-processing (e.g., grain milling), different manufacturing industries, for instance, carpentry, tailoring, welding, among others [47]. These manufacturing industries aim to increase income or productivity of communities' people. Thus, such industries can be defined as small productive processes (SPPs).

Because of the potential benefits of the SPPs previously mentioned, several initiatives have been deployed worldwide to contribute to the alluded socio-economic development of rural communities. In [49], the authors present some examples of the PUE and the resulting SPPs that provide economic benefits to rural communities' people. A brief description of such SPPs and their main characteristics are described below.

Ice making: This kind of PUE can be useful, particularly in isolated and hot locations. The SPP for this activity can include stand-alone freezers (nominal power less than a kW) or large commercial ice makers, which may consume tens of kW. The ice produced can be used for several purposes, such as preserving food and cooling drinks. Figure 2.2 shows an example of commercial ice making to produce ice for businesses.

Figure 2.2 Large commercial ice maker [49]

Milling: Rural communities in Africa usually produce flour through milling different products, for example, maize, cassava or sorghum. Besides, the husking and shredding of rice are common activities in such locations. Because of the lack of electricity in rural areas, milling SPP is commonly performed through grinding, pounding by hand or by small mills powered by diesel generators. An example of a milling SPP powered by a diesel generator is shown in Figure 2.3. Nevertheless, to achieve environmental benefits, electric motor-driven mills can be preferable to diesel-driven mills.

Figure 2.3 Small milling productive process powered by a diesel generator [49]

11

Carpentry: This kind of activity and other woodworking activities are widely carried out in rural locations in Africa and other countries. Carpentry is often performed manually, but carpenters can travel to an electrified location or use diesel generators. The electric equipment used in carpentry SPPs ranges from small drills to large machines, which have larger power requirements. Figure 2.4 shows an example of a carpentry workshop.

Figure 2.4 Carpentry workshop [49]

Egg incubation: This productive activity may be an attractive business for rural communities because of its low up-front investment cost and potentially high returns. The incubation equipment requires electricity, and the success of the business depends on the adequate use of such equipment. Figure 2.5 shows an example of egg incubation equipment.

Figure 2.5 Egg incubation equipment [49]

Water treatment and sales: Access to clean water for drinking, cooking, and hygiene is important for sustainable development, especially in rural communities. Some water treatment methods in rural locations are, for example, chemical treatment, filtration, and reverse osmosis. These methods usually use electrical energy to perform the treatment SPP. A water treatment system and a system which is filling bottles are shown in Figure 2.6.

Figure 2.6 Water treatment system and filling bottles [49]

Other productive uses: The authors in [50] have summarized several SPPs deployed worldwide, primarily in developing countries to support the socio-economic growth of communities. Examples of such SPPs are food processing, lighting, irrigation, food preparation, cooling, among others. Table 2.2 presents an overview of various examples of the SPPs and some aspects of them.

Table 2.2 Overview of several examples of the SPPs deployed worldwide (adapted from [50])

Technology	Need/Application	Country/Region	Ownership
Efficiency improvement	Lighting	Mexico	Institution
Biogas	Food processing & preparation	India	Implementing organization
Solar cookers	Food preparation	Argentina	Individual
Solar PV	Lighting	Kenya	Cooperative
Micro Hydro Power	Lighting	Philippines	Implementing organization + community
Efficient pumps	Irrigation	India	Community
Solar PV	Electrification	Togo	Individual
Pico hydro	Lighting	Sri Lanka	Community
Solar PV	Lighting	East Timor	Community
Solar PV	Electrification	Thailand	Individual
Biogas	Electrification	India	Community
Biogas	Food processing	India	Community
Biogas	Food preparation	China	Community

Table 2.2 Overview of several examples of the SPPs deployed worldwide (adapted from [50])
(Continued)

Technology	Need/Application	Country/Region	Ownership
Biogas	Food preparation	Guatemala	Individual
Biogas	Cooling	Pakistan	Individual
Solar cookers	Food processing	Morocco	Institution
Solar cookers	Food preparation	Argentina	Individual
Solar PV and wind power	Irrigation	Tanzania	Institution
Efficient lanterns	Lighting	Sri Lanka	Individual
Biogas	Food processing	Latin America	Individual/Communities
Solar oven	Food preparation	Gambia	Implementing organization
Micro hydro power	Electrification	Brazil	Cooperative
Efficient stoves	Food preparation	Sierra Leone	Individual
Solar dryer	Food conservation	Mozambique	Cooperative
Solar PV & micro hydro power	Electrification	Peru	Community
Solar cookers	Food preparation	Burkina Faso	Cooperative
Biomass gasification	Industry	India	Individual
Biomass combustion	Food processing	Burkina Faso	Implementing organization
Solar cookers	Food preparation	Paraguay	Individual
Solar dryer	Food conservation	Afghanistan	Implementing organization

Despite the enormous potential of the PUE to improve the socio-economic aspects of rural communities, the great majority of rural electrification projects still focus primarily on domestic energy use [51]. Therefore, it can be expected that more initiatives will be developed to promote PUE in communities.

2.1.2 Small Productive Solar Processes in Chile

Solar energy is the source of almost all energy that is used in the earth. Plants use solar energy for photosynthesis. Then, herbivorous animals indirectly absorb a small amount of the energy contained in organic matter by eating plants and vegetables, while carnivores indirectly absorb a smaller amount by eating herbivores [52]. Fossil fuels are solar energy stored from a very remote geological age. Biomass is organic plant or animal waste. Wind energy uses currents generated from hot air and the rotation of the Earth. Hydropower relies on the evaporation of water and its subsequent return to Earth in the form of rain to supply rivers, lakes, and reservoirs. In addition, waves carry all the energy received from the winds as they travel across the ocean [52].

As can be seen, solar energy is very versatile and can be transformed into other forms of energy. Figure 2.7 presents different forms of solar energy conversion, associated technologies, and their end use. As can be seen in Figure 2.7, solar energy conversion ranges from green chemistry to

evaporation, resulting in different technologies for harnessing solar energy such as reactors, dryers, heaters, PV panels, among others.
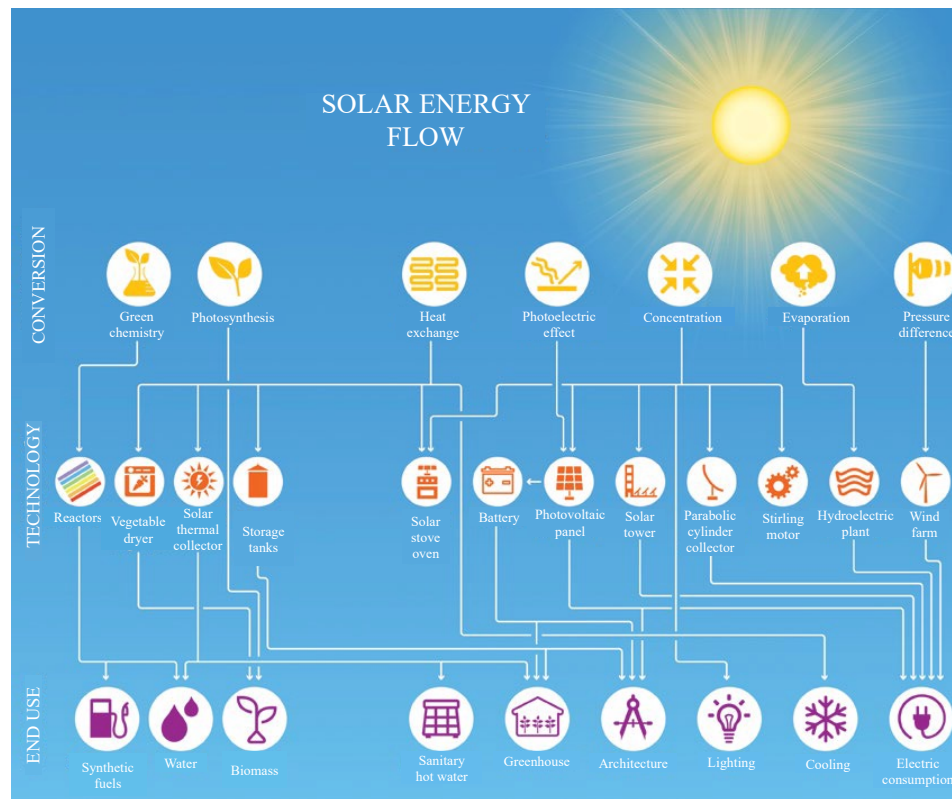
Figure 2.7 Solar energy flow (adapted from [52])

Regarding the solar potential around the world, very few regions have annual global horizontal irradiation (GHI) values above 2,500 kWh/m^2, for example, Tucson, Arizona, USA exhibits a value around 2,080 kWh/m^2 [3]. Accordingly, as can be seen in Figure 2.8, Chile has areas with annual GHI values exceeding 2,500 kWh/m^2. Consequently, there is a potential in the use of solar technologies in Chile as half of the country has a GHI above 1,826 kWh/m^2 (see Figure 2.9). Furthermore, the Atacama Desert presents great advantageous conditions with 2,556 kWh/m^2 besides its exceptionally clear sky, with an annual average clearness index that at 0.72 is close to the world's maximum of 0.8 [3].

In this context, taking advantage of Chile's solar potential, its solar history starts in 1872 when the world's first solar water distillation plant was built at Las Salinas in the Province of Antofagasta by Carlos Wilson [53]. Then, between 2004 and 2016, there was a flourishing of solar energy in the country where several initiatives appeared, motivated primarily by government incentives. For example, in 2007, around 3,000 small-scale stand-alone photovoltaic (PV) systems were installed and promoted by a program for rural electrification in the northern regions of Chile [54]. In 2008, the government established that the energy matrix of the system will have to be composed of 10% of renewable energy by 2024, which was updated to be required to reach 20% by 2025 [55]. A more detailed of history of solar development in Chile can be found in [52], [56].

15
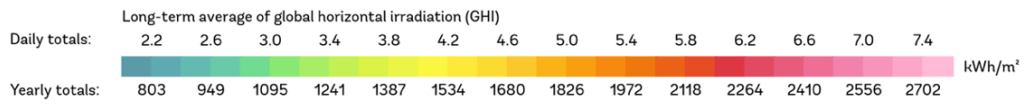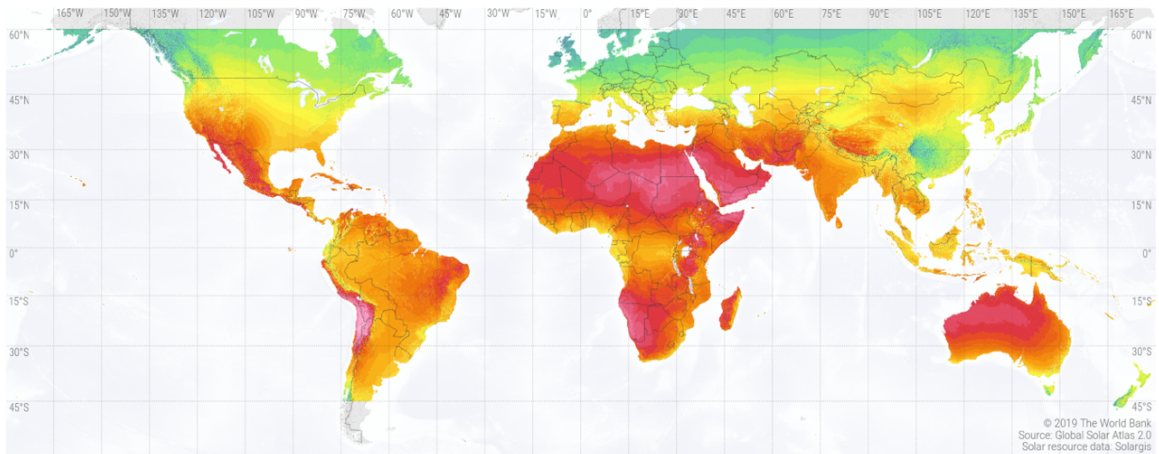
Figure 2.8 Map of global horizontal irradiation worldwide [57]
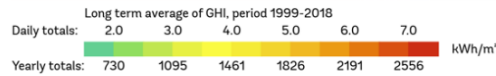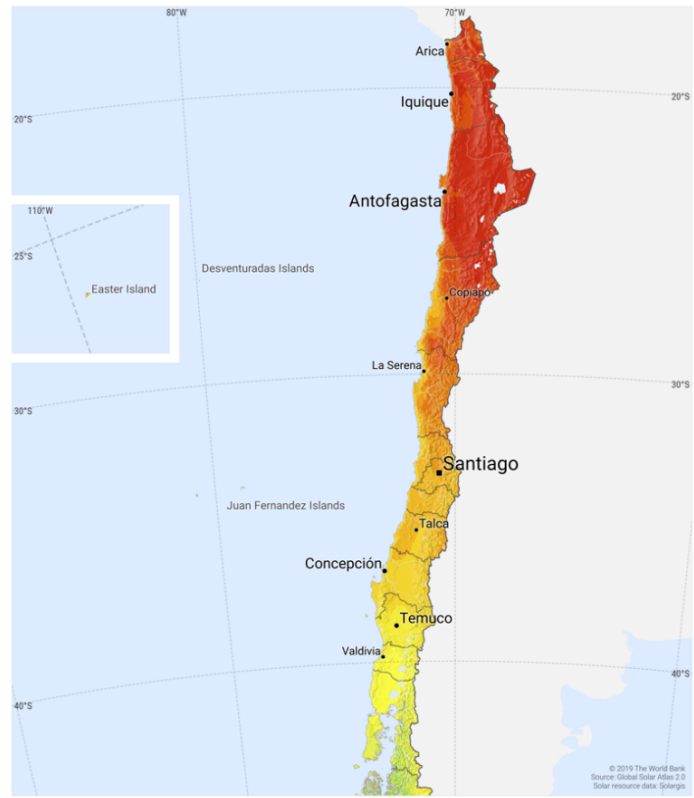
Figure 2.9 Map of global horizontal irradiation in Chile [57]

Considering the mentioned above, both the solar potential of Chile and the forms of solar energy conversion, several solar plants of different technologies (e.g., PV, solar water heater (SWH), concentrating solar thermal (CST)) have been installed in the country to supply primarily large consumption centers and large-scale industry. Figure 2.10 shows an overview of north-central Chile with its solar potential for solar project development, the location of solar projects under evaluation or operation, and the location of the main residential and industrial consumption.

It is important to note that Figure 2.10 illustrates the state of Chile's solar sector until the end of 2015. Furthermore, in this year the central-northern part of the country was still divided into two electricity subsystems, the Central Interconnected System (SIC) and the Northern Interconnected System (SING). In this context, with the interconnection of these two subsystems in 2017, the National Electric System (SEN) was created. In addition, the development of solar energy projects has had a strong growth in recent years. Therefore, updated statistics regarding solar energy projects developed in Chile can be found in [58], [59].
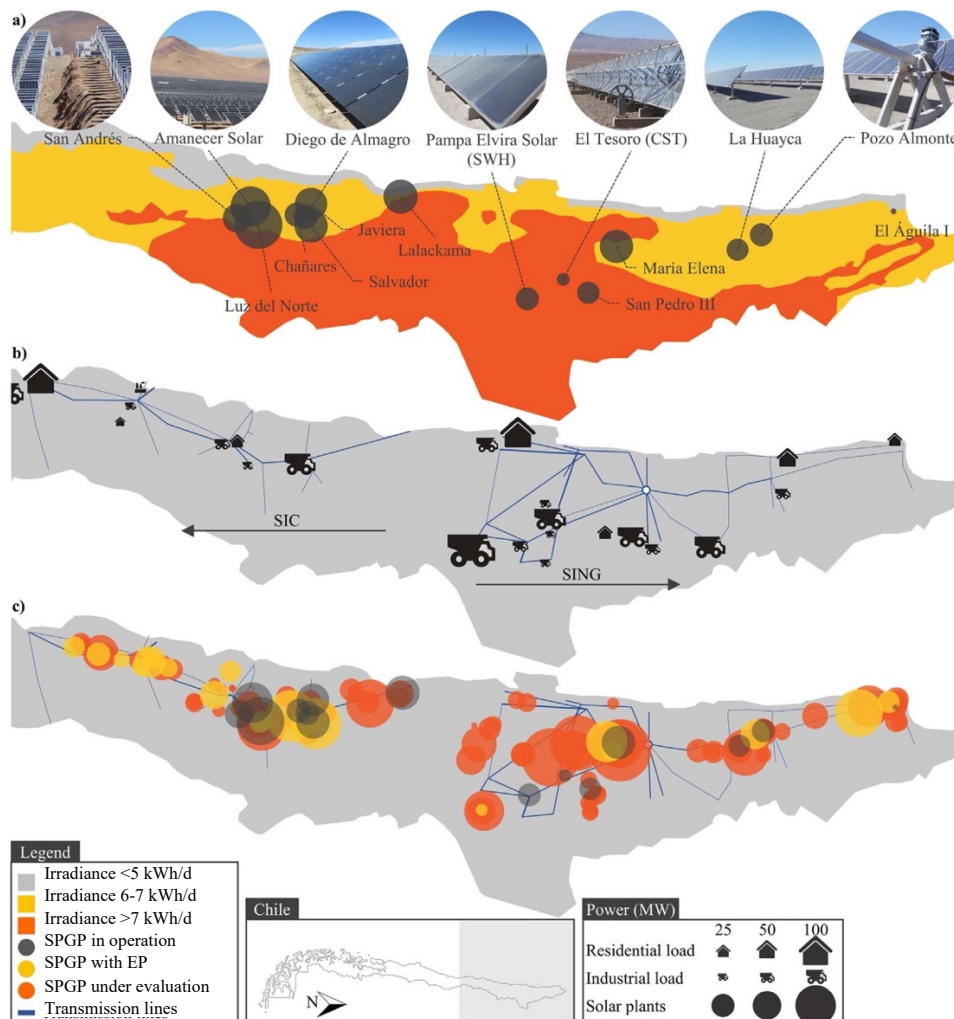
Figure 2.10 (a) Map of the main (> 3 MW) solar energy plants in operation by 2015, (b) load centers in Chile's SIC and SING, and (c) solar power generation plants (SPGP) larger than 3 MW in operation, evaluation and with environmental permit (EP) [56]

17

Although Chile has experienced a significant development of large-scale solar energy projects, the same level of development has not been seen in small-scale projects (i.e., DES). In fact, there are only a few initiatives, for instance, 300 small-scale PV installed in 2007 [54], a 23 kW PV array installed in Huatacondo, Chile's first microgrid [60]. Nevertheless, in 2014 through the net-billing approach, the regulation for rooftop systems was established. Consequently, the connection of PV systems to the distribution system was encouraged, although there was not a large deployment of PV systems at the beginning [61].

While there is interest in developing small-scale solar projects in Chile, it has been mainly for residential use [62]. In other words, the main objective is not to promote PUE. Nevertheless, there are some initiatives that foster the productive use of solar energy at small-scale level [6]. In this context, the small productive solar processes (SPSPs) can be defined as small-scale projects that use solar energy to add value to the productive activities (i.e., productive use of solar energy) of the people in the communities. Moreover, since these types of productive processes are based primarily on solar anergy, their behavior may be influenced by external weather variables such as solar radiation, ambient temperature, wind speed, relative humidity, calendar day, among others.

In Chile in recent years, with the support of governmental institutions and universities, several types of SPSPs have been promoted, primarily in the areas of agriculture, aquaculture, and livestock. The most common SPSPs in Chile are, for example, solar irrigation water pumping, solar-powered greenhouse [63], solar drying, river shrimp farming based on solar energy [6], camelid fiber collection and processing using solar energy [64]. The following is a general description of the most common SPSPs in Chile, considering their productive purpose, mode of operation and the external weather variables that may influence their electrical behavior.

Solar irrigation water pumping: This type of project aims to allow farmers to cultivate water-intense summer crops, to enhance land use and to increase the adoption of clean energy [65]. In conventional irrigation systems in remote locations, water pumping is supplied by a diesel generator, which requires expensive fuels and creates air pollution. In contrast, a solar-based (i.e., PV) irrigation system uses a sprinkler connected to a solar-powered water pump to reduce both water consumption and electricity consumption [66]. Besides, solar-based pumping systems present less maintenance cost and do not have fuel cost [67]. The main components of a solar irrigation system are: solar panel, converter, transformer, pump, battery and sprinkler [66]. A more detailed description of this type of project and its main components can be found in [68]. Some examples of the application of this type of SPSP in Chile can be found in [69]. It should be noted that solar radiation is the external variable that directly influences the electrical behavior of this SPSP because the pumped water flow rate depends on the incident solar radiation and on the size of the PV array [66].

Solar-powered greenhouse: The objective of this type of SPSP is to generate electricity using a PV system to supply the lighting, and heating/cooling subsystems of the greenhouse to increase crop productivity [70]. Traditionally, fossil fuel-based generators are used to feed the electrical systems of greenhouses to maintain the internal conditions of the greenhouse (i.e., temperature, humidity, etc.) [71]. However, continuing to use this technology is neither cost-efficient nor environmentally friendly; therefore, using solar energy as the main source to supply the greenhouse electrical systems is an attractive alternative [72]. In this sense, the Foundation for Agrarian Innovation (FIA by its Spanish acronym) has funded several demonstration systems of PV-powered greenhouses in Chile [62]. A further description of the operation and components of this type of process is presented in [72]. Regarding the external weather variables that may affect this type of SPSP, illumination has a direct impact on indoor temperature, relative humidity, soil illumination, plant growth, product quality and quantity, water consumption and evapotranspiration [71]. Therefore, depending on the level of external lighting, to maintain adequate conditions inside the greenhouse, ventilation or heating or artificial lighting will be activated in the greenhouse which leads to a variation in the electricity consumption profile.

Solar drying: Traditionally, this type of process is used for food preservation. In this sense, the solar drying process consists of taking advantage of solar energy for removing moisture from products mainly to inhibit the growth of microorganisms that can damage the food [73]. Besides, dehydration reduces the weight and volume of the products, thus reducing transportation and storage and helps to store the food at ambient temperature [74]. However, to promote the socio-economic development of the people in the communities, this type of SPSP adds value to the crops produced by the farmers, allowing them to access new markets to sell their products. An example of the application of this type of SPSP in the communities of northern Chile can be found in [6]. For further details regarding the solar drying process and its equipment see [73], [74].

The external weather variables that may influence the drying process are mainly solar radiation, temperature and relative humidity [74]. The temperature determines the quality of the dried product; therefore, to keep the drying temperature within the permissible ranges, the electrical consumption of the process will change depending on the availability of solar radiation and also on the ambient temperature. For example, in periods of high solar radiation it would be necessary to activate the ventilation in order to prevent the temperature from exceeding the maximum allowed. On the contrary, when there is low solar contribution, it would be required to activate the heating devices to maintain an adequate drying temperature. In the same way, the relative humidity is a driving force in a natural convection system. Thus, a lower relative humidity of the air will lead to an increase in the drying rate which can help to reduce the drying time [74].

River shrimp farming based on solar energy: River shrimp (*Cryphios caementarius*) farming has been a productive activity carried out by the inhabitants of northern Chile for several decades [75]. To achieve successful farming, the water must have adequate conditions of temperature (from 17ºC to 27ºC), salinity (from 0 to 21.6 ppt), pH (between 7.5 and 8.0), among others [75]. In addition, because arsenic is present in many ecosystems in northern Chile [76], including in rivers, it is essential to remove arsenic from the water in which the shrimp will be cultivated to prevent poisoning in humans [77]. For this purpose, technological equipment based on solar energy can be used to take advantage of the abundant solar radiation of northern Chile and perform arsenic removal through a photochemical process [78]. In addition, to maintain suitable water conditions (mainly temperature) this SPSP includes pumps to recirculate the water. In this sense, the power consumption of this process can vary depending on the ambient temperature and on the solar radiation that directly influences the photochemical procedure of arsenic removal.

Camelid fiber collection and processing using solar energy: Camelid livestock are mostly practiced in the northern part of Chile [79] and this is one of the main economic activities of the people in the communities. Once the people shear the camelid fiber, it is taken to a storage center for later processing. Generally speaking, fiber processing involves ten stages: categorization and classification, opening, scouring (at this stage the fibers are also washed with hot water, usually between 48 ºC and 55 ºC), drying, carding, gilling and combing, top finishing, blending, bleaching and dyeing, and spinning [80]. In this context, PV technology and solar collectors have been integrated into conventional fiber processing. The PV to supply the machinery and the collectors to heat the water needed for one of the fiber processing stages. In addition, to achieve a good quality fiber it is necessary that it does not contain too much moisture, therefore if the relative humidity of the environment increases or decreases, the process will require a higher or lower amount of energy for drying. In addition, this SPSP uses hot water from solar collectors, but in the case that the solar radiation is not enough to heat the water to an adequate temperature, it will be necessary to activate electric heating devices.

Taking advantage of the productive use of solar energy, in 2017, through an initiative of SERC-Chile with the support of the BHP Billinton Foundation, the Ayllu Solar Project was created [6]. This project aims to promote the sustainable development of urban and rural communities in the Arica and Parinacota region of northern Chile through the productive use of solar energy. In this context, the Ayllu Solar project consists of different small-scale projects deployed in various locations in such region, for example, the processing of agricultural products with solar energy, river shrimp farming, camelid fiber collection and processing center [64], among others [78] as seen in Figure 2.11. A more detailed description of the specific objectives and the reference projects of the Ayllu project is shown in Annexed B.
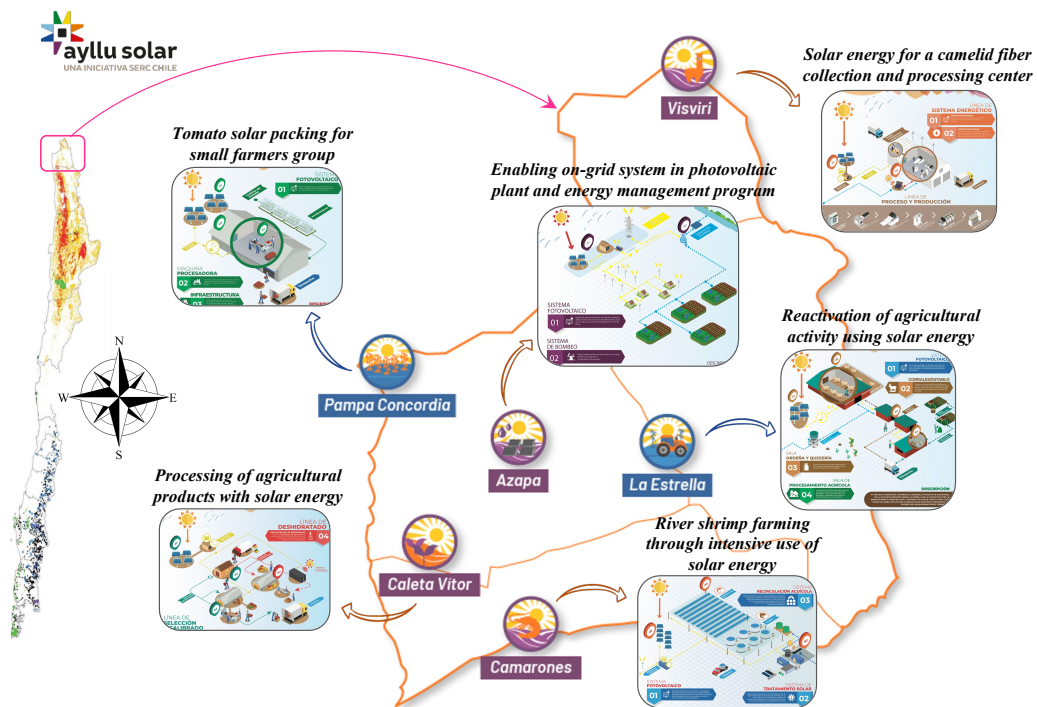
Figure 2.11 Ayllu Solar small productive solar processes (SPSPs) located in the Arica and Parinacota region (adapted from [78])

2.2 Microgrids: operation and control

2.2.1 MG concept

Small electrical systems have been used to provide power mainly in remote communities where connecting to the main grid is not feasible due to technical and/or economic difficulties. Fossil fuel-based generation sources (e.g., diesel) have been the main alternative to supply remote systems for several years because of their competitive costs, flexible and continuous operation. However, te characteristics of DER (e.g., low operating costs and low to zero emissions) have led them to be increasingly considered as alternatives to conventional generation. Nevertheless, the integration of DER into electrical systems is a challenging task.

The MG concept appeared as an appealing alternative to deal with the challenges to integrating DER into electrical systems. The MG concept was first defined in [81], [82] as a self-contained electrical power system consisting of DER, such as DG and energy storage systems (ESS), and loads (controllable loads in some cases) that are coupled to MG through the point of connection; and all of them comprise a single controllable system. Figure 2.12 shows a sample MG with its main elements such as DG (e.g., wind turbine, PV, among others) and the possible connections to the main grid and other MGs.
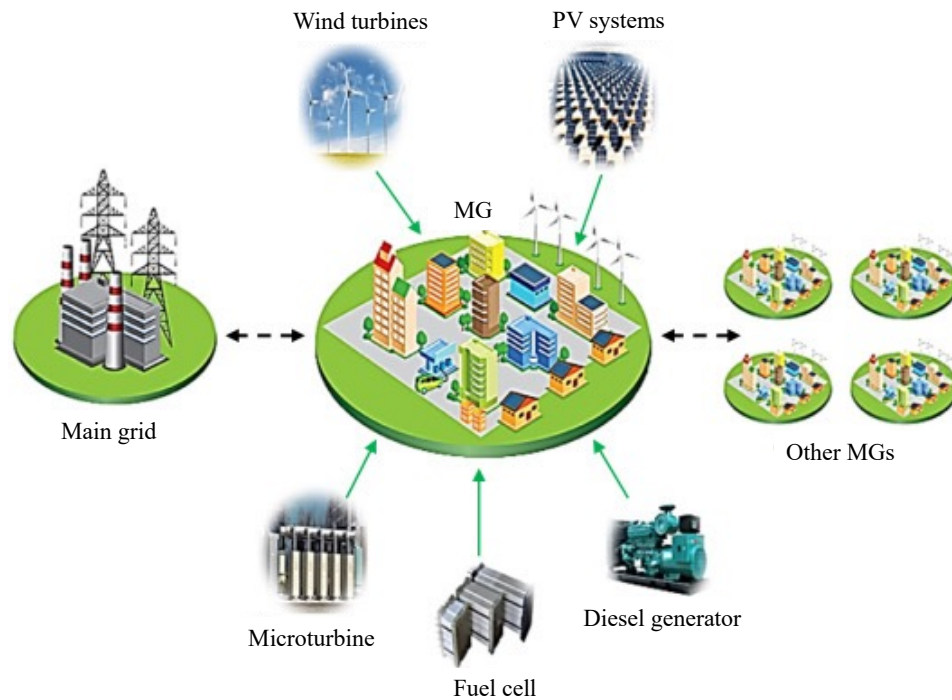
Figure 2.12 Sample MG with its main elements [83]

Due to their versatility, capabilities and benefits, MGs have been deployed in different parts of the world [10], [84], [85], and in Latin America especially in remote locations that are difficult to access where MGs provide electric energy to people in remote communities [86]–[88]. Figure 2.13 presents some examples of MGs installed in different countries in Latin America such as Chile, Ecuador, Argentina, Brazil, among others.
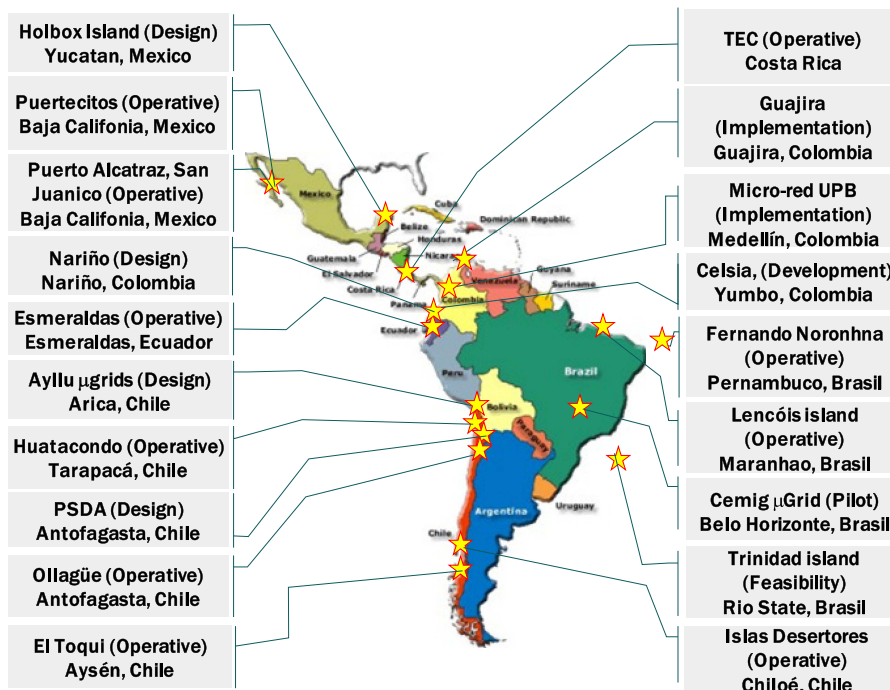
Figure 2.13 Examples of MGs installed in several countries in Latin America [89]

2.2.2 Operation and control of MGs

Regarding the control and operation of these small electrical systems, MGs can have three operating modes: i) on-grid mode, i.e., connected to the main grid through the point of common coupling (PCC) as illustrated in Figure 2.14, ii) off-grid mode, i.e., MGs that do not have a PCC, and iii) switch from on-grid mode to off-grid mode and vice versa depending on the operating conditions in the main grid. The main characteristics of each operating modes are described below.
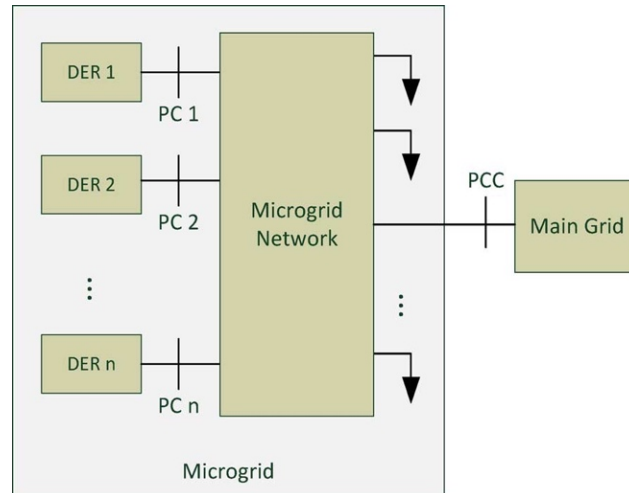
Figure 2.14 Schematic diagram of a generic multiple-DER MG [90]

On-grid operating mode [90]: In this mode of operation, the main grid determines the frequency of the MG and the voltage at PCC. The main role of the MG in this case is to manage the active and reactive power generated by the DER units, and the load consumption. Besides operating in on-grid mode, MGs can support the main grid in different manners such as voltage control, frequency control, and can provide more flexibility and reliability [91].

Off-grid operating mode [90]: This mode of operation is also known as stand-alone, isolated or islanded, in this case the MG operates as an autonomous entity. This operating mode is more challenging than the on-grid mode because of the need to maintain the critical demand-supply equilibrium. Thus, it requires more accurate load sharing mechanisms to balance sudden active power mismatches. Frequency and voltages are controlled by different DER units; thus, the main objective is to ensure that all units contribute to supply the load consumption in a predefined way.

Transition from on-grid mode to off-grid mode [92]: While MG is operating in on-grid mode, the main grid provides the reference of frequency and voltage at PCC. However, if disturbances (e.g., blackouts, faults, voltage sag, voltage swell, load switching, among others) occur in the main grid, the MG switches to an isolated operation. This capability of the MGs may ensure uninterrupted supply to critical loads [93]. Nevertheless, the implementation of MG control strategies to enable smooth transition between operating modes, i.e., on-grid/off-grid, is mandatory.

An adequate control of MG is required for stable, economically reliable, and efficient operation. Thus, the principal tasks of the MG control structure are [94]:

- voltage and frequency regulation for on-grid and off-grid operating modes
- proper load sharing and DER coordination
- resynchronization with the main grid
- power flow control between MG and the main grid
- optimizing the MG operating cost

The tasks mentioned above have different characteristics and occur in different time scales, thus, to fulfill such tasks a hierarchical control strategy is commonly used. The hierarchical control scheme consists of three control levels such as primary, secondary, and tertiary. Each of them differs in their i) speed response and time frame at which they operate, and ii) infrastructure requirements (e.g., communications requirements) [90]. The primary control reacts instantaneously when local events occur, while the secondary control responds within a few minutes. Finally, the tertiary control operates in the range of several minutes. A brief description of their main features is presented below. Figure 2.15 illustrates the three control levels with their respective time scaling.

Primary control: This is the first and the fastest level of control and is also known as local control or internal control because it is based on local measurements and does not require communication infrastructure between the MG DER. Due to its speed requirements and dependence on local measurements, islanding detection, output control and power sharing and balance control are considered in this level [90]. Analogous to power system generators, output control and power sharing are carried out by the governor, voltage regulator, and the inertia of MG synchronous generators.

Secondary control: This level of control is also called the MG EMS, and is responsible for the reliable, secure, and economical operation of MG in either on-grid or off-grid. Besides, such tasks are particularly challenging in stand-alone MGs due to the presence of variable energy sources, where the update rate of the unit dispatch command should be high enough to follow the sudden changes of load and non-dispatchable generators [90]. One of the objectives of the secondary control is to restore the voltage and frequency deviations produced by the action of the primary control [90]. Nevertheless, the main objective of the EMS consists of achieving the optimal (or near optimal) Unit Commitment (UC) and Economic Dispatch (ED) set points for the available DER units in the MG.

Tertiary control [90]: This is the highest level of control and sets long term and typically "optimal" operating set points according to the requirements of the main grid. In addition to establishing the coordination requirements with the main grid (e.g., voltage support, frequency

24

regulation, etc.), the tertiary control is in charge of coordinating the operation of multiple MGs in case this type of configuration is considered. The tertiary control can be considered as part of the host grid, and not the MG itself [90].
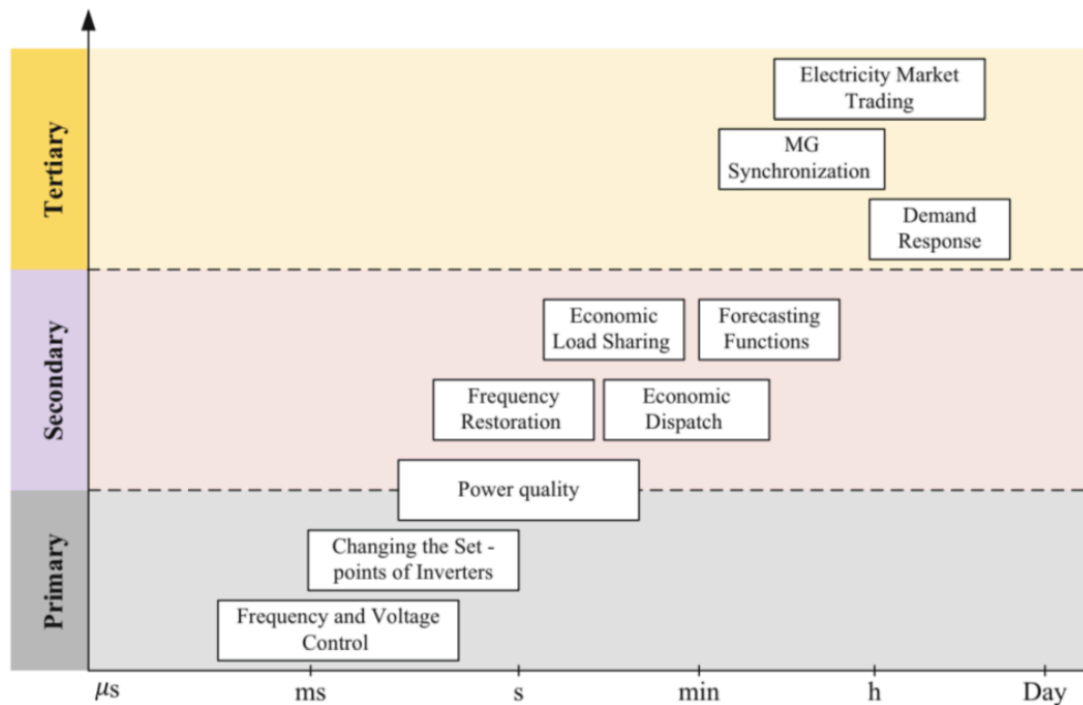
Figure 2.15 Different control level for the MG [95]

It should be noted that both the primary and the tertiary control are beyond the scope of this study, however, a more detailed description of them can be found in [10], [90], [95]. However, the secondary control (i.e., EMS) is a fundamental part of this work, therefore, it is further described in the following section.

2.2.3 Energy management systems for MGs

As previously mentioned, EMS is responsible for determining the optimal (near optimal) operating set points of dispatchable units in an MG by solving an UC and/or an ED problem [96]. For this purpose, the EMS considers different information such as load forecasting, power generation available from DER, energy available from storage, weather forecasts, energy prices, etc.[40]. Depending on the control architecture, EMSs can be classified into four categories: centralized, descentralized, distributed and hybrid [95]. Figure 2.16 shows an overview of the different types of EMS control architectures.

In centralized control architecture, a central controller makes the decisions and then sends the optimal (or near optimal) operating setpoint to the local DER controllers. This central controller usually minimizes the total operating cost by preventing the removal of critical loads under any possible adverse conditions [95]. With this aim, the central controller used information from the

forecasting systems, for example, load consumption, wind speed, solar radiation, etc. Moreover, this type of architecture presents a simple structure and in isolated mode, it has acceptable reliability [95]. Nevertheless, this control architecture can be more expensive because it requires high communication infrastructure. Practical applications of this approach are demonstrated in [41], [97].

In a decentralized control architecture, the energy management problem is solved while a highest independence to DER units and loads is provided [90]. All control decisions are primarily made locally, nevertheless, this control architecture can still consider the hirarchical control scheme. This type of control architecture is highly dependent on the main grid when it operates in on-grid mode. Thus, an increase in uneconomical costs can be expected. Consequently, the EMS with decentralized architecture operating in either on-grid mode or off-grid mode is not very useful or resilient [95].

Due to the particular characteristics of the decentralized architecture, it has been addressed in the literature through a multi-agent system (MAS) approach. Generally speaking, a MAS can be defined as a system composed of multiple intelligent agents, provided with local information, that interact with each other to achieve multiple global and local objectives [90]. A detailed analysis of the advantages, drawbacks, control and operational challenges, and challenges in communications requirements can be found in [98].

When a distributed architecture is considered, autonomous agents perform control in a cooperative manner to meet the objectives of the MG [99]. This type of control architecture is also known as communication-based decentralized control [100] where MG's agents directly communicates with each other, which improves scalability because it avoids single-point faults. However, this control architecture requires high processing power at each local conroller, thus, an increase in the system cost is expected [101].

Given the advantages and disadvantages of control architectures described above, a hybrid EMS can deal with the issues of such control architectures, which eventually have to rely on communication to some extent [101]. This hybrid control architecture may include several central controllers with a distributed topology that is coordinated. In addition, each central controller may consider various local controllers that can operate independently [95].
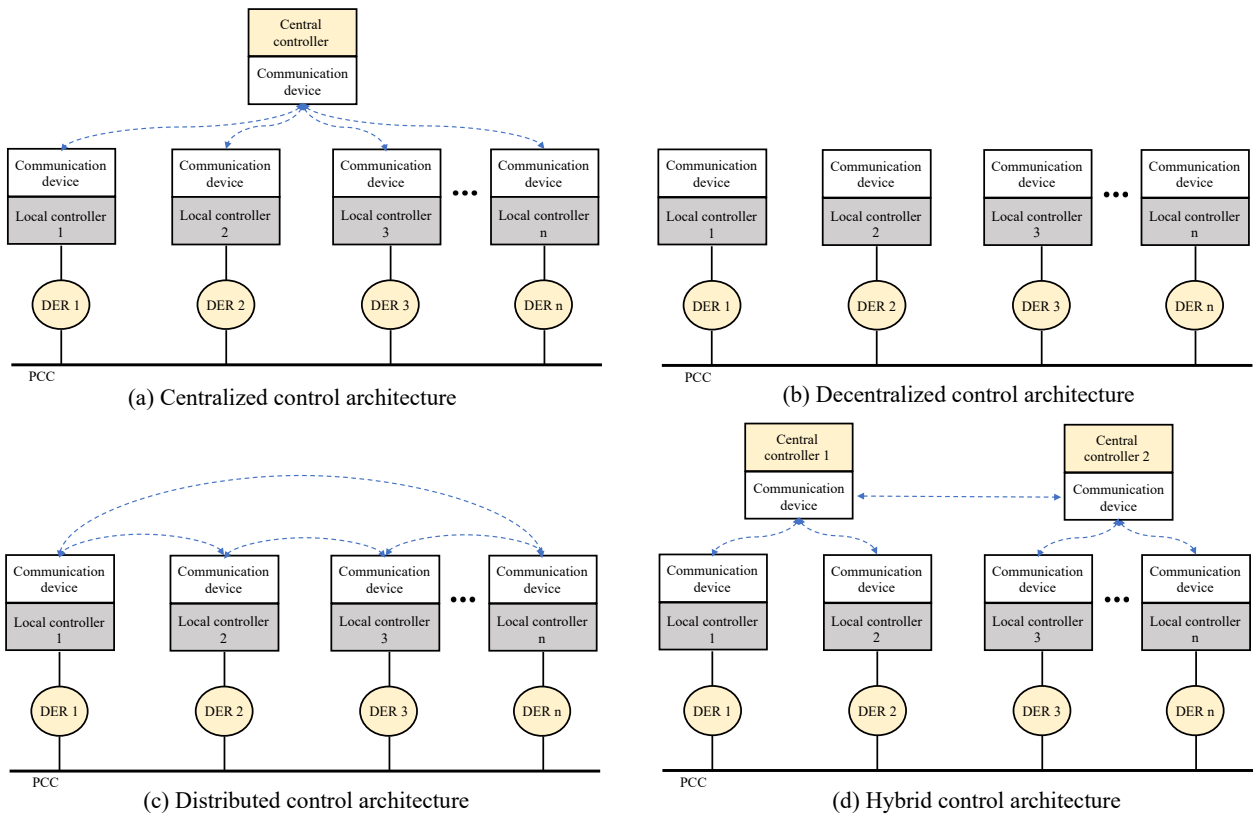
Figure 2.16 Different types of EMS control architectures (adapted from [102])

The type of MG control architecture designed for the MG depends on DER ownership, MG size, available technologies, and communication infrastructures [95]. In this sense, in Chile the most commonly used MG control architecture in real implementations is the centralized architecture, [60], [97], thus, this is considered in this work. Consequently, a brief overview of the main attributes of centralized EMS and its challenges are presented below. Nevertheless, the methodological approach presented in this work may be applied in other EMS control architectures.

D. Espín-Sarzosa *et al.* [40] proposed a taxonomy of the main attributes of the centralized EMS (see Figure 2.17). Such taxonomy consists of five levels such as control architectures, fields of interest, selected topics, main features, and level of complexity (each with its own particular characteristics).

Based on the taxonomy mentioned above and a revision of a nearly 200 articles addressing the topic of centralized EMS for MGs, D. Espín-Sarzosa *et al.* [40] conducted a cluster analysis to find the main trends in EMSs focused on centralized control architectures. The identified clusters are presented in Figure 2.18. Each cluster represents a research trend in centralized EMSs.
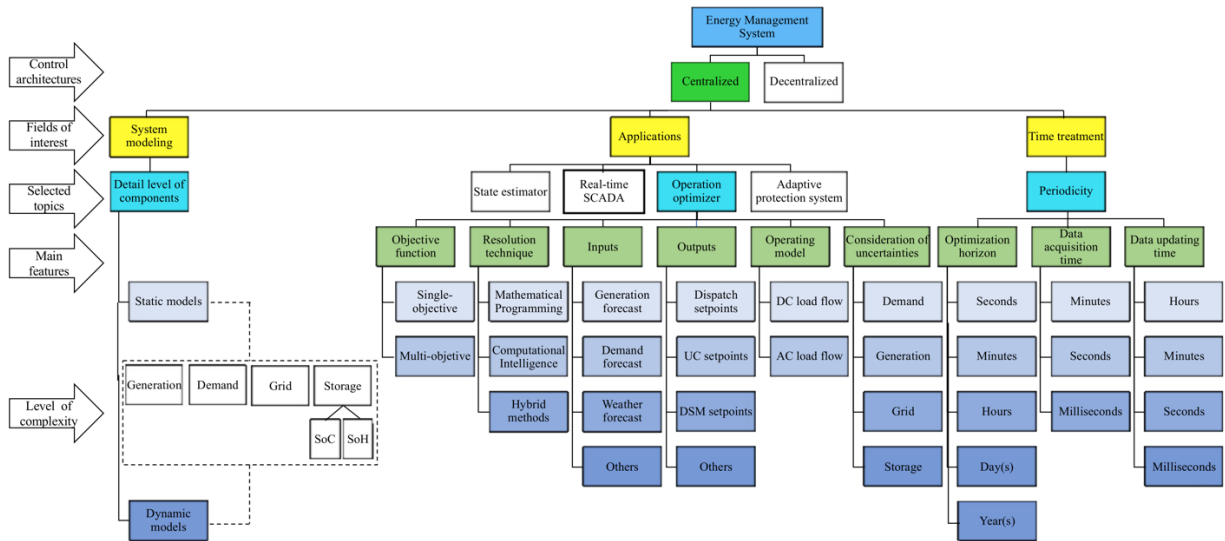
Figure 2.17 Taxonomy of the main attributes of the centralized EMS [40]
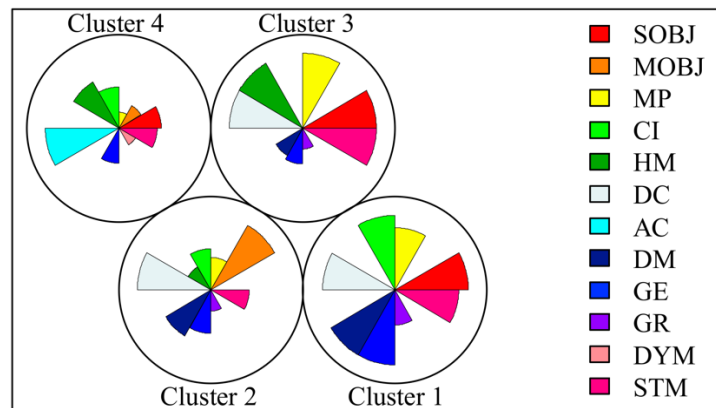
Figure 2.18 Identified clusters that represent research trends in centralized EMS [40]

Based on the cluster analysis and the identified research trends, some of the distinguished key challenges and future research directions are [40]:

- Decentralized energy solutions (i.e., SPPs and SPSPs) will increasingly integrate local RES, thus, more complex customers' behaviors are expected. Consequently, the modeling of this type of loads involves new complexities and the need of new simulation strategies that exceeds the traditional ZIP model approach or a time series analysis.

- Some obstacles for the researchers to cope with regarding additional modeling challenges that occur on a simultaneous basis have been identified, e.g., multiple objective functions, full AC network representations, and the application of hybrid solution methods. Each of these combinations constitutes new challenges in this research area.

- Most of the reviewed studies hold a high consideration of DC load flow. However, reactive power is also an important part of MG and should be considered in energy management to

28

achieve a reliable and secure system. However, this consideration introduces non-linear equations that increase formulation complexity and computational burden. Therefore, research efforts should focus on developing low complexity and computationally efficient AC load flow models.

- There is no evidence of a research cluster where all EMS development challenges were dealt with on a simultaneous basis. In fact, research proposals in every cluster are mainly focused on the improvement of specific areas, while making some simplifications in others. This is due to the complexity of the mathematical problem resulting from trying to consider all EMS development challenges.

2.3 Load representation and modeling in energy management systems for MGs

As mentioned in the previous section, the EMS determines the optimal (near optimal) operating setpoints based on expected demand and generation. Thus, to achieve such desired setpoints, adequate models for representing load consumption are needed.

Regarding load modeling, two broad approaches are aimed at determining model parameters: the component-based and the measurement based. The former is based on developing and aggregate load model by using information about the composition of each load type and characteristics of each load component [103]. While the latter aims to develop load models through measurements gathered *in situ*. The models developed through this approach have a significant advantage, i.e., they are more accurate than those developed using the component-based approach [103].

As stated above, one way to represent the electrical loads is to use the aggregated consumption information available at the measurement points in the MG. Then, the measurements are utilized either to estimate model parameters or to train forecasting models. In this sense, there are different alternatives in the scientific literature, of which those based on statistical models, AI approaches, and physical representation models stand out. Figure 2.19 presents a summary of the different approaches to represent electrical consumption in MGs.
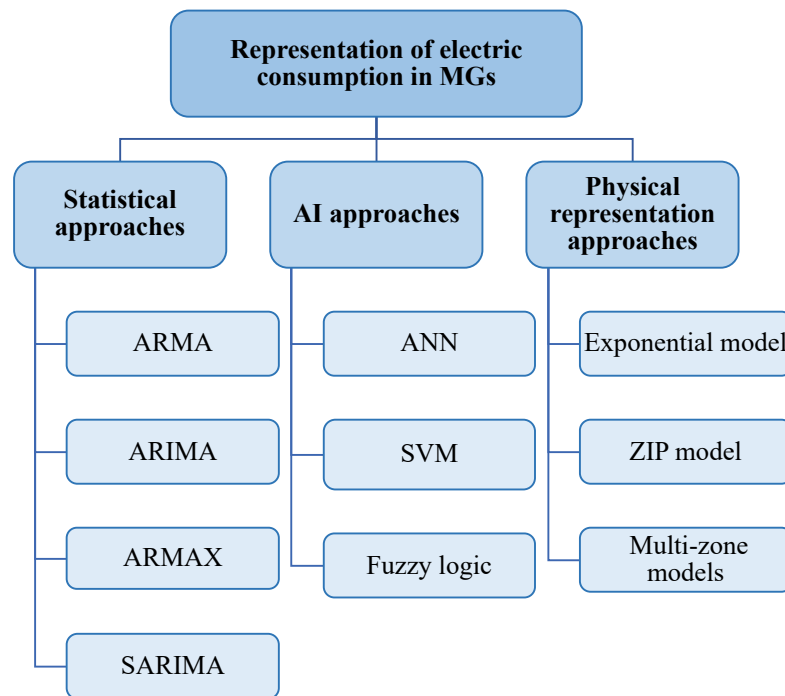
Figure 2.19 Approaches to represent electrical consumption in MGs

2.3.1 Statistical approaches

The statistical approaches are also known as time series models, where the most widely used are the Autoregressive Integrated Moving Average (ARIMA) and the Autoregressive Moving Average (ARMA), and they were introduced by George Box and Gwilym Jenkins in the 70's [104]. The basic ARMA model comprises an autoregressive model (AR) and a moving average model (MA). In addition, the autoregressive model is a linear regression of the current value based on one or more previous values [105]. An important feature is that to consider an ARMA model, the time series should be stationary. If that is not the case, the stationarity is achieved by differencing a non-stationary series first, thus leading to a new model called ARIMA [105]. Moreover, to consider the seasonality, the seasonal ARIMA or SARIMA can be used. In general, statistical approaches are adaptable, can deal with seasonality and with non-stationary [105] and only requires the past value of a time series [106]. Nevertheless, such approaches are subjective and require a good understanding of the underlying statistics [106]. Finally, to consider the effect of exogenous variables (e.g., weather conditions), the autoregressive moving average with exogenous (ARMAX) variables has been used [107]. However, this approach can get trapped in a local optimum caused by the exogenous variable. Therefore, to face this challenge it is required to combine the ARMAX model with other approaches such as particle swarm optimization (PSO) [108]. A more detailed description of these statistical approaches can be found in [109].

2.3.2 Artificial intelligence approaches

ANN is an AI approach based on the structure of the human brain. Similar to the human brain, the ANN comprises neurons and interactions within multiple layers that emulate biological synapses. The wires that connect one neuron to another are known as weights. Generally speaking, there are

three main characteristics that define an ANN: i) the architecture of the net (feedforward or recurrent), ii) the learning rule used to determine the weights during training (e.g., perceptron, Hebbian, etc.), and iii) the activation function between input and output neurons [105]. One of the most widely used ANN architectures is the multilayer perceptron (MLP) which is based on a backpropagation rule that evaluates the output's error from the output back to the hidden layer [105]. ANN may be used to represent complex loads considering the effect of external weather variables [26]. Nevertheless, it is worth mentioning that this approach is useful when the model structure is unknown or it is hard to be mathematically represented and for systems that have already been developed [16]. The latter because a large volume of data is needed for ANN training, and there is not always sufficient data at the initial stage of systems development. A comprehensive review of studies regarding ANN and applications in several areas can be found in [110]. Moreover, the authors in [111] present some examples about the use of ANN in the context of MGs.

The support vector machine (SVM) model is based on a structure risk minimum principal instead of the empirical minimization principle implmented by most of the traditional ANN models [112]. The SVM model shares a lot of similarities with standard MLP neural networks (e.g., network parameter selecting challenges), but it is more efficient than the ANN. The SVM model is equivalent to solve a linear constrained quadratic programming problem, thus, its solution is globally optimal [112]. The main advantages of this approach are [113]: the user can avoid overfitting due to regularization, expert knwoledge about the problem can be built through kernel trick and because it is defined by a convex optimization problem, it can reach global optimum and there are efficient methods to solve it. In contrast, some of the principal disadvantages are [113]: the biggest limitation depends on the choice of kernel, limitation in speed and size for both training and testing stages, and it is significantly slow in the testing stage. Consequently, the SVM approach has been improved by combining it with other approaches, for example, Genetic Algorithms (GA) [114], self-organizing maps (SOM) [115].

Fuzzy logic has the ability to emulate human decision making because it deals with ambiguous and uncertain information. Besides fuzzy logic is user friendly, robust and simple to design, thus, it is preferred over the ANN [116]. In general, fuzzy logic is a oversimplification of real-world problems and considers degrees of truth instead of usual true/false or 1/0 equivalent to Boolean logic [117]. In general, fuzzy logic comprises two parts: fuzzification and defuzzification. The former is the process of transforming a crisp set to a fuzzy set or a fuzzy set to fuzzier set, while the latter is the process of reducing a fuzzy set into a crisp set of to convert a fuzzy member into a crisp member [117]. Further, fuzzy logic regression can face some of the limitations of linear regression, for example, the poor relationship between the response variable and predictor variable, among others [118]. Moreover, in fuzzy regression the errors between the observed and the estimated values are assumed to be dependent on the indefiniteness of the system structure [118]. In general, the main advantages of fuzzy logic in load forecasting applications are [119]: this approach uses fuzzy sets that enabled us to condense large amount of data into a smaller set of

variable rule, fuzzy logic controllers are based on heuristics and therefore able to incorporate human intuiton and experience. Nevertheless, calibrating the parameters to obtain good quality results can be challenging. Therefore, several alternatives have been proposed in the scientific literature to address this challenge, e.g., bio-inspired metaheuristics [120].

2.3.3 Physical representation approaches

As previously mentioned, to obtain the operating setpoints for dispatchable units in an MG, the EMS performs an ED and/or UC problem [96]. The former usually only considers the limits of the generator, and the constraint that supply must meet demand. However, to achieve more realistic results, the ED must consider the power flow equations, either a DC approximation [121] or an AC approach [121]. The DC approximation considers the power flow limits of the lines (in a linearized representation) and the active power, but reactive power and losses are not part of the formulation (these assumptions are typically valid for high-voltage transmission systems [121]). However, MGs feeders similar to distribution networks have a low X/R ratio, which increases the coupling between active and reactive power [90], thus, the DC approach needs to be carefully used [122]. In contrast, the AC approach comprises a full detail of network constraints, active and reactive power flows, bus voltages (i.e., multi-bus) and branch losses. However, the full AC network representation is non-convex in its original form [123], thus, it is required to consider convexification techniques to achieve a global optimum [124], [125].

In the context of MG, usually a single-bus EMS approach where network constraints are neglected [97], [126]–[128] or a multi-node EMS approach that considers physical network constraints such as bus voltages, line flow limits, etc. can be considered [129]–[132]. However, not considering the underlying network constraints can lead to bus voltages that significantly violate the tolerance constraints [129]. Nevertheless, the authors in [133] have shown that considering certain assumptions regarding the characteristics of the MGs, a single-bus EMS that also includes the reactive power of the MG can be formulated.

The traditional AC approach considers variants of CP representations (i.e., PQ nodes) for representing aggregated loads [134]. In this context, the load forecasting results obtained through the approaches discussed in Sections 2.3.2 and 2.2.3 may be used as inputs for the OPF. However, the CP load representations do not consider the voltage dependence, therefore, they do not represent the behavior of the loads as observed from real measurements. For example, in the B.C. Hydro system where it was shown that decreasing the substation voltage by 1% will cause that the active and reactive demand decrease by 1.5% and 3.4%, respectively [135]. Besides, this effect can be observed in residential loads, for instance, a 5% reduction in voltage will lead to a decrease in the load consumption by around 7.6% [136].

To adequately represent the relationship between the power and voltage, two of the most commonly used models are the exponential and the ZIP load model. The former relates the power and voltage through an exponential mathematical representation [16]. While the latter considers a polynomial expression (that combines constant impedance, constant current and constant power) to represent the relationship between the power and voltage. Figure 2.20 illustrates the behavior for each ZIP characteristic.
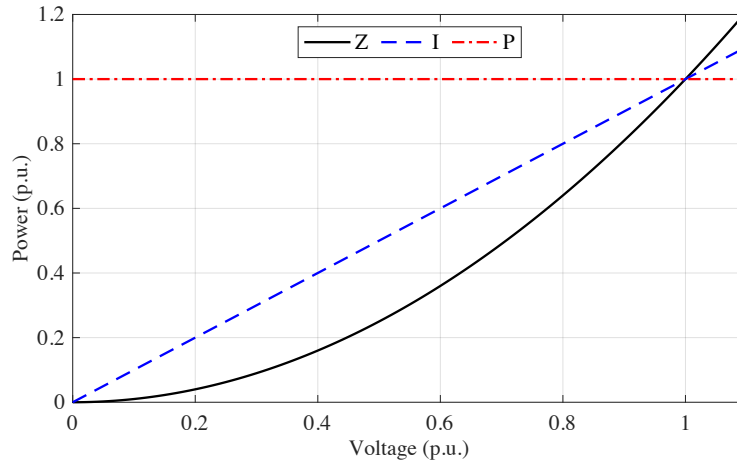
Figure 2.20 Load behavior for constant impendance (Z), constant current (I) and constant power (P) characteristics

Although the exponential model has fewer parameters than the ZIP load model, according to [137], the ZIP model has physical significance. In other words, the constant impedance can represent pure resistive loads, for example, space heaters, incandescent lights, hot plates, etc. [138]. Similarly, the constant power component can represent induction motor loads, while the constant current feature would represent power supplies and variable frequency drive loads [138].

Both the exponential model and the ZIP model are able to represent conventional electrical loads, however, with the introduction of complex loads such as electronics, electric vehicles, among others, these models are not sufficient to represent the complicated behavior of complex loads [38], [39]. For example, in the case of an electronic load, if the voltage is higher than a threshold value, the electronic load behaves as constant power. While if the voltage is between two different threshold values, the active and reactive power of the electronic load are linearly reduced to zero [38]. Further, when considering the charging of the battery of an electric vehicle (EV), at the beginning of the process the current absorbed by the battery is constant, but after the state-of-charge (SOC) reaches a certain level, the voltage becomes constant but the current gradually decreases until it reaches a very small value when the battery is close to its maximum charge [39].

In addition, as mentioned in Section 2.1.2, SPSPs have appeared in recent years to promote sustainable development in communities. However, these SPSPs also present a complex electrical behavior because they are based on solar energy and may be influenced by changes in external

weather variables, for example, if we consider a solar drying process, besides the fact that the electrical consumption varies due to voltage changes, the process also varies depending on the solar radiation and the ambient temperature.

Consequently, to capture and adequately represent the electrical behavior of complex loads, multi-zone models have been proposed, which are also known as multi-stage or multi-step models [38], [39], [139], [140]. These models have the property that depending on the zones or periods of operation they can vary their structure (e.g., combining physical representation models) to provide a more accurate representation of complex loads. For example, in the case of electronic charging, the authors in [38] propose a composite model that presents 5 modes of operation where in each of them the model parameters change depending on the operating voltage level. Further, to capture the electrical behavior of EV charging, a multi-stage time-variant model was proposed in which the ZIP model parameters change depending on the charging time [39].

In the case of SPSPs, D. Espín-Sarzosa *et al.* [141] present a methodology that considers an EMZ-ZIP load model to capture the complex behavior of this type of these processes. The EMZ-ZIP load model consists of combining electrical devices that may belong to an SPSP [141]. In this context, the structure of the EMZ-ZIP changes according to operating zones. Moreover, to assess the performance of the EMZ-ZIP, the authors in [141] have conducted a performance analysis that comprises a bias-variance tradeoff analysis (second-order Akaike's Information Criterion (AICc)) [142] and an analysis through forecasting indexes (RMSE, MAE, MAPE, and R^2) [143]. Considering these analyses, the EMZ-ZIP is compared with other approaches frequently used in the literature such as time-variant ZIP model (TV-ZIP) [144], ZI model [145], exponential model based on both a linearized technique [133] and a variable transformation [146], SVM, gaussian process regression (GPR), and long short-term memory (LSTM) [147]. Table 2.3 summarizes the results of the performance analysis.

Table 2.3 Performance analysis results [141]

Model	AICc	RMSE	MAE	MAPE (%)	R^2
TV-ZIP	−29,703.57	0.01870	0.012326	6.586	0.98474
LSTM	−1703.42	0.14153	0.020032	11.141	0.98507
EMZ-ZIP	−1556.63	0.01874	0.012344	6.577	0.98484
Var-exp	−535.21	0.01879	0.012247	6.575	0.99234
Lin-exp	−534.63	0.01871	0.012304	6.580	0.98446
GPR	−369.01	0.02564	0.018614	12.960	0.97250
SVM	−368.52	0.02906	0.023662	15.280	0.96093
ZI	99.09	0.01870	0.012329	6.586	0.98477

It can be seen from Table 2.3 that the TV-ZIP model has the lowest AICc value. This implies that from the model selection point of view, the TV-ZIP model is the best to represent the power consumption of the SPSP considered in the case study in [141]. Nevertheless, the AICc value of

the EMZ-ZIP model is much lower than the other physical representation models (i.e., exponential models) considered in Table 2.3. Therefore, it has a better bias-variance tradeoff, consequently, it has a better representation of the complex consumption of SPSPs. A further analysis of the EMZ-ZIP load model can be found in [141].

Moreover, Figure 2.21 shows the evolution of parameters that capture voltage sensitivity. As can be observed in Figure 2.21 (b), The TV-ZIP model assumes that the aggregate electrical consumption of the SPSP behaves as a constant impedance type for most of the time. This behavior does not apply in practice because SPSPs have a combination of several load types, not only constant impedance. In contrast, Figure 2.21 (a) shows the evolution of the EMZ-ZIP parameters which show a better result in capturing the sensitivity of the SPSP loads to voltage. Therefore, although the EMZ-ZIP model contemplates more parameters, it is the better model to properly represent the sensitivity of the SPSP loads to voltage. This is because of the incorporation of more knowledge about the load structure of the SPSP [141].
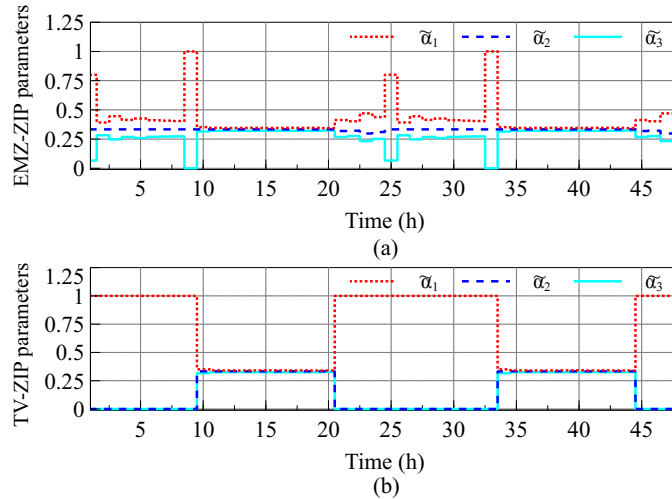
Figure 2.21 Evolution of parameters that capture voltage sensitivity: (a) EMZ-ZIP model and (b) TV-ZIP model [141]

2.4   Summary

This chapter presents the theoretical background of the main topics treated in this thesis. Firstly, Section 2.1 describes and showed examples of SPSPs deployed in various parts of the world. In addition, the concept of SPSPs was defined, describing their main characteristics and the most common projects in Chile. Secondly, in Section 2.2 the concept of the MG is described, in addition the operation and control characteristics for MGs are presented with a particular focus on the centralized architecture EMS because it is the main interest in this work. Finally, Section 2.3 describes different alternatives for representing loads in EMS in the context of MGs. Therefore, due to the voltage dependence of the SPSPs loads and the characteristics of a centralized EMS considering an ED formulation that includes the network constraints, the physical representation approaches, particularly the EMZ-ZIP model, are of special interest in this thesis.

3 Proposed Methodology
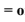
In this chapter, the proposed methodology for modeling the SPSPs and their integration into an EMS for operating a MG is presented. A general overview of the proposed methodology and a general description of its main stages are addressed in Section 3.1. The development of a database with ZIP load models of specific devices that belong to SPSPs is described in Section 3.2. The development of the EMZ-ZIP load model is presented in Section 3.3. The EMZ-ZIP load model parameter identification procedure is described in Section 3.4. The procedure to integrate the EMZ-ZIP load model into an EMS formulation is discussed in Section 3.5. The details of the MG and ESM operation procedure are described in Section 3.6. The most relevant aspects for the implementation of MG model, databases and EMS routines that comprise the proposed methodology are described in Section 3.7. Some feasible extensions to the proposed methodology are discussed in Section 3.8. Finally, Section 3.9 summarizes the main topics treated in this chapter.

3.1 General overview of the proposed methodology for modeling the SPSPs

The proposed methodology for modeling the SPSPs and their integration into EMS for the operation of an MG consists of five main stages with its respective inputs and outputs as presented in D. Espín-Sarzosa *et al.* [141] (see Figure 3.1). First, stage A refers to the development of a database which includes the ZIP load model parameters of the electrical devices that an SPSP may include. Such ZIP parameters can be obtained from either experimental data or existing databases.

Second, an extended TV-ZIP load model is developed in stage B. For this purpose, we gathered information through semi-structured surveys and/or from existing SPSPs and used it later. This is feasible and convenient, considering the engagement of customers promoted by an MG owner. Next, through the gathered information we can know an approximation of both the structure of the SPSPs (i.e., specific electrical devices that an SPSP may include) and the time in which the devices may be used (i.e., time of use of energy). Table 3.1 shows an example of the semi-structured survey employed to gather information from an SPSP. It should be noted that this survey is similar to those used in the gathering of information to estimate electrical demand in the design and planning of MGs [148]. Then, the extended TV-ZIP load model is developed. It combines a generic flexible TV-ZIP, and the ZIP load models for specific devices stored in the previously created database. Moreover, by using the information related to external weather variables (e.g., solar irradiation, temperature, wind speed, humidity, among others) that may influence the SPSPs' electrical behavior and the time of use of energy, the zone classification approach performs a zone division. After this, an extended ZIP load model can be established for each identified zone leading to the formulation of the extended EMZ-ZIP load model.

Table 3.1 Overview of the semi-structured survey to gather information from an SPSP

	Type of device	Nominal active power	Nominal reactive power	Nominal voltage	Quantity	Time of use of energy (▨ = on, ▧ = off)																							
						1	2	3	4	5	6	7	8	9	10	11	12	13	14	15	16	17	18	19	20	21	22	23	24
SPSP	Device$_1$	$P_{0,1}$	$Q_{0,1}$	$V_{0,1}$	Qty$_1$																								
	Device$_2$	$P_{0,2}$	$Q_{0,2}$	$V_{0,2}$	Qty$_2$																								
	Device$_3$	$P_{0,3}$	$Q_{0,3}$	$V_{0,3}$	Qty$_3$																								
	⋮	⋮	⋮	⋮	⋮																								
	Device$_n$	$P_{0,n}$	$Q_{0,n}$	$V_{0,n}$	Qty$_n$																								

Figure 3.1 Overview of the proposed methodology [141]

Third, the parameters of the EMZ-ZIP load model are identified in stage C. This procedure is performed through an optimization problem and the use of the historical data of power and voltage measurements. In this stage, the estimated parameters of the EMZ-ZIP load model and statistical information of residuals are provided. It should be noted that for SPSPs in the design phase, measurements from similar existing SPSPs, results from system simulations or information gathered through structured surveys [148] could be used.

Fourth, stage D refers to the integration of the EMZ-ZIP load model into an EMS approach. With this aim, the identified parameters of the EMZ-ZIP load model with the information of other MG elements are integrated into the system operation modeling of EMS. Moreover, due to the voltage sensitivity of the developed models, an AC approach is required. For example, an AC multi-period optimal power flow (OPF) will be able to define the operating conditions for the scheduling horizon of EMS. Furthermore, additional technical information about MG elements may be integrated at this stage. For example, cost information for generation/storage units, supplementary technical constraints (e.g., maximum and minimum limits, ramps, efficiencies, among others), and parameters of other individual loads in MG.

Finally, once EMS is parameterized, it is able to perform the MG operation (stage E). To achieve this, EMS requires MG measurements such as power, voltage, among others, as well as historical data related to power, voltage, weather and time. After that, EMS runs its optimizing routines and sends the operating setpoints to dispatchable units and other devices. This procedure is carried out in a predefined period (e.g., 5 min, 10 min, 15 min) until a predetermined condition such as those described below is detected.

At the initial time k_0 all stages (A–E) are performed following the sequence in Figure 3.1. However, if at the time $k_0 + \Delta k$ considerable changes are detected in analysis blocks 1 or 2, certain stages are conducted again. In this context, analysis block 1 evaluates statistical information from historical data. Therefore, if a significant variation in the errors in either the zone transitions or in the zone length is detected, it is necessary to execute stage B and, consequently, the other stages are executed too. For example, if the analysis window is in hours, it is evaluated whether it is improved by extending or reducing the current zone duration. Besides, new historical power and voltage data are available as MG operates; thus, it is necessary to identify the parameters of the EMZ-ZIP model by running stage C. This procedure can be performed after a predefined time, for example, every 24 hours.

Alternatively, analysis block 2 analyzes the structural changes in either MG or the SPSPs, or both. For example, if new devices are installed in the SPSPs, it will be necessary to run from stage A again. Thus, the EMZ-ZIP model will include the ZIP models of the newly added devices. Moreover, if analysis block 2 detects structural changes in MG (e.g., changes in the topology, adding or removing generation units or loads different from those of the SPSPs), it is necessary to execute stage D to re-parameterize the EMS to include these structural changes.

In addition, changes may occur in the scheduling of activities in the SPSPs, for example, advance or delay of the work shift. In this sense, the EMS includes a routine to detect these changes

and takes advantage of the zoning feature of the EMZ-ZIP model to move the zones (consequently, the identified parameters) to face these changes in the scheduling of productive activities.

Finally, the proposed methodology for modeling the SPSPs and their integration into an EMS involves the aforementioned five stages. This strategy is compatible with different EMS approaches. Nevertheless, stages D and E are highly dependent on the specific EMS approach; thus, a detailed description of the formulation of the EMS approach selected in this work and the integration of the EMZ-ZIP model into this approach is presented in Section 3.5.

3.2 Development of a database with ZIP load models of SPSP's specific devices

As mentioned in Section 2.3.3, the ZIP load model is one of the most appealing alternatives for load modeling. The mathematical expressions of the ZIP load models for the active and reactive power at any discrete time step k ($k \in \mathbb{Z}^+$) are expressed as follows:

$$P(k) = P_0 \left(\alpha_1 \left(\frac{V(k)}{V_0} \right)^2 + \alpha_2 \left(\frac{V(k)}{V_0} \right) + \alpha_3 \right) \tag{1}$$

$$Q(k) = Q_0 \left(\beta_1 \left(\frac{V(k)}{V_0} \right)^2 + \beta_2 \left(\frac{V(k)}{V_0} \right) + \beta_3 \right) \tag{2}$$

$$\alpha_1 + \alpha_2 + \alpha_3 = 1 \tag{3}$$

$$\beta_1 + \beta_2 + \beta_3 = 1 \tag{4}$$

where $P(k)$ and $Q(k)$ denote the total active and reactive power consumed by the load at any time step k, respectively; $V(k)$ is the current voltage at time step k; P_0 and Q_0 are the active and reactive power at nominal voltage V_0; α_1, α_2, α_3, and β_1, β_2, β_3 represent the ZIP coefficients for the active and reactive power, respectively, and they must satisfy (3) and (4), respectively.

As mentioned previously, based on the information gathered through semi-structured surveys/cadasters or information about existing SPSPs, it is feasible to know the structure of such SPSPs in terms of the type and number of specific devices that they comprise, such as a "fingerprint" of each SPSP. Thus, it is feasible to acquire the ZIP parameters (i.e., α_1, α_2, α_3, β_1, β_2, β_3) of each potential device used by the SPSPs from either experimental data or existing load model databases, for example, from [16], [33]. It should be noted that the ZIP parameters obtained from sources are typical, but not exact values for the devices that an SPSP may include. This may lead to inaccuracies; however, to deal with this the ZIP parameters can be updated with measurements from the SPSP devices. In addition, as will be discussed below, the flexible component of the EMZ-ZIP is key to dealing with such inaccuracies. Then, the acquired ZIP parameters are stored in a database, which will be the main source of information for the next

stages. Figure 3.2 illustrates the procedure for the development of the database containing the ZIP parameters of the potential electrical devices used by the SPSPs.
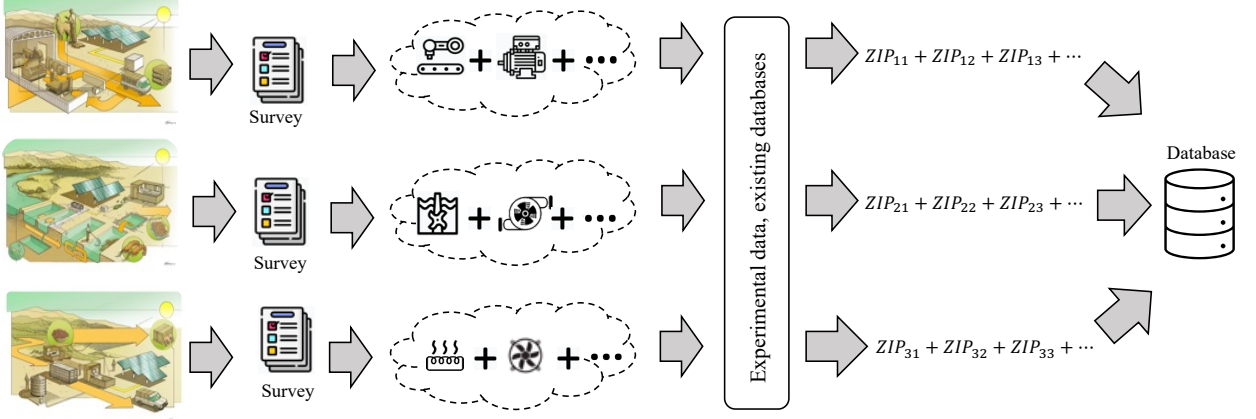
Figure 3.2 Overview of the development of the database that includes the ZIP parameters of potential electrical devices used by the SPSPs

To illustrate the use of the database, let us assume that an SPSP consists of the following devices: i) a conveyor belt; ii) an electrical heater; and iii) two water pumps. Then, the ZIP parameters for each device are acquired from reported specialized literature (for instance, from [33]) and stored in the database. Consequently, the ZIP parameters $\alpha_{1,\omega}, \alpha_{2,\omega}, \alpha_{3,\omega}, \beta_{1,\omega}, \beta_{2,\omega}, \beta_{3,\omega}$ ($\omega \in$ {heater, belt, pumps}) are available for the next stages.

3.3 Development of the EMZ-ZIP load model

3.3.1 Extending the ZIP load model

Although the ZIP model captures the effect of voltage on load consumption, uncertainties of load behavior in the SPSPs could remain. In fact, some devices from the survey/cadaster could be missed or the assigned device from the database could mismatch the load behavior for specific devices. Thus, the first extension of the ZIP model based on the incorporation of a generic extra flexible ZIP component is proposed. More concretely, the TV-ZIP load model was used to account for these changes [141]. The TV-ZIP component for the active power is thus mathematically expressed as (5). Moreover, for notation simplicity, (6) is established for the remainder of this work; hence,

$$P(k) = P_0(k)\left(\tilde{\alpha}_1(k)\tilde{V}^2(k) + \tilde{\alpha}_2(k)\tilde{V}(k) + \tilde{\alpha}_3(k)\right) \tag{5}$$

$$\tilde{V}(k) = (V(k)/V_0) \tag{6}$$

$$\tilde{\alpha}_1(k) + \tilde{\alpha}_2(k) + \tilde{\alpha}_3(k) = 1 \tag{7}$$

where $P(k)$ represents the active power at time step k, $P_0(k)$ stands for the nominal active power at nominal voltage V_0, $V(k)$ is the current voltage at time step k; $\tilde{\alpha}_1(k)$, $\tilde{\alpha}_2(k)$, $\tilde{\alpha}_3(k)$ are the time-dependent ZIP parameters, which represent the load features of constant impedance, constant current, and constant power, respectively. Moreover, as in the conventional ZIP load

model case, the coefficients must fulfill (7) for every time step k. It should be noted that, for reactive power representation, the mathematical expressions (5)-(7) are valid, except that they must consider the ZIP coefficients for reactive power.

Consequently, the authors in [141] have proposed an extended TV-ZIP load model that combines both the TV-ZIP load model and the ZIP models of the set of active devices of the SPSPs. Let $\delta_\omega(k)$ denote the contribution of each load category of the set of active devices to the total load consumption. Then, the extended TV-ZIP load model is expressed in (8)-(11).

$$P(k) = ZIP_{flex}(\tilde{V}(k)) + \sum_{\omega=1}^{\Omega} \delta_\omega(k) ZIP_\omega(\tilde{V}(k)) \tag{8}$$

$$\sum_{\omega=1}^{\Omega} \delta_\omega(k) \leq 1 \tag{9}$$

$$ZIP_{flex}(\tilde{V}(k)) = P_{flex}(k)\big(\tilde{\alpha}_1(k)\tilde{V}^2(k) + \tilde{\alpha}_2(k)\tilde{V}(k) + \tilde{\alpha}_3(k)\big) \tag{10}$$

$$ZIP_\omega(\tilde{V}(k)) = P_{0,\omega}\big(\alpha_{1,\omega}\tilde{V}^2(k) + \alpha_{2,\omega}\tilde{V}(k) + \alpha_{3,\omega}\big) \tag{11}$$

where, $P(k)$ represents the total load consumption at time step k, $ZIP_{flex}(\tilde{V}(k))$ represents the flexible component of the extended TV-ZIP load model for which it is necessary to identify all its parameters (i.e., $P_{flex}(k), \tilde{\alpha}_1(k), \tilde{\alpha}_2(k), \tilde{\alpha}_3(k)$). The term $ZIP_\omega(\tilde{V}(k))$ represents each active electrical device of the SPSP for which its ZIP coefficients (i.e., $P_{0,\omega}, \alpha_{1,\omega}, \alpha_{2,\omega}, \alpha_{3,\omega}$) are already given (see Section 3.2). Thus, solely the identification of its contribution $\delta_\omega(k)$ is needed. Equation (9) reflects the contribution of each load category of the SPSP through the values of $\delta_\omega(k)$. Finally, the term Ω ($\Omega \in \mathbb{Z}^+$) represents the set of devices that belong to an SPSP.

3.3.2 Zoning the extended TV-ZIP load model

The electrical behavior of the SPSPs may change influenced by external weather variables (see Section 2.1.2) such as solar irradiation, temperature, wind, humidity, among others. For example, in a solar drying process, the electrical resistances are not needed when there is a high solar irradiation contribution. Therefore, during periods of low solar contribution, the electrical resistances will be active, while they will be inactive during periods of high solar contribution. Besides, based on the information gathered from semi-structured surveys, the time in which the different electric devices that belong to an SPSP may be active can be known in advance. Then, to properly capture the complex behavior of SPSPs, a zone division of the analysis window (e.g., 24 h) can be performed. According to [141], this is useful for two reasons: i) it significantly decreases the complexity of the parameter identification process (because solely a subset of parameters are identified instead of estimating all of them), and ii) it improves the representation of the sensitivity of SPSP loads to voltage variations.

The zoning procedure is based on the information regarding the type of SPSP, the information of the variables that may influence its electrical behavior, the time of use of energy obtained through the semi-structured surveys, and an ANN approach for classification [149], [150]. Figure 3.3 shows the general ANN architecture, which consists of an input layer, a hidden layer, and an output layer. In the hidden layer and the output layer, the artificial neurons are interconnected via adaptive weights. These weights are obtained through a training process utilizing input and output data. Each artificial neuron is activated through an activation function, for example, threshold activation function, sigmoidal function, among others [151]. The most commonly used activation function is a sigmoidal function [152]; thus, it is considered in this work. Besides, the ANN training process can be performed by using different algorithms, for instance, the Levenberg-Marquardt (LM) backpropagation, the gradient descent backpropagation, among others [153]. The LM algorithm is used in this work because it is successful in reducing errors in classification applications compared to other algorithms [154], [155].
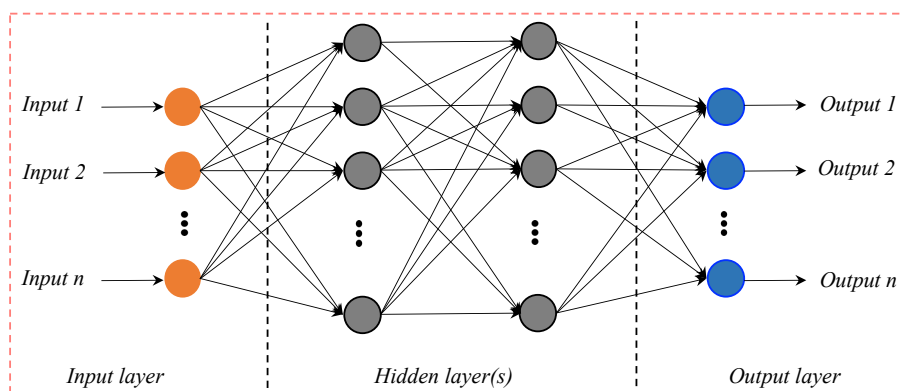
Figure 3.3 General ANN architecture

Determining the number of inputs, outputs, hidden neurons, and the number of hidden layers is known as the definition of an ANN architecture [156]. However, there is no general rule to define the best ANN architecture, i.e., the determination of various parameters, such as the number of hidden layers, number of nodes in the hidden layer etc. [110]. Therefore, a method to calibrate the ANN architecture based on trial & error (i.e., in an empirically way [149]) is proposed in [157] and is used in this work.

As illustrated by Figure 3.3, the ANN approach consists of an input layer, a hidden layer, and an output layer. In this context, the input data are selected depending on the type of SPSP and the external weather variables that may affect its electrical behavior as previously described in Section 2.1.2. Whereas the output data for training are pre-identified zones (e.g., zone 1, zone 2, etc.) based on expert knowledge analysis [158], [159] considering the influence of external weather variables on the operation of the SPSP electrical devices and the time of use of energy. This information is gathered through semi-structured surveys (see Section 3.1). It should be noted that a zone is a period during a day where a device or a set of devices may be active. Then, the ANN associates the inputs (external weather variables data) with the output vector (zones). Once the ANN is trained, it is able to anticipate changes that may occur in the definition of zones. For instance,

during a cloudy day, there will be a considerable change in energy usage in the SPSP. Thus, the ANN will adjust the zones to handle the day's change in energy use due to the cloudy day.

For illustrative purposes, let us consider a basic example where an SPSP has the daily active power profile shown in Figure 3.4 and is composed by three devices (cooler, heater, and water pump) represented by ZIP_{cooler}, ZIP_{heater}, and ZIP_{pump}, respectively. Then, considering the information gathered through the semi-structured survey related to the effect of solar radiation and the ambient temperature on the time of use of energy of the SPSP, it is feasible to define the following zones. The period between 00:00 and 7:59 where there is no solar contribution, the heater can be active; then, it corresponds to zone 1. Next, between 8:00 and 17:59 due to increased solar radiation and ambient temperature, the cooler and fan will be activated. Thus, such period can be defined as zone 2. Finally, between 18:00 and 23:59 again the heater will be active because of poor solar contribution. This last period of the day can be considered as zone 3. Note that solar radiation and ambient temperature measurements are used as input data, and the pre-identified zones based on expert knowledge analysis are used as output data to train the ANN. This procedure can be performed considering information from several months, including seasons and changes in the environmental conditions, so that ANN performs the predictions to adjust the zones in case of detecting such changes.
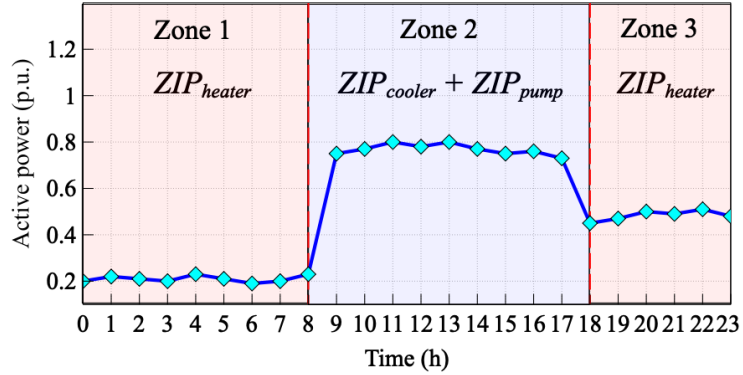
Figure 3.4 Determined operating zones and active devices in each zone

Once zones have been identified, the general mathematical expression of the EMZ-ZIP load model is expressed as in (12)-(15).

$$P(k) = ZIP_{flex}(\tilde{V}(k)) + \sum_{\omega=1}^{\Omega_\psi} \delta_\omega(k) ZIP_\omega(\tilde{V}(k)) \tag{12}$$

$$\sum_{\omega=1}^{\Omega_\psi} \delta_\omega(k) \le 1 \tag{13}$$

$$ZIP_{flex}(\tilde{V}(k)) = P_{flex}(k)\left(\tilde{\alpha}_1(k)\tilde{V}^2(k) + \tilde{\alpha}_2(k)\tilde{V}(k) + \tilde{\alpha}_3(k)\right) \tag{14}$$

$$ZIP_\omega(\tilde{V}(k)) = P_{0,\omega}\left(\alpha_{1,\omega}\tilde{V}^2(k) + \alpha_{2,\omega}\tilde{V}(k) + \alpha_{3,\omega}\right) \tag{15}$$

43

where, as can be seen, the expressions are similar to those of the extended TV-ZIP model. However, the term Ω_ψ ($\Omega \in \mathbb{Z}^+$) that denotes the number of SPSPs' active devices in each zone ($\psi \in \mathbb{Z}^+$).

It should be noted that the zones for the output set for ANN training are based on expert knowledge analysis, i.e., they are identified heuristically, which can lead to significant errors if misidentified. Nevertheless, the flexible component of the EMZ-ZIP (i.e., $ZIP_{flex}(k)$) plays a key role in dealing with this issue. This is because the flexible component can represent any device or a combination of devices, which may be ignored due to misidentification of zones. Besides, the flexible component can be updated at each time step k using available measurements data.

3.4   Parameter identification of the EMZ-ZIP load model

The parameter identification procedure corresponds to the stage C of the proposed methodology (see Section 3.1). In this sense, to identify the parameters of the EMZ-ZIP load model, an optimization problem based on a least-squares approach is used [160]. Let $\hat{P}(k)$ denote the estimated active power at time step k for zone ψ, $\vec{P}_d(k)$ and $\tilde{V}_d(k)$ ($d \in D$) represent the vectors of active power and voltage measurements for each time step k, respectively, and D stands for the set of measurements. Consequently, the minimization problem to identify the set of parameters of the EMZ-ZIP load model at each time step k is expressed in (16)-(22).

$$\underset{\substack{P_{flex}(k),\ \delta_\omega(k),\tilde{\alpha}_1(k),\\ \tilde{\alpha}_2(k),\ \tilde{\alpha}_3(k)}}{minimize} \sum_{d=1}^{D} \left(\vec{P}_d(k) - \hat{P}(k)\right)^2 \tag{16}$$

Subject to:

$$\hat{P}(k) = P_{flex}(k)\left(\tilde{\alpha}_1(k)\tilde{V}_d^2(k) + \tilde{\alpha}_2(k)\tilde{V}_d(k) + \tilde{\alpha}_3(k)\right)$$

$$+ \sum_{\omega i=1}^{\Omega_\psi} \delta_\omega(k)P_{0,\omega}\left(\alpha_{1,\omega}\tilde{V}_d^2(k) + \alpha_{2,\omega}\tilde{V}_d(k) + \alpha_{3,\omega}\right) \tag{17}$$

$$\sum_{\omega=1}^{\Omega_\psi} \delta_\omega(k) \leq 1 \tag{18}$$

$$\tilde{\alpha}_1(k) + \tilde{\alpha}_2(k) + \tilde{\alpha}_3(k) = 1 \tag{19}$$

$$0 \leq \delta_\omega(k) \leq 1 \tag{20}$$

$$0 \leq \tilde{\alpha}_1(k), \tilde{\alpha}_2(k), \tilde{\alpha}_3(k) \leq 1 \tag{21}$$

$$0 \leq P_{flex}(k) \tag{22}$$

Analyzing the minimization problem above it can be seen that, $P_{flex}(k)$ is a non-identifiable [161] and unbounded variable, hence, the big-M method is utilized to bound it. Besides, it is worth mentioning that the big-M value should be selected as proposed in [162]. Note that the objective

function in (16) and the constraints (18)-(22) are all convex. However, the constraint (17) is non-convex due to the product between the variables $P_{flex}(k)$ and $\tilde{\alpha}_\varphi(k)$ ($\varphi \in \{1,2,3\}$) (i.e., bilinear terms) [163], thus, it cannot be addressed directly. In this sense, several approaches to overcome this challenge can be found the specialized literature, for example, those reported in [164] and the convexification procedure presented in [141] (see Annexed C). Nevertheless, the well-known McCormick's (MK) relaxations approach [165] is considered first in this work because of its benefits, such as applicability and easy implementation computationally. Moreover, these relaxations are typically stronger than those resulting from convexification or linearization procedures [166].

By applying the MK [165], [167] to the product of variables $P_{flex}(k)\tilde{\alpha}_\varphi(k)$ ($\varphi \in \{1,2,3\}$) in the constraint (17), a new set of variables is defined as $z_\varphi(k) = P_{flex}(k)\tilde{\alpha}_\varphi(k)$ ($\varphi \in \{1,2,3\}$). Let $(\cdot)^U$ and $(\cdot)^L$ denote the upper bound and lower bound of a variable, respectively. Consequently, the MK inequalities are formulated as follows:

$$z_\varphi(k) \geq P_{flex}^L \tilde{\alpha}_\varphi(k) + P_{flex}(k)\tilde{\alpha}_\varphi^L - P_{flex}^L \tilde{\alpha}_\varphi^L, (\varphi \in \{1,2,3\}) \tag{23}$$

$$z_\varphi(k) \geq P_{flex}^U \tilde{\alpha}_\varphi(k) + P_{flex}(k)\tilde{\alpha}_\varphi^U - P_{flex}^U \tilde{\alpha}_\varphi^U, (\varphi \in \{1,2,3\}) \tag{24}$$

$$z_\varphi(k) \leq P_{flex}^U \tilde{\alpha}_\varphi(k) + P_{flex}(k)\tilde{\alpha}_\varphi^L - P_{flex}^U \tilde{\alpha}_\varphi^L, (\varphi \in \{1,2,3\}) \tag{25}$$

$$z_\varphi(k) \leq P_{flex}(k)\tilde{\alpha}_\varphi^U + P_{flex}^L \tilde{\alpha}_\varphi(k) - P_{flex}^L \tilde{\alpha}_\varphi^U, (\varphi \in \{1,2,3\}) \tag{26}$$

Then, by replacing $z_\varphi(k) = P_{flex}(k)\tilde{\alpha}_\varphi(k)$ ($\varphi \in \{1,2,3\}$), introducing the MK inequalities derived above into the minimization problem (16)-(22) and considering the respective upper and lower bounds of the variables, the following convex minimization problem is obtained for each step k:

$$\underset{\substack{z_1(k),z_2(k)\, z_3(k),P_{flex}(k) \\ \tilde{\alpha}_1(k),\tilde{\alpha}_2(k),\tilde{\alpha}_3(k),\delta_\omega(k)}}{minimize} \sum_{d=1}^{D} \left(\vec{P}_d(k) - \hat{P}(k)\right)^2 \tag{27}$$

Subject to:

$$\hat{P}((k)) = \left(z_1(k)\tilde{V}_d^2(k) + z_2(k)\tilde{V}_d(k) + z_3(k)\right)$$
$$+ \sum_{\omega=1}^{\Omega_\psi} \delta_\omega(k)P_{0,\omega}\left(\alpha_{1,\omega}\tilde{V}_d^2(k) + \alpha_{2,\omega}\tilde{V}_d(k) + \alpha_{3,\omega}\right) \tag{28}$$

$$\sum_{\omega=1}^{\Omega_\psi} \delta_\omega(k) \leq 1 \tag{29}$$

$$\tilde{\alpha}_1(k) + \tilde{\alpha}_2(k) + \tilde{\alpha}_3(k) = 1 \tag{30}$$

$$z_\varphi(k) \geq M\tilde{\alpha}_\varphi(k) + P_{flex}(k) - M, (\varphi \in \{1,2,3\}) \tag{31}$$

$$z_\varphi(k) \leq M\tilde{\alpha}_\varphi(k), (\varphi \in \{1,2,3\}) \tag{32}$$

45

$$z_\varphi(k) \leq P_{flex}(k) \tag{33}$$

$$0 \leq \delta_\omega(k) \leq 1 \tag{34}$$

$$0 \leq \tilde{\alpha}_1(k), \tilde{\alpha}_2(k), \tilde{\alpha}_3(k) \leq 1 \tag{35}$$

$$0 \leq P_{flex}(k) \leq M \tag{36}$$

Although MK relaxations provides stronger results for bilinear terms than convexification or linearization procedures, it may be difficult to prove its global optimality, i.e., the result of the relaxed problem may still be far from the best solution, which naturally increases the chances of failure with respect to finding the global optimal solution [168]. Thus, to cope with this drawback, more sophisticated approaches are needed, such as recursive MK relaxation, piecewise MK relaxations [167] global optimization (GO) [169], among others [170]. Indeed, according to [171], if an optimization problem has constraints involving bilinear terms, then, GO techniques are mandatory for its solution.

Thus, to deal with bilinear term challenge, a GO technique is used in this work. Generally speaking, the goal of GO is to find a global solution (maximum or minimum) of a given optimization problem in some region of interest [172]. In the specialized literature exists various GO algorithms that can be used. For example, simulated annealing (SA), genetic algorithms (GA), PSO, among others [169].

While GO increases the chances to find the global optimum, the local optimization techniques are an important element of a GO methodology [173]. In other words, a typical GO procedure is always a trade-off between two objectives: globally and locally search [173]. More concretely, globality of algorithms provides their capability of narrowing the area of search, and the problem of finding the global optimal point is solved by a local optimization technique [173]. In this sense, the Global-Search strategy together with a Scatter Search algorithm [174] and the local solver *fmincon* are used in this work (an applied research to an engineering problem can be found in [175]).

It is worth mentioning that the local solver used in this work (i.e., *fmincon*) is a gradient-based method. Thus, it is a faster algorithm, however, its convergence performance is highly dependent on the starting point [176], [177], as shown in Figure 3.5(a). If the searching starts from initial point 1, it will stop at local minimum. In contrast, if it starts from initial point 2, it can find global optimum, which in this case is the minimum. This same analogy can be applied in the case of finding the global maximum (see Figure 3.5(b)).

46
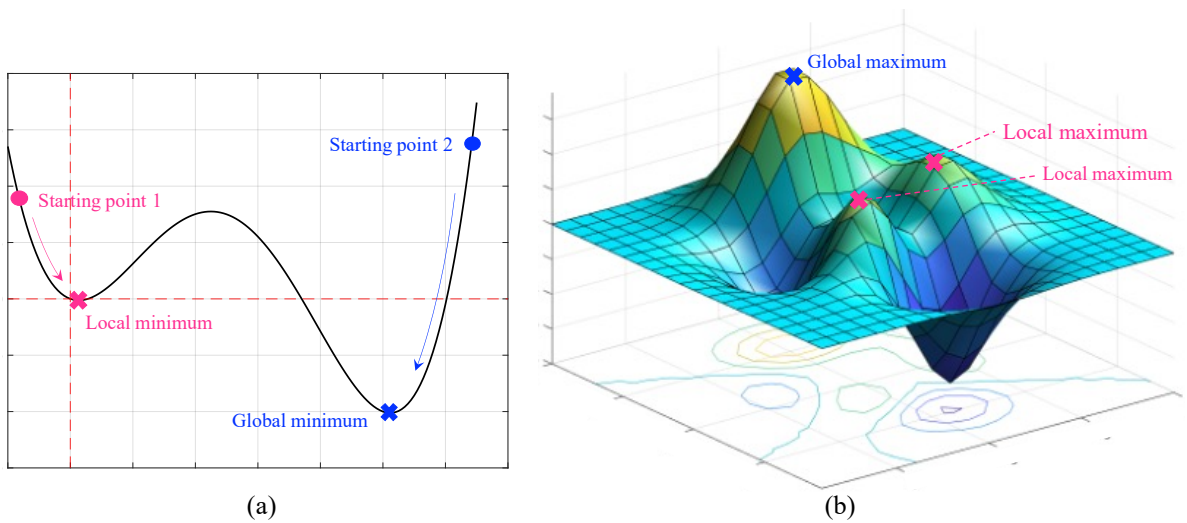
Figure 3.5 Local and global optimal solutions: (a) minimum, and (b) maximum

Due to the high dependence on the starting point, it may not be desired that a starting point is close to a non-feasible or local stationary point. Consequently, we propose the use of the result of the minimization problem (27)-(36) (i.e., resulting optimization problem of applying MK) as starting point for the GO approach. Then, the parameters of the minimization problem (16)-(22) can be identified. Figure 3.6 shows an overview of the scheme for the parameter identification procedure (GO-MK) described above.
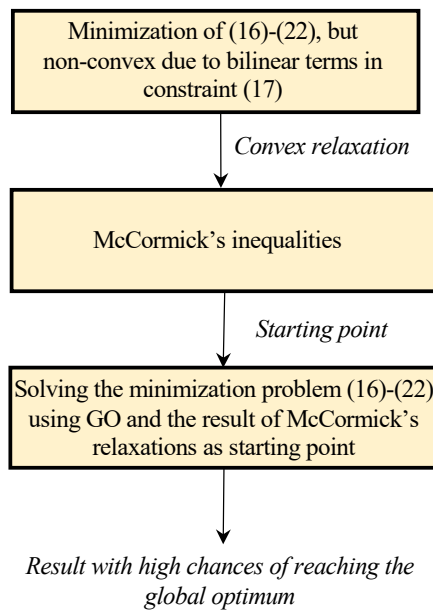
Figure 3.6 Overview of the scheme for the parameter identification procedure

3.4.1 Illustrative example

This section presents an illustrative example where the procedure described above (i.e., parameter identification) is applied to identify the parameters of the loads that are connected to the small low voltage system shown in Figure 3.7. As can be seen, the small system contains three loads which are represented through ZIP load models.

$$ZIP_1 = P_{0,1}\left(\alpha_{1,1}\left(\frac{V}{V_0}\right)^2 + \alpha_{2,1}\left(\frac{V}{V_0}\right) + \alpha_{3,1}\right)$$

$$ZIP_2 = P_{0,2}\left(\alpha_{1,2}\left(\frac{V}{V_0}\right)^2 + \alpha_{2,2}\left(\frac{V}{V_0}\right) + \alpha_{3,2}\right)$$

$$ZIP_3 = P_{0,3}\left(\alpha_{1,3}\left(\frac{V}{V_0}\right)^2 + \alpha_{2,3}\left(\frac{V}{V_0}\right) + \alpha_{3,3}\right)$$
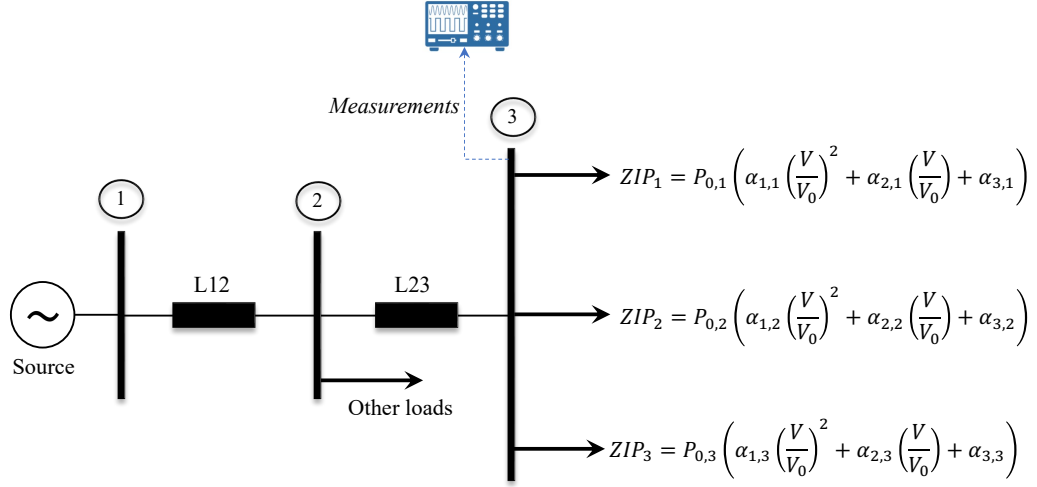
Figure 3.7 Small low voltage system including loads represented through ZIP load models

The small test system is a three-phase 220 V system that includes three ZIP loads, they represent an electric heater, an electric fan, and a set of electric lamps, respectively. The nominal active powers of each considered load are $P_{0,res} = 2000\ (W)$, $P_{0,,fan} = 610\ (W)$, and $P_{0,lamp} = 944\ (W)$. Whereas the ZIP parameters of the mentioned loads were obtained from [33].

The experiment consists of, first, collecting the measurements of voltage and power every 10 minutes at bus 3. Second, preprocessing the collected measurements to be used in the parameter identification procedure. Third, establishing the extended TV-ZIP load model for the small system by using (8)-(11). It is worth mentioning that the flexible part of the extended TV-ZIP model is responsible for representing the set of electric lamps. Next, identifying the parameters of the resulting extended TV-ZIP model using the collected measurements and, on the one hand, the minimization problem (27)-(36) solved through the MK, on the other hand, the minimization problem (16)-(22) solved through the proposed GO-MK strategy. It is worth mentioning that noise can affect the performance of parameter identification methods [178]. Usually, data collection methods are frequently corrupted by noise. Then, to improve the accuracy of parameter identification, filtering techniques can be used to preprocess the measurements to reduce noise [38]. However, the analysis of the effect of noise on parameter identification results is beyond the focus of this paper.

We considered three cases to assess the performance of the parameter identification procedure by using the MK and the GO-MK approach. First, considering only one device switched on. Second, assuming that two devices are active. Third, considering that all three devices are active. Each of the considered cases and their respective resulting extended TV-ZIP model are further described below. It should be noted that, for simplicity, the experiments solely consider the estimation of the set of parameters for a time step k; nevertheless, this can be extended for all time steps considered in the study horizon.

48

Case 1: In this case, we have assumed that only the set of electric lamps is switched on. Thus, the aim is to use the measurements collected at bus 3 to identify all the parameters of the equation (37) (i.e., $P_{flex}(k), \tilde{\alpha}_1(k), \tilde{\alpha}_2(k), \tilde{\alpha}_3(k)$) and that the resulting identified parameters are close to the original ZIP values. Figure 3.8(a) and Figure 3.8(b) show the input data of active power and voltage that were gathered at bus 3 and we used for the parameter identification procedure. As can be seen in Figure 3.8 (b), the voltage profile is between 0.95 p.u. and 1.05 p.u., which corresponds to normal operating conditions. Further, the active power consumption in Figure 3.8(a) varies due to the voltage effect in the ZIP model of the electric lamps.

The original ZIP values and the results of the parameter identification procedure are given in Table 3.2. The estimated parameters indicate that the results obtained through MK have a higher error compared to those obtained with the GO-MK strategy. For example, the $\tilde{\alpha}_{3,k}$ estimated through MK has an error of 460%, while the values estimated through the GO-MK has an error of 0.00%. Therefore, the parameters estimated using the GO approach are closer to the original ZIP parameter values. In this case, the estimated values using the GO-MK strategy are practically equal to the original values.

Figure 3.9 shows the results of the active power estimated using a new voltage profile and the parameters already estimated through the MK (Figure 3.9(a)) and GO strategy (Figure 3.9(b)). Comparing Figure 3.9(c) and Figure 3.9(d) it can be seen that the active power estimated using the parameters obtained with the MK has an error by around 11.5%, while using the parameters obtained through GO-MK the error of the new active power profile is below $1x10^{-5}$%. It should be noted that the error made in the estimated power magnitude using the MK (Figure 3.9(a)) is due to the estimation error of the P_0 parameter.

$$P(k) = P_{flex}(k)\left(\tilde{\alpha}_1(k)\tilde{V}^2(k) + \tilde{\alpha}_2(k)\tilde{V}(k) + \tilde{\alpha}_3(k)\right) \tag{37}$$

Figure 3.8 (a) Active power measurements and (b) voltage measurements for case 1

Table 3.2 Original values and results of the parameter identification by using the MK and the GO-MK approach for case 1

ZIP Parameter	Original values	MK results	Relative error (%)	GO-MK results	Relative error (%)
P_0	0.944	0.843	10.69	0.944	0.00
$\tilde{\alpha}_1$	0.520	0.444	14.62	0.520	0.00
$\tilde{\alpha}_2$	0.450	0.388	13.78	0.450	0.00
$\tilde{\alpha}_3$	0.030	0.168	460.00	0.030	0.00
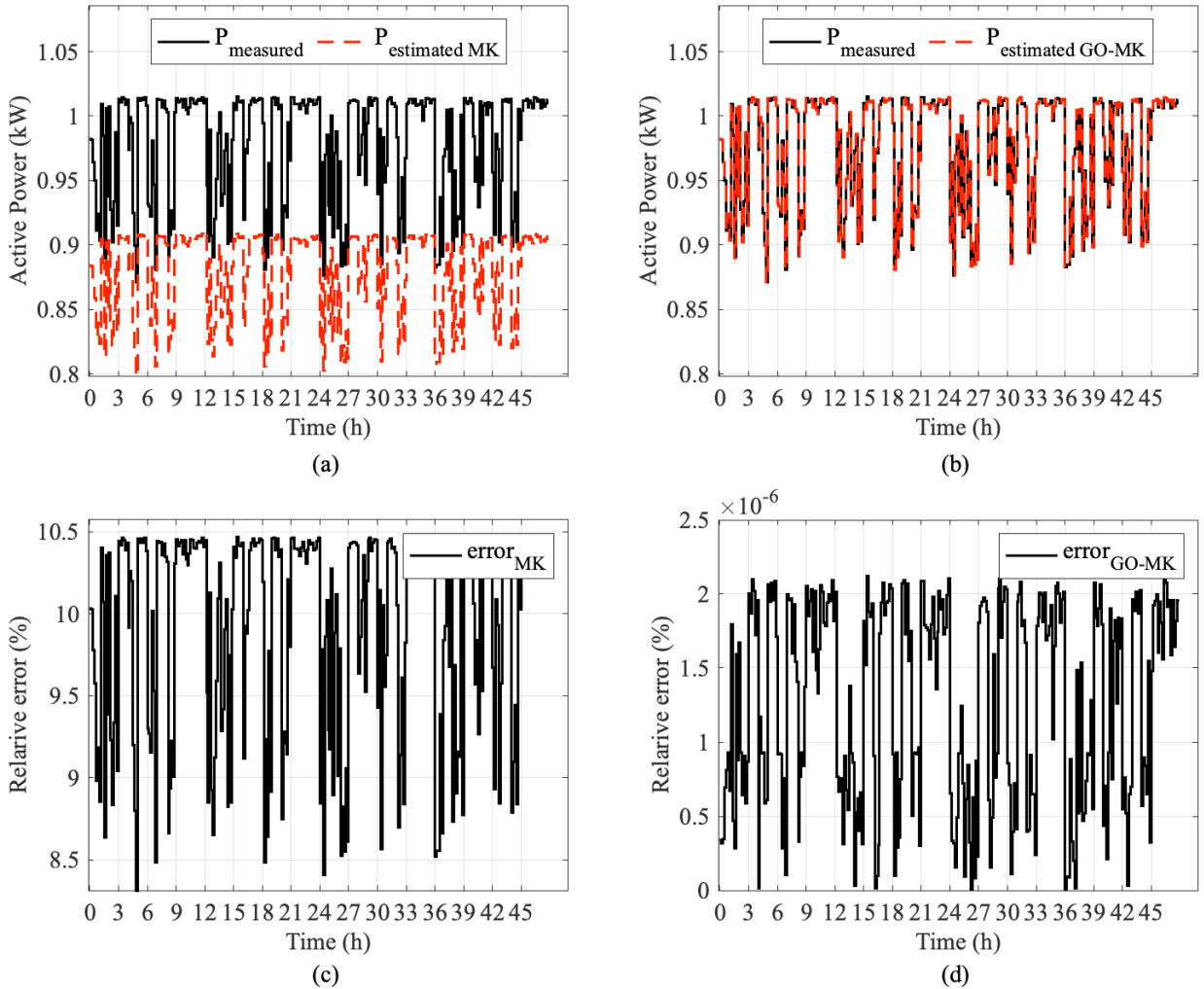
Figure 3.9 (a) Estimated active power using the parameters obtained through MK, (b) estimated active power using the parameters obtained through GO-MK, (c) relative estimation error using the parameters obtained through MK, and (d) relative estimation error using the parameters obtained through GO-MK for case 1

Table 3.3 shows the type of programming model and size (number of decision variables) of the GO strategy considering a random starting point and using the MK result as the starting point. Similarly, Figure 3.10 and Figure 3.11 show the convergence characteristics of the GO considering a random starting point and the GO using the MK result as starting point (GO-MK), respectively.

On the side of the GO approach with the randomized starting point, we performed 100 experiments with random points following a uniform distribution. Figure 3.10 shows the values of the relative probability and the cumulative relative probability for the number of local solver calls and function evaluations that the GO approach with random starting point performs to reach the best value of the objective function.

On the one hand, as can be seen in Figure 3.10, the GO approach with random starting point has a probability of approximately 25% of conducting less than 12 calls to the local solver and around 30% of conducting less than 5000 function evaluations to reach the best value of the objective function. On the other hand, it can be seen from Figure 3.11 that the GO-MK approach performs 12 calls to the local solver and about 5000 function evaluations to reach the best value of the objective function. These results can be explained by the fact that although the MK result is suboptimal, as previously shown, it is close to the value of the global optimum. Then, the GO strategy, which is a nonlinear programming (NLP) type, takes less function evaluations and calls to the local solver to find the best solution when using the MK result as a starting point. Moreover, although the size of the programming model type increases from 4 variables in GO to 11 variables in GO-MK (see Table 3.3), the McCormik's relaxations optimization model is a linear programming (LP) type which does not considerably increase the computational burden because it can be solved in polynomial time [179].

Table 3.3 Type of programming model and size of the GO strategy considering a random starting point and using the MK result as the starting point for case 1

Strategy	Type of programming model	Size (number of decision variables)
GO	NLP	4
GO-MK	LP+NLP	11
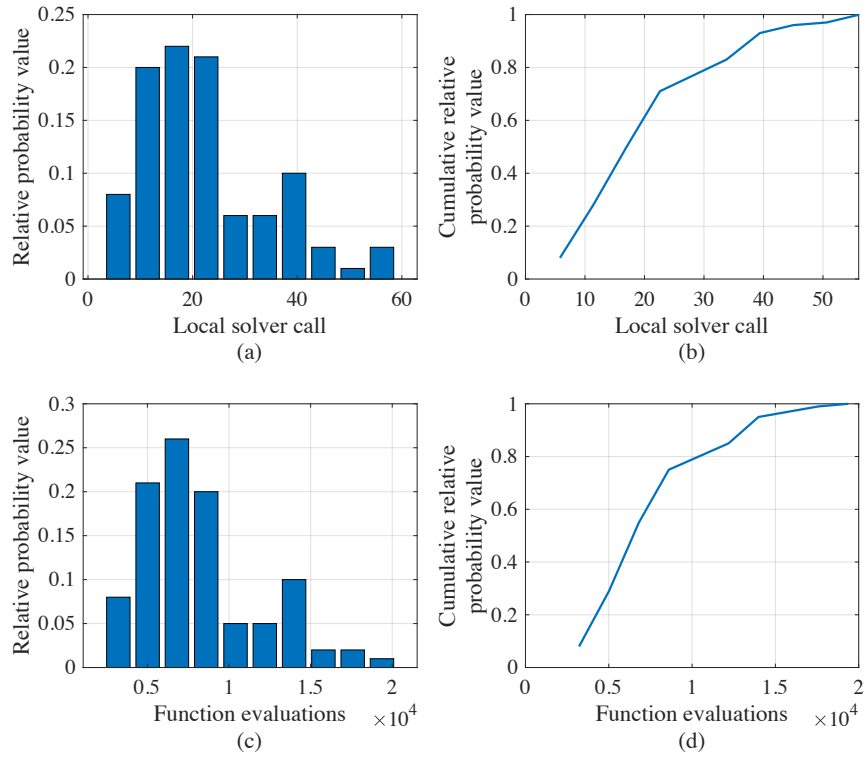
Figure 3.10 Convergence characteristics of GO considering a random starting point (case 1): (a) relative probability value and (b) cumulative relative probability value for the number of local solver calls, and (c) relative probability value and (d) cumulative relative probability value for the number of function evaluations

Figure 3.11 Convergence characteristics of GO-MK (case 1): (a) function value and (b) function evaluations

Case 2: In this case, we have assumed that two loads are switched on: the electric fan and the set of electric lamps. Thus, the aim is to use the measurements collected at bus 3 to identify all the parameters of the flexible component and the contribution $(\delta_1(k))$ of the electric fan to total load consumption in (38). Figure 3.12(a) and Figure 3.12 (b) depict the input data of active power and voltage that were gathered at bus 3 and we used for the parameter identification procedure. Voltage profile variations are within normal operating limits similar to the previous case. Further, the active power consumption in Figure 3.12 (a) is higher than the previous case because two devices are active, besides, it varies due to the voltage effect on the ZIP models of the individual loads.

The original ZIP values and the results of the parameter identification procedure are given in Table 3.4. As in the previous case, the estimated parameters indicate that the results obtained through MK have a higher error compared to those obtained with the GO-MK strategy (see Table 3.4). Nevertheless, because the extended ZIP model in (38) considers one more parameter (i.e., $\delta_1(k)$), the values estimated through the GO-MK strategy present a higher error than the previous case. Despite this, the parameters estimated using the GO-MK approach are closer to the original ZIP parameter values than using the MK.

Figure 3.13 shows the results of the active power estimated using a new voltage profile and the parameters already estimated through the MK (Figure 3.13(a)) and GO using the McCormick result as starting point, i.e., GO-MK (Figure 3.13(b)). Comparing Figure 3.13(c) and Figure 3.13(d) shows that the active power estimated using the parameters obtained with the MK has an error by around 10.9%, while using the parameters obtained through GO-MK the error of the new active power profile is below $5 \times 10^{-3}\%$.

$$P(k) = P_{flex}(k)\left(\tilde{\alpha}_1(k)\tilde{V}^2(k) + \tilde{\alpha}_2(k)\tilde{V}(k) + \tilde{\alpha}_3(k)\right) + \delta_1(k)ZIP_{fan}(\tilde{V}(k)) \tag{38}$$
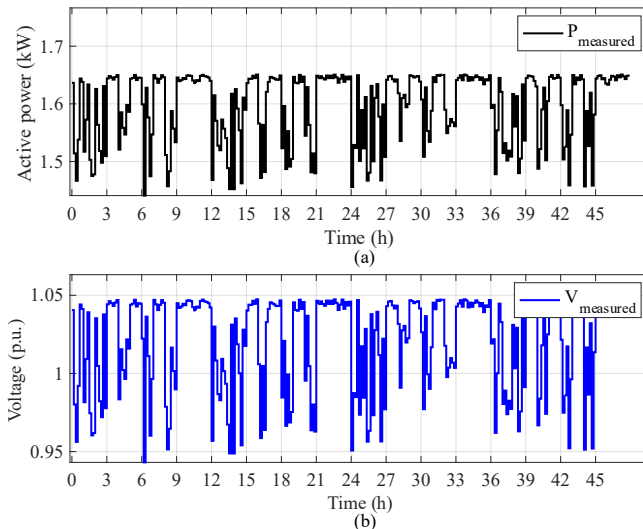
Figure 3.12 (a) Active power measurements and (b) voltage measurements for case 2

53

Table 3.4 Original values and results of the parameter identification by using the MK and the GO-MK approach for case 2

ZIP Parameter	Original values	MK results	Relative error (%)	GO-MK results	Relative error (%)
P_0	0.944	0.885	6.25	0.944	0.00
$\tilde{\alpha}_1$	0.520	0.424	18.46	0.524	0.77
$\tilde{\alpha}_2$	0.450	0.431	4.22	0.442	1.78
$\tilde{\alpha}_3$	0.030	0.145	383.33	0.034	13.33
δ_1	1.000	0.831	16.90	1.000	0.00
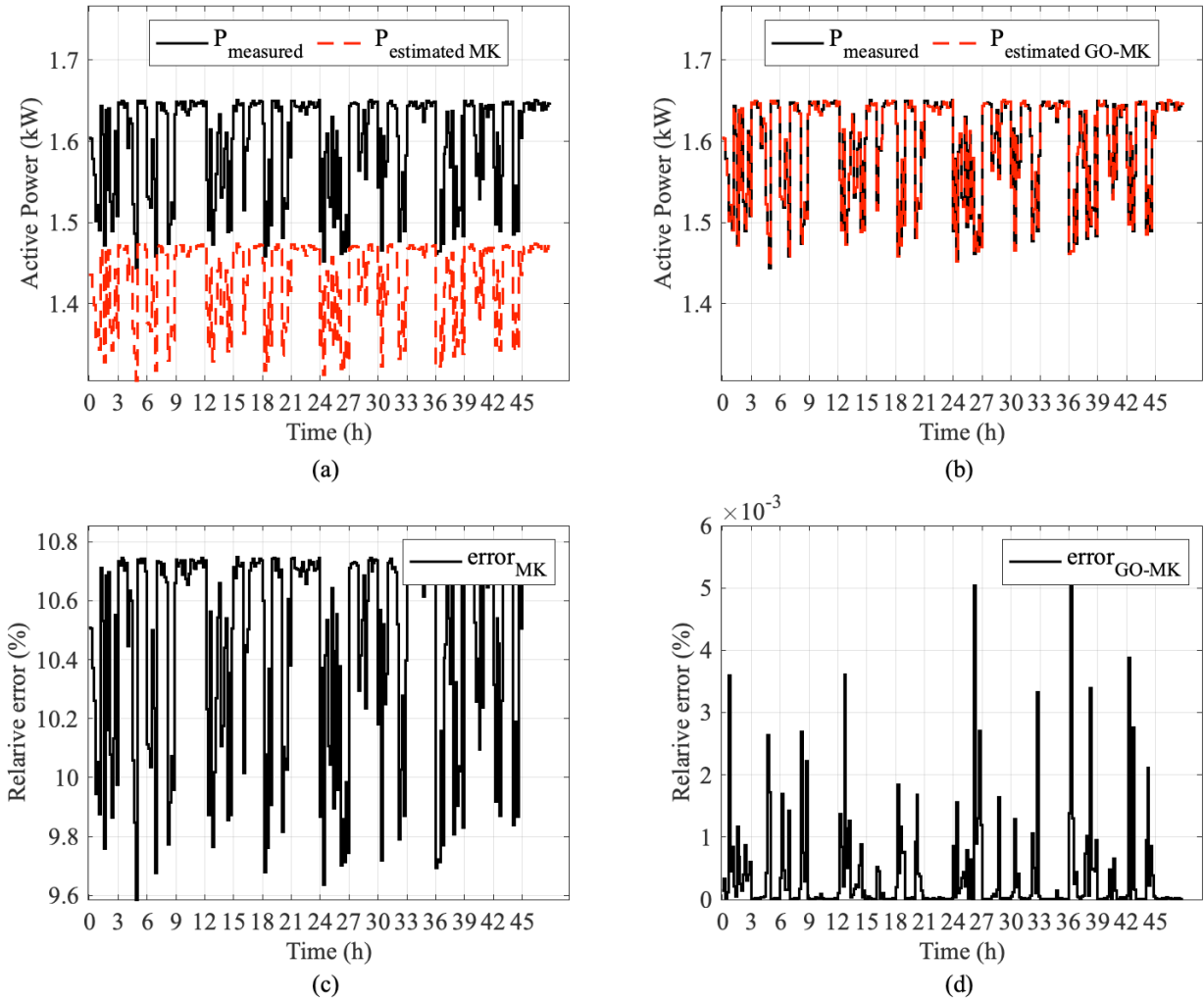
Figure 3.13 Estimated active power using the parameters obtained through MK, (b) estimated active power using the parameters obtained through GO-MK, (c) relative estimation error using the parameters obtained through MK, and (d) relative estimation error using the parameters obtained through GO-MK for case 2

Table 3.5 shows the type of programming model and size (number of decision variables) of the GO strategy considering a random starting point and using the MK result as the starting point. Similarly, Figure 3.14 and Figure 3.15 show the convergence characteristics of the GO considering a random starting point and the GO using the MK result as starting point (GO-MK), respectively.

Figure 3.14 shows the values of the relative probability and the cumulative relative probability for the number of calls to the local solver and the function evaluations that the GO approach with random starting point performs to reach the best value of the objective function. On the one hand, it can be seen from Figure 3.15 that the GO-MK approach performs 2 calls to the local solver and around 1800 function evaluations to reach the best value of the objective function. On the other hand, as can be seen in Figure 3.14, the GO approach with random starting point has a 0% probability of both performing less than 2 calls to the local solver and conducting less than 1800 function evaluations to reach the best value of the objective function. Finally, as can be seen in Table 3.5, the size of the programming model type increases from 5 variables in GO to 13 variables in GO-MK. However, as mentioned above, the McCormik's relaxations optimization model is LP type which does not considerably increase the computational burden because it can be solved in polynomial time.

Table 3.5 Type of programming model and size of the GO strategy considering a random starting point and using the MK result as the starting point for case 2

Strategy	Type of programming model	Size (number of decision variables)
GO	NLP	5
GO-MK	LP+NLP	13
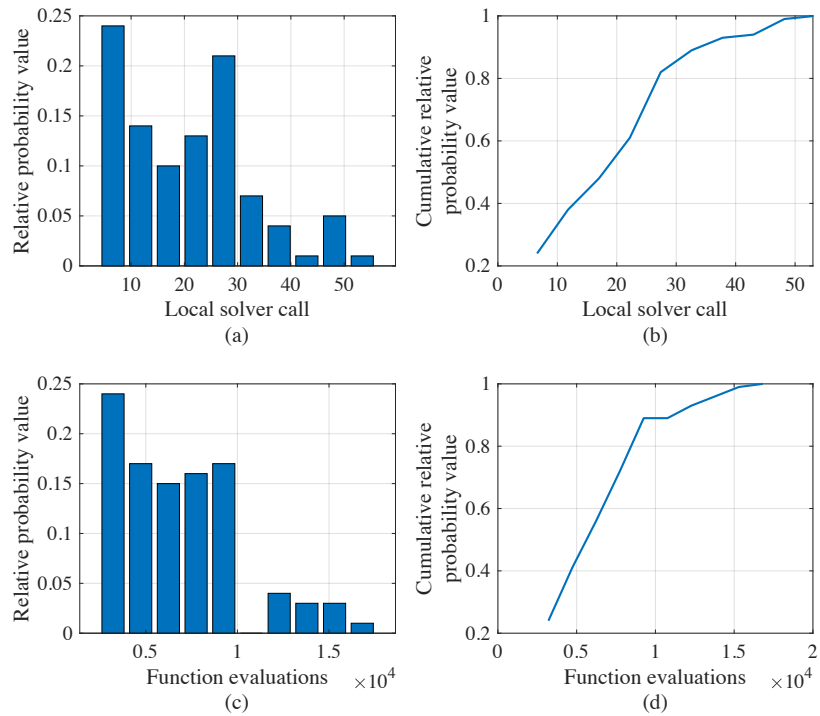
Figure 3.14 Convergence characteristics of GO considering a random starting point (case 2): (a) relative probability value and (b) cumulative relative probability value for the number of local solver calls, and (c) relative probability value and (d) cumulative relative probability value for the number of function evaluations
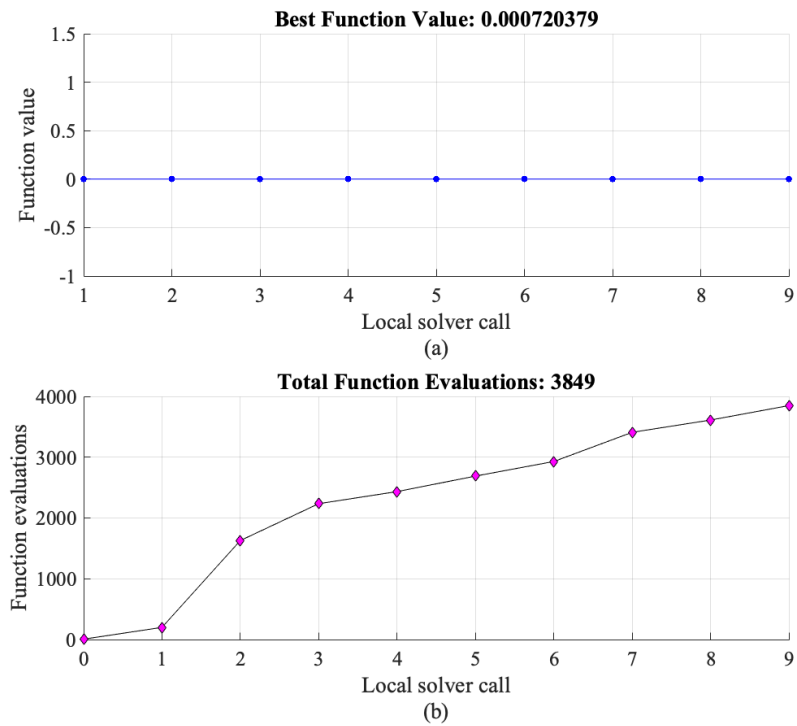
Figure 3.15 Convergence characteristics of GO-MK (case 2): (a) function value and (b) function evaluations

56

Case 3: The main difference between this case and the previous ones is that this one considers three devices turned on. Furthermore, in this case the parameters of the flexible part and the contributions of the electric fan ($\delta_1(k)$) and the heater ($\delta_2(k)$) must be estimated. Figure 3.16(a) and Figure 3.16(b) show the input data of active power and voltage that were gathered at bus 3 and we used for the parameter identification procedure. As in the two previous cases, the voltage profile varies between normal operating limits, and it influences active power consumption of the individual loads.

The original ZIP values and the results of the parameter identification procedure are given in Table 3.6. As in the previous case, the estimated parameters obtained through MK have a higher error compared to those obtained with the GO-MK strategy (see Table 3.6). In the same way as in the case 2, but the extended ZIP model in (39) considers two additional parameters in this case, the values estimated through the GO-MK strategy are closer to the original ZIP parameter values than using the MK.

Figure 3.17 shows the results of the active power estimated using a new voltage profile and the parameters already estimated through the MK (Figure 3.17(a)) and GO using the McCormick result as starting point, i.e., MK (Figure 3.17(b)). Comparing Figure 3.17(c) and Figure 3.17(d), it can be seen that the active power estimated using the parameters obtained with the MK has an error by around 6.6%, while using the parameters obtained through GO-MK the error of the new active power profile is below 0.02%.

$$P(k) = P_{flex}(k)\left(\tilde{\alpha}_1(k)\tilde{V}^2(k) + \tilde{\alpha}_2(k)\tilde{V}(k) + \tilde{\alpha}_3(k)\right) + \delta_1(k)ZIP_{fan}\left(\tilde{V}(k)\right)$$
$$+ \delta_2(k)ZIP_{heater}\left(\tilde{V}(k)\right) \tag{39}$$

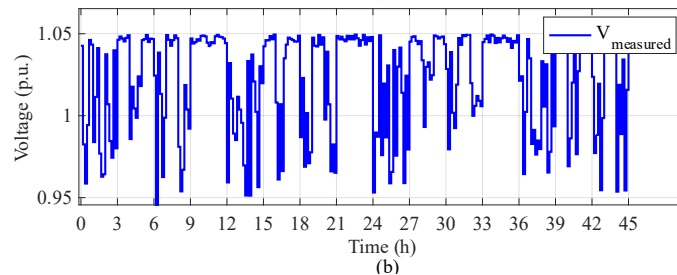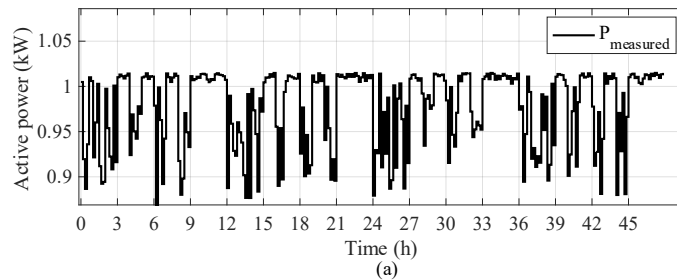$$\sum_{\omega=1}^{2} \delta_\omega(k) \leq 1 \tag{40}$$
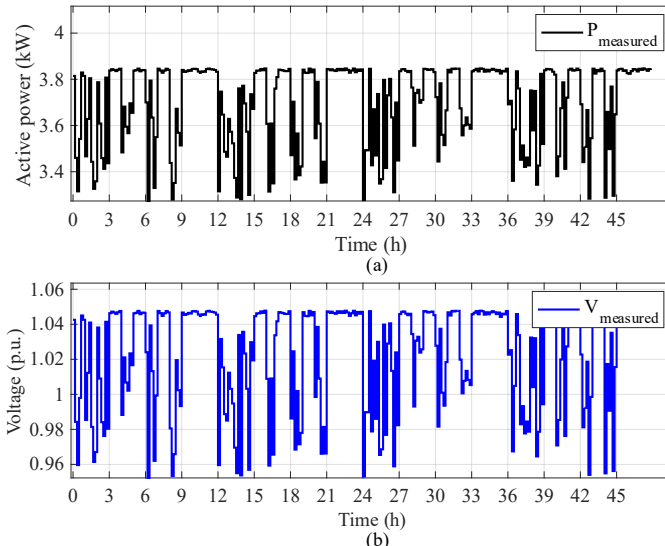
Figure 3.16 (a) Active power measurements and (b) voltage measurements for case 3

Table 3.6 Original values and results of the parameter identification by using the MK and the GO-MK approach for case 3

| ZIP Parameter	Original values	MK results	Relative error (%)	GO-MK results	Relative error (%)
P_0	0.944	0.912	3.39	0.944	0.00
$\tilde{\alpha}_1$	0.520	0.482	7.31	0.550	5.77
$\tilde{\alpha}_2$	0.450	0.383	14.89	0.388	13.78
$\tilde{\alpha}_3$	0.030	0.135	350.00	0.062	106.67
δ_1	1.000	0.828	17.20	1.000	0.00
δ_2	1.000	0.953	4.70	1.000	0.00
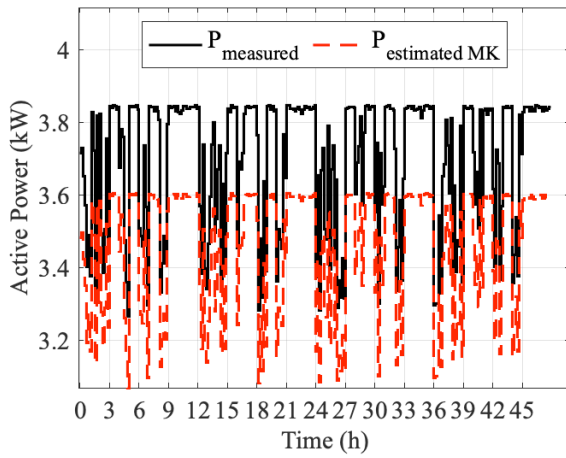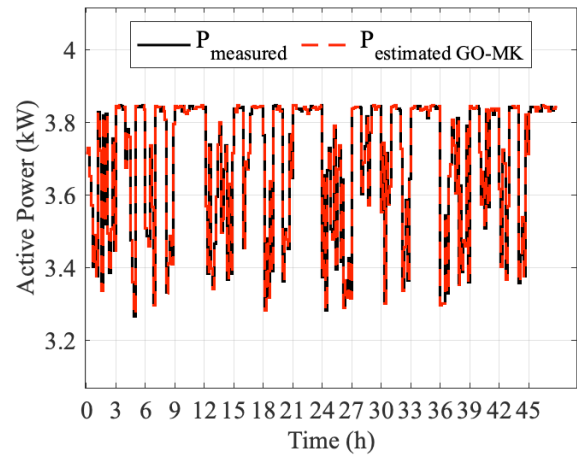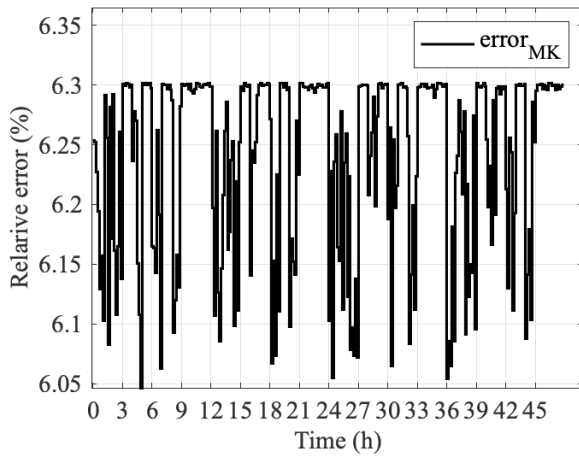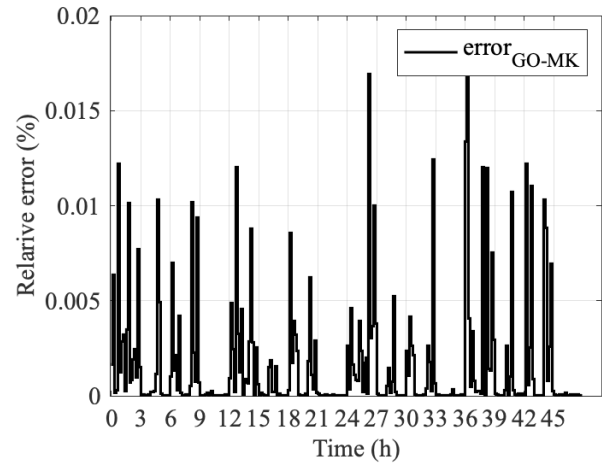
Figure 3.17 Estimated active power using the parameters obtained through MK, (b) estimated active power using the parameters obtained through GO-MK, (c) relative estimation error using the parameters obtained through MK, and (d) relative estimation error using the parameters obtained through GO-MK for case 3

Table 3.7 shows the type of programming model and size (number of decision variables) of the GO strategy considering a random starting point and using the MK result as the starting point. Similarly, Figure 3.18 and Figure 3.19 show the convergence characteristics of the GO considering a random starting point and the GO using the MK result as starting point (GO-MK), respectively.

Figure 3.18 shows the values of the relative probability and the cumulative relative probability for the number of calls to the local solver and the function evaluations that the GO approach with random starting point performs to reach the best value of the objective function. On the one hand, it can be seen from Figure 3.19 that the GO-MK approach performs 12 calls to the local solver and around 4200 function evaluations to reach the best value of the objective function. On the other hand, as can be seen in Figure 3.18, the GO approach with random starting point has a probability of approximately 10% of conducting less than 12 calls to the local solver and around 9% of conducting less than 4200 function evaluations to reach the best value of the objective function. Finally, as can be seen in Table 3.7, the size of the programming model type increases from 5 variables in GO to 13 variables in GO-MK. However, as mentioned above, the McCormik's relaxations optimization model is LP type which does not considerably increase the computational burden because it can be solved in polynomial time.

Table 3.7 Type of programming model and size of the GO strategy considering a random starting point and using the MK result as the starting point for case 3

| Strategy	Type of programming model	Size (number of decision variables)
GO	NLP	6
GO-MK	LP+NLP	15
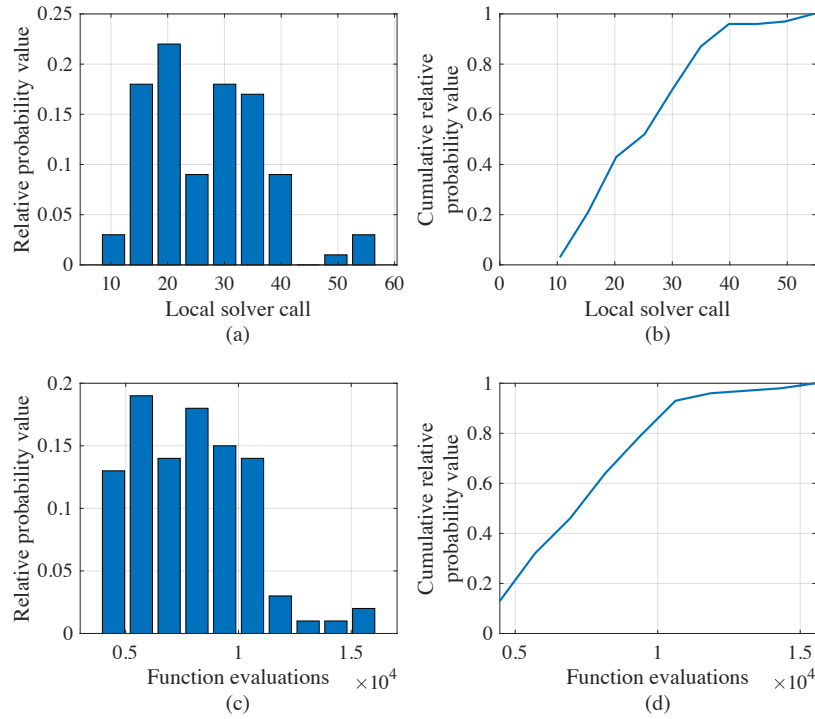
Figure 3.18 Convergence characteristics of GO considering a random starting point (case 3): (a) relative probability value and (b) cumulative relative probability value for the number of local solver calls, and (c) relative probability value and (d) cumulative relative probability value for the number of function evaluations
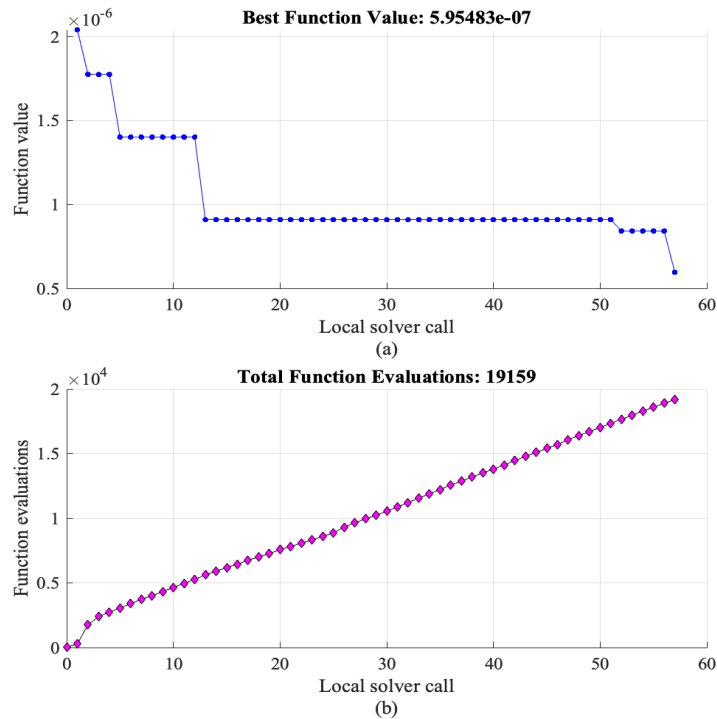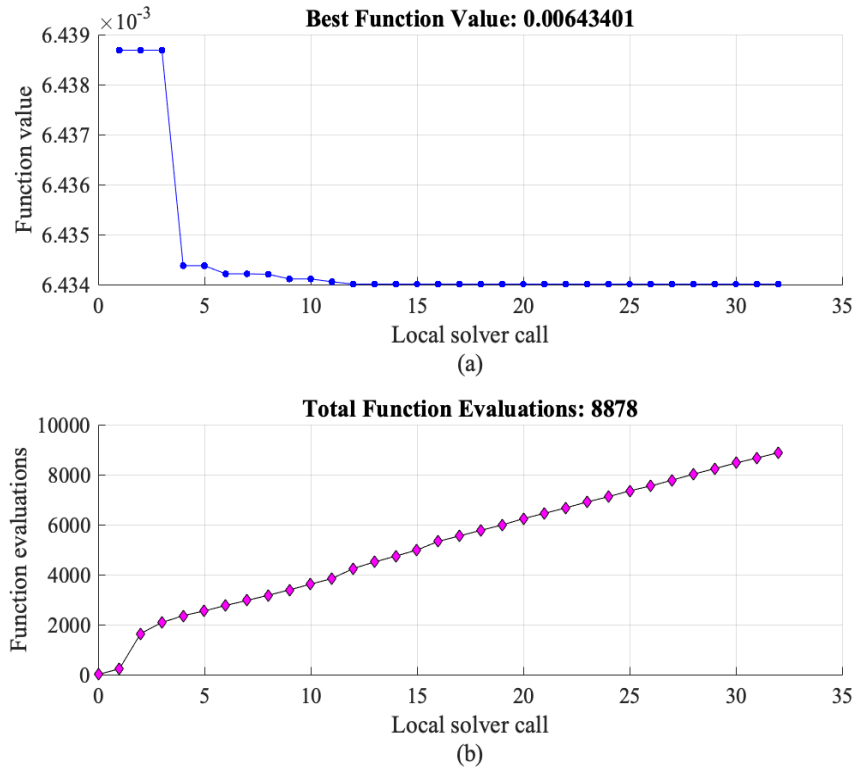

Figure 3.19 Convergence characteristics of GO-MK (case 3): (a) function value and (b) function evaluations

Discussion: Overall, the three selected cases showed that the values estimated using the GO-MK strategy have a high probability of reaching the global optimum compared to the MK. However, when more active devices (i.e., more parameters) are considered in the extended TV-ZIP model, the errors between the original ZIP values and the estimated parameters of the flexible part increase, especially the parameter with the smallest original value which in this case is $\tilde{\alpha}_3$. Nevertheless, although the estimation error of the parameter $\tilde{\alpha}_3$ has a considerable increase, its value is much lower compared to parameters $\tilde{\alpha}_1$ and $\tilde{\alpha}_2$; therefore, it is not significant. In this sense, the estimation error of new active power values is considerably small, below $5 \times 10^{-3}\%$ in case 2 and 0.02% in case 3. On the contrary, if only MK are considered, the estimated parameters values will always be far from the global optimum compared to the GO-MK strategy. Consequently, the error of estimation of new active power values considering the parameters obtained through MK will be considerably higher, e.g., about 10.9% in case 2 and 6.6% in case 3.

Regarding the convergence characteristics, in general, the GO requires less solver calls and less objective function evaluations, to reach the best objective function value when using the MK result as the starting point. Consequently, GO-MK presents less computational burden than GO with random starting point. This can be explained by the fact that, although the MK result is suboptimal, it is close to the global optimum value. Moreover, although the size of the programming model type increases in GO-MK, the McCormik's relaxations optimization model is a LP type which does not considerably increase the computational burden because it can be solved in polynomial time.

3.5   Integration of the EMZ-ZIP load model into an EMS

3.5.1 Approaches for integrating the EMZ-ZIP load model into EMS formulation

As previously described, the extended TV-ZIP model is based on the polynomial ZIP model (see Section 3.3.1). In this sense, although relatively simple, the ZIP model makes the mathematical formulation of the EMS non-convex due to the constant impedance part which has a quadratic dependence on voltage. Therefore, to integrate the ZIP model and consequently the EMZ-ZIP model into the EMS formulation, it is necessary to consider convex approximations of these models.

In the specialized literature, depending on the type of problem, different alternatives can be found to either convexify or linearize the ZIP model [133], [145], [180], [181]. Nevertheless, for this work we have considered two alternatives: one based on an approximation using Taylor series [133] and the other based on the binomial expansion method [181]. Then, from these two alternatives we used only one to integrate the EMZ-ZIP to the EMS based on the analysis that is presented later in this section.

The first alternative to linearize the quadratic voltage dependence is proposed by the authors in in [133]. Although this linearization is focused on the exponential model, it can be extended to the ZIP model as shown below. Furthermore, the main assumption of this approach is that the bus voltages in a network are close to 1.00 p.u., thus, the voltage can be represented as in (41).

$$V = 1 + \Delta V \tag{41}$$

In addition, because the bus voltage limits commonly lie between 0.95 p.u. and 1.05 p.u., the range for ΔV is ± 0.05, which yields a negligible range for ΔV^2 equal to ± 0.0025 [133]. Consequently, the exponential term of the voltage can be linearized using the first-order Taylor series approximation method (TAM) [133] resulting in (42).

$$V^\alpha = (1 + \Delta V)^\alpha \approx 1 + \alpha \Delta V \tag{42}$$

Accordingly, based on these assumptions and replacing (42) in (5), the linearized ZIP load model for the active power is expressed as follows:

$$P = P_0(\tilde{\alpha}_1(1 + 2\Delta V) + \tilde{\alpha}_2(1 + \Delta V) + \tilde{\alpha}_3) \tag{43}$$

The second alternative considered in this work is based on the binomial approximation method (BAM) as presented in [181]. This approximation approach makes use of the same assumption as the TAM, i.e., the bus voltages in a network stay close to 1.00 p.u. This results in the same expression in (42). However, the BAM makes use of an auxiliary variable by denoting the bus voltage squared as u. Then, replacing this new variable in (41) results in (44).

$$u = 1 + \Delta u \tag{44}$$

Moreover, establishing $\alpha = 2$ in (42), the following key relationship is obtained:

$$\Delta u \approx 2\Delta V \tag{45}$$

Next, by including u and (41) into (5), the new expression is as follows:

$$P \approx P_0(\tilde{\alpha}_1 u + \tilde{\alpha}_2(1 + \Delta V) + \tilde{\alpha}_3) \tag{46}$$

Then, by replacing (45) in (46) results in:

$$P \approx P_0\left(\tilde{\alpha}_1 u + \tilde{\alpha}_2\left(1 + \frac{\Delta u}{2}\right) + \tilde{\alpha}_3\right) \tag{47}$$

Finally, by substituting (44) in the expression (47) and rearranging the terms, we obtain the expression of the ZIP model approximated through the BAM.

$$P \approx P_0\left(\left(\tilde{\alpha}_1 + \frac{\tilde{\alpha}_2}{2}\right)u + \left(\tilde{\alpha}_3 + \frac{\tilde{\alpha}_2}{2}\right)\right) \tag{48}$$

Note that, the constant current term of the original ZIP model was equally divided between the constant impedance and constant current terms in the approximate ZIP model [181].

Both alternatives can be valid for integrating the ZIP model into the EMS, however, to determine the most appropriate one, we performed a comparative analysis. This consists of a relative error analysis of the load representation and a sensitivity analysis of the ZIP parameters. The former was developed in [181] by considering the ZIP parameters of one load, but, in this work we considered four loads (a heater, a copier, a light, and an electronic load) having different characteristics (i.e., constant impedance, constant current and constant power). Then, we varied the voltage between 0.85 p.u. and 1.15 p.u. with a step of 0.01 and analyzed the relative error between the original ZIP model representation and each of the two approximation methods for each load considered. The ZIP parameters were taken from [33]. Figure 3.20 shows the results of the comparative analysis of the relative error of load representation considering both the TAM and the BAM. Further, the sensitivity analysis of the ZIP parameters is presented in Annexed D.
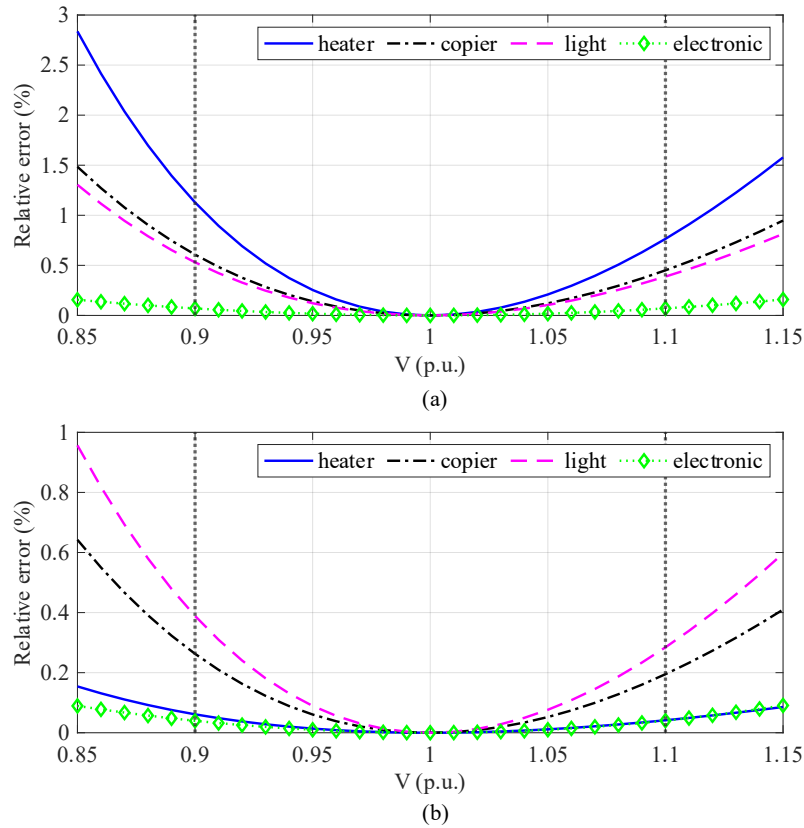
Figure 3.20 Results of the comparative analysis of the relative error of load representation considering: (a) TAM and (b) BAM

It can be seen from Figure 3.20 that the two approximations (i.e., the TAM and the BAM) have a representation of the electric loads similar to the original ZIP models because they have a relative error below 5% in all cases. However, when considering the approximation errors between the voltage levels at the normal operating limits (i.e., 0.9 p.u. and 1.1 p.u.) the TAM presents a

63

maximum relative error of approximately 1.45% in the case of the heater, the copier and light, and only in the case of the electronic load the maximum error is below 0.4%, while the BAM presents a maximum error below 0.4% in all cases. As can be seen from the analysis, the TAM presents a higher error in most of the cases compared to the BAM considering the normal operating range. Besides, the results of the sensitivity analysis presented in Annexed D show that the BAM has a better performance than the TAM. Therefore, based on the results described above, in this work we used the BAM to approximate the EMZ-ZIP model as presented in the next Section.

3.5.2 Multi-bus convex AC EMS integrating the EMZ-ZIP load model

As mentioned earlier, an EMS ensures efficient and economical operation of an MG by determining the optimal (near optimal) operating setpoints of the dispatchable DG units present in a MG. In this context, the most typically used EMS approach that considers the minimization MG operating costs and is formulated in (49)-(61) as a mixed-integer linear programming (MILP) [97], [182]–[186]. It should be noted that the system is assumed to be three-phase balanced.

$$\underset{P_{gi}(k),P_{BESSj}(k),P_{US}(k)}{minimize} \sum_{k=1}^{K} \left(\sum_{i=1}^{I} C_{gi}P_{gi}(k) + \sum_{j=1}^{J} C_{Bj}P_{BESSj}(k) + C_{US}P_{US}(k) \right) \Delta_k \qquad (49)$$

Subject to:

$$\sum_{i=1}^{I} P_{gi}(k) + \sum_{j=1}^{J} P_{BESSj}(k) + P_{US}(k) = \sum_{n=1}^{N} P_{Ln}(k) - \sum_{m=1}^{M} P_{DGm}(k) \qquad (50)$$

$$\vartheta_{gi}^{min} \leq \vartheta_{gi}(k) \leq \vartheta_{gi}^{max} \qquad (51)$$

$$P_{gi}^{min} \leq P_{gi}(k) \leq P_{gi}^{max} \qquad (52)$$

$$P_{BESSj}(k) = \eta_{BESSj}^{dis}P_{BESSj}^{dis}(k) - \frac{P_{BESSj}^{ch}(k)}{\eta_{BESSj}^{ch}} \qquad (53)$$

$$0 \leq P_{BESSj}^{ch}(k) \leq P_{chBESSj}^{max}y_{BESSj}^{ch}(k) \qquad (54)$$

$$0 \leq P_{BESSj}^{dis}(k) \leq P_{disBESSj}^{max}y_{BESSj}^{dis}(k) \qquad (55)$$

$$y_{BESSj}^{ch}(k) + y_{BESSj}^{dis}(k) \leq 1 \qquad (56)$$

$$y_{BESSj}^{ch}(k), y_{BESSj}^{dis}(k) \in \{0,1\} \qquad (57)$$

$$E_{BESSj}(k) = E_{BESSj}(k-1) + \Delta_k \frac{P_{BESSj}^{ch}(k)}{\eta_{BESSj}^{ch}} - \Delta_k \eta_{BESSj}^{dis}P_{BESSj}^{dis}(k) \qquad (58)$$

$$E_{BESSj}^{init}(k) = E_{BESSj}^{final}(k) \qquad (59)$$

$$E_{BESSj}^{min} \leq E_{BESSj}(k) \leq E_{BESSj}^{max} \qquad (60)$$

$$P_{US}(k) \geq 0 \qquad (61)$$

where Δ_k represents the duration of time sub-period k; C_{gi} and $P_{gi}(k)$ denote the generation cost and the active power provided by the *i-th* diesel generation unit, respectively; C_{ESSj}, $P_{ESSj}(k)$, $P_{ESSj}^{ch}(k)$, $P_{ESSj}^{dis}(k)$, η_{ESSj}^{ch}, η_{ESSj}^{dis}, $y_{ESSj}^{ch}(k)$ and $y_{ESSj}^{dis}(k)$ represent the operating cost, the injected/consumed active power, the charging power, the discharging power, the charging efficiency, the discharging efficiency, the charging binary variable and the discharging binary variable of the *j-th* battery energy storage system (BESS), respectively; $P_{US}(k)$ and C_{US} stand for the unserved power and the cost of the unserved power in the system, respectively; $P_{Ln}(k)$ is the load consumption in the *n-th* load center of the system; $P_{DGm}(k)$ denotes the active power supplied by the *m-th* DG unit (e.g., PV plant, wind turbine, etc.). Likewise, ϑ_{gi}^{min} and ϑ_{gi}^{max} denote the minimum and maximum volume of the diesel generator fuel tank; P_{gi}^{min} and P_{gi}^{max} are the minimum and maximum limits of active power generated by the *i-th* diesel generator; P_{chESSj}^{max} and $P_{disESSj}^{max}$ denote the maximum charging and discharging allowed values of active power of the *j-th* BESS; $E_{BESSj}(k)$, E_{BESSj}^{min} and E_{BESSj}^{max} represent the energy stored at time step k, and the minimum and maximum allowed values of energy stored by the *j-th* BESS, respectively. E_{BESSj}^{init} and E_{BESSj}^{final} represent the BESS's initial and final energy. Finally, *I, J, M, N* and *K* denote the sets of diesel generators, BESSs, DG units and load centers of the MG, and the scheduling horizon, respectively.

It is evident that the EMS formulation in (49)-(61) only considers the balance between generation and consumption. However, since network model is not considered, it is not possible to guarantee that the power scheduled and produced by the generation units can be transferred to the electricity consumption centers [96]. Indeed, the network constraints are required to achieve a MG operation within the operating voltage limits and system losses restriction [187], [188]. Moreover, because bus voltages are not considered in the EMS formulation above, the voltage effect on the SPSPs' loads cannot be fully captured.

Consequently, to address the challenges mentioned above, the network constraints are added to the EMS formulation. Let the MG branch model consists of the single-branch equivalent circuit illustrated in Figure 3.21. If the branch power flow from bus r to bus s, then, $S_{r,s}$, $P_{r,s}$ and $Q_{r,s}$ represent the apparent, the active, and the reactive powers flowing through the branch.

$$\hat{V}_r = |\hat{V}_r| \angle \theta_r \qquad\qquad \hat{V}_s = |\hat{V}_s| \angle \theta_s$$

$$S_{r,s} = P_{r,s} + jQ_{r,s}$$

$$Y_{r,s} = G_{r,s} + jB_{r,s}$$
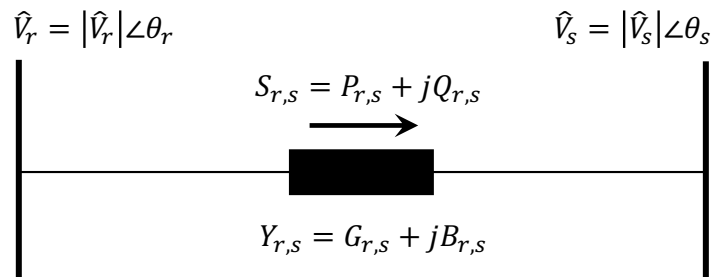
Figure 3.21 MG branch model

Then, the admittance matrix that comprises the complex rectangular representation of all MG branch admittances (conductance and susceptance) is denoted as follows:

$$Y_{bus} = G + jB \tag{62}$$

Besides, expressing the bus voltages through their polar form as in (63).

$$\widehat{V}_r = |\widehat{V}_r| \angle \theta_r \tag{63}$$

Moreover, for the simplicity in notation let $V_r = |\widehat{V}_r|$. Then, the resulting active and reactive powers injected at an arbitrary bus r of the system [189] are expressed as in (64)-(65).

$$\begin{aligned} P_r(k) = V_r{}^2(k)G_{r,r} \\ + \sum_{\substack{s=1 \\ s \neq r}}^{\Upsilon} \left[V_r(k)V_s(k)G_{r,s}\cos(\theta_r(k) - \theta_s(k)) + V_r(k)V_s(k)B_{r,s}\sin(\theta_r(k) - \theta_s(k)) \right] \end{aligned} \tag{64}$$

$$\begin{aligned} Q_r(k) = -V_r{}^2(k)B_{r,r} \\ - \sum_{\substack{s=1 \\ s \neq r}}^{\Upsilon} \left[V_r(k)V_s(k)G_{r,s}\cos(\theta_r(k) - \theta_s(k)) - V_r(k)V_s(k)B_{r,s}\sin(\theta_r(k) - \theta_s(k)) \right] \end{aligned} \tag{65}$$

where Υ denotes the number of buses in the MG, $P_r(k)$ and $Q_r(k)$ represent the difference between the generated and demanded power at the *r-th* bus, $V_r(k)$ is the voltage at the *r-th* bus, $\theta_r(k)$ represents the voltage angle at the *r-th* bus, and $r, s \in \{\Upsilon\}$. Note that, expressions in (64)-(65) are non-convex because they involve trigonometric functions (i.e., sine and cosine). Besides, the active and reactive power balance could be achieved through several values of $P_r(k)$, $Q_r(k)$, $V_r(k)$ and $\theta_r(k)$. Therefore, to efficiently integrate the network equations into the mathematical formulation of the EMS requires expressing them in their convex equivalents. For this purpose, we considered the convex approximation proposed in [190]. It should be noted that, the McCormick envelopes can be also used to convert the non-convex feature of the optimal power flow model into a convex quadratic constrained programming problem as shown in [191].

Power losses are caused because active and reactive currents pass through the lines (i.e., $\zeta_{r,s}$). For notation simplicity, define $\ell_{r,s} = |\zeta_{r,s}|^2$. Then, the current expression is expressed in (66) and the branch active ($P_{r,s}^{loss}(k)$) and reactive ($Q_{r,s}^{loss}(k)$) power losses are expressed in (67) and (68) [192], respectively.

$$\ell_{r,s}(k) = \frac{P_{r,s}^2(k) + Q_{r,s}^2(k)}{V_r{}^2(k)} \tag{66}$$

$$P_{r,s}^{loss}(k) = \ell_{r,s}(k) \cdot \Re(Y_{r,s}) \tag{67}$$

$$Q_{r,s}^{loss}(k) = \ell_{r,s}(k) \cdot \Im(Y_{r,s}) \tag{68}$$

Next, by following [190], the expressions below are defined:

66

$$R_{r,s}(k) = V_r(k)V_s(k)\cos(\theta_r(k) - \theta_s(k)) \tag{69}$$

$$T_{r,s}(k) = V_r(k)V_s(k)\sin(\theta_r(k) - \theta_s(k)) \tag{70}$$

$$u_r(k) = \frac{V_r^2(k)}{\sqrt{2}} \tag{71}$$

By substituting $R_{r,s}(k)$, $T_{r,s}(k)$ and $u_r(k)$ in (64)-(65), we obtain:

$$P_r(k) = \sqrt{2}G_{r,r}u_r(k) + \sum_{\substack{s=1 \\ s \neq r}}^{Y}\left[G_{r,s}R_{r,s}(k) + B_{r,s}T_{r,s}(k)\right] + \sum_{\substack{s=1 \\ s \neq r}}^{Y}P_{r,s}^{loss}(k) \tag{72}$$

$$Q_r(k) = -\sqrt{2}B_{r,r}u_r(k) - \sum_{\substack{s=1 \\ s \neq r}}^{Y}\left[B_{r,s}R_{r,s}(k) - G_{r,s}T_{r,s}(k)\right] + \sum_{\substack{s=1 \\ s \neq r}}^{Y}Q_{r,s}^{loss}(k) \tag{73}$$

Next, by considering the properties of $\sin(x)$ and $\cos(x)$ the following relations can be derived:

$$R_{r,s}(k) = R_{s,r}(k) \tag{74}$$

$$T_{r,s}(k) = -T_{s,r}(k) \tag{75}$$

$$2u_r(k)u_s(k) = R_{r,s}^2(k) + T_{r,s}^2(k) \tag{76}$$

Nevertheless, the expressions in (66) and (76) need to be transformed into their conic programming formats; thus, by following [193] we get:

$$\ell_{r,s}(k)u_r(k) \geq P_{r,s}^2(k) + Q_{r,s}^2(k) \tag{77}$$

$$2u_r(k)u_s(k) \geq R_{r,s}^2(k) + T_{r,s}^2(k) \tag{78}$$

Next, by adding $P_{r,s}^{loss}(k)$ in (50) yields (79). Besides, since network constraints are considered and these involve reactive power, it is also required to consider the reactive power balance equation (80) in the EMS formulation.

$$\sum_{i=1}^{I}P_{gi}(k) + \sum_{j=1}^{J}P_{BESSj}(k) + P_{US}(k) = \sum_{n=1}^{N}P_{Ln}(k) + \sum_{\substack{s=1 \\ s \neq r}}^{Y}P_{r,s}^{loss}(k) - \sum_{m=1}^{M}P_{DGm}(k) \tag{79}$$

$$\sum_{i=1}^{I}Q_{gi}(k) + \sum_{j=1}^{J}Q_{BESSj}(k) = \sum_{n=1}^{N}Q_{Ln}(k) + \sum_{\substack{s=1 \\ s \neq r}}^{Y}Q_{r,s}^{loss}(k) \tag{80}$$

Additionally, the constraints of minimum and maximum limits of bus voltages, and maximum power flow limits through branches are expressed in (81) and (82), respectively.

$$\frac{\left(V_r^{min}\right)^2}{\sqrt{2}} \leq u_r(k) \leq \frac{\left(V_r^{max}\right)^2}{\sqrt{2}} \tag{81}$$

$$\left|Y_{r,s}(u_r(k) - u_s(k))\right| \leq S_{r,s}^{max}(k) \tag{82}$$

Consequently, the resulting convex AC EMS optimization problem is formulated as follows:

minimize (49)

Subject to: (79), (80), (72), (73), (51), (52), (53), (54), (55), (56), (57), (58), (60), (61), (77), (78), (81), (82)

Next, to integrate the EMZ-ZIP load model expressed in (12)-(15) into the EMS formulation, it is required to derive its convex approximation by applying the BAM described in Section 3.5.1. Subsequently, the resulting convex approximation of the EMZ-ZIP model is formulated as follows:

$$P_{SPSP}(u_r(k)) \approx ZIP_{flex}(u_r(k)) + \sum_{\omega=1}^{\Omega_\psi} \delta_\omega(k) ZIP_\omega(u_r(k)) \tag{83}$$

$$\sum_{\omega=1}^{\Omega_\psi} \delta_\omega(k) \leq 1 \tag{84}$$

$$ZIP_{flex}(u_r(k)) = P_{flex}(k)\left(\left(\tilde{\alpha}_1(k) + \frac{\tilde{\alpha}_2(k)}{2}\right) u_r(k) + \left(\tilde{\alpha}_3(k) + \frac{\tilde{\alpha}_2(k)}{2}\right)\right) \tag{85}$$

$$ZIP_\omega(u_r(k)) = P_{0,\omega}\left(\left(\alpha_{1,\omega} + \frac{\alpha_{2,\omega}}{2}\right) u_r(k) + \left(\alpha_{3,\omega} + \frac{\alpha_{2,\omega}}{2}\right)\right) \tag{86}$$

It should be noted that the same procedure is applicable to derive the reactive power expression, i.e., $Q_{SPSP}(u_r(k))$ of the EMZ-ZIP load model. Accordingly, by replacing $P_{SPSP}(u_r(k))$ and $Q_{SPSP}(u_r(k))$ in the energy balance expressions (50), (79), and in the load flow expressions (72), (73) considering that they are buses where the SPSPs may be connected besides other loads, the following resulting expressions are obtained.

$$\sum_{i=1}^{I} P_{gi}(k) + \sum_{j=1}^{J} P_{BESSj}(k) + P_{US}(k)$$
$$= \sum_{n=1}^{N} [P_{Ln}(k) + P_{SPSP}(u_r(k))] + \sum_{\substack{s=1 \\ s \neq r}}^{\Upsilon} P_{r,s}^{loss}(k) - \sum_{m=1}^{M} P_{DGm}(k) \tag{87}$$

$$\sum_{i=1}^{I} Q_{gi}(k) + \sum_{j=1}^{J} Q_{BESSj}(k) = \sum_{n=1}^{N} [Q_{Ln}(k) + Q_{SPSP}(u_r(k))] + \sum_{\substack{s=1 \\ s \neq r}}^{\Upsilon} Q_{r,s}^{loss}(k) \tag{88}$$

$$P_r(k) - P_{SPSP}(u_r(k)) = \sqrt{2}G_{r,r}u_r(k) + \sum_{\substack{s=1 \\ s \neq r}}^{\Upsilon} [G_{r,s}R_{r,s}(k) + B_{r,s}T_{r,s}(k)] + \sum_{\substack{s=1 \\ s \neq r}}^{\Upsilon} P_{r,s}^{loss}(k) \tag{89}$$

$$Q_r(k) - Q_{SPSP}(u_r(k)) = -\sqrt{2}B_{r,r}u_r(k) - \sum_{\substack{s=1 \\ s \neq r}}^{\Upsilon} [B_{r,s}R_{r,s}(k) - G_{r,s}T_{r,s}(k)] + \sum_{\substack{s=1 \\ s \neq r}}^{\Upsilon} Q_{r,s}^{loss}(k) \qquad (90)$$

To avoid the integer variables in (54)-(57), the nonlinear convex BESS model [194] or the convex relaxation proposed in [187] can be considered. The resulting EMS optimization problem is expressed as follows:

minimize (49)

Subject to: (87), (88), (89), (90), (51), (52), (53), (54), (55), (56), (57), (58), (59), (60), (61), (77), (78), (81)

Finally, it is important to note that the resulting EMS optimization problem that integrates the EMZ-ZIP load model is convex due to both the BAM applied to the EMZ-ZIP model and the variable transformation used to convexify the power flow constraints. As a result of the latter procedure, the EMS became a second-order cone programming (SOCP) optimization problem that can be efficiently solved in a finite number of steps [195] and it has a lower computational complexity [196] which scales with the square-root of the problem size [197], i.e., the number of decision variables [198]. Therefore, these properties allow scalability of the resulting EMS and a certain degree of flexibility for its application in actual MGs and large-scale problems [196].

3.6   Operation of MG-EMS

The timetable in Figure 3.22 shows the procedures performed at each EMS run time. At the beginning, i.e., at run time t_0 the EMS is in safe mode. Consequently, a set of predefined settings are stored in the EMS, which is ready to execute a black-start procedure to initiate the operation of the MG [199], [200]. For this purpose, the MG generation units use their local controllers to maintain synchronism in the MG based among others on the droop curves [201].

t_0	t_1	t_2	t_3	t_4	*Transition*		t_5	t_6
Executing black-start procedure	Acquisition of renewable generation and loads forecasts except those from SPPs	Definition of current operating zone	Selection of the EMZ-ZIP model for future time intervals	Executing optimization routines	If optimization procedure has converged: follow to t_5	If optimization procedure has not converged: keep the previous setpoints and follow to t_5	Sending operating setpoints	Restart procedures

New execution cycle

Figure 3.22 Timetable of EMS operation

It should be noted that, at t_0 stages A, B, and C in Figure 3.1 are already developed, which correspond to the EMZ-ZIP model and the identification of its parameters. Then, at run time t_1 the EMS acquires the renewable generation and load forecasts except the SPSPs. At run time t_2, based on the local time and zones determined in step 2 (see Figure 3.1), an EMS routine determines the

current operating zone candidate for each SPP based on the predefined zones (see Figure 3.4). For this purpose, the available measurement of an SPP consumption is compared with the two load estimations (i.e., Zone 1 vs Zone 2 EMZ-ZIPs) in the transition zone depicted in red color (see Figure 3.23). The duration of the transition zone corresponds to a predefined value based on the practical observations of an existing SPSP. The zone with the lowest accumulated error (ε) based on the available measurements is selected for the SPSP load forecast used by the EMS in the transition period. In t_3, for the remaining future time intervals the predefined zone definition is considered.
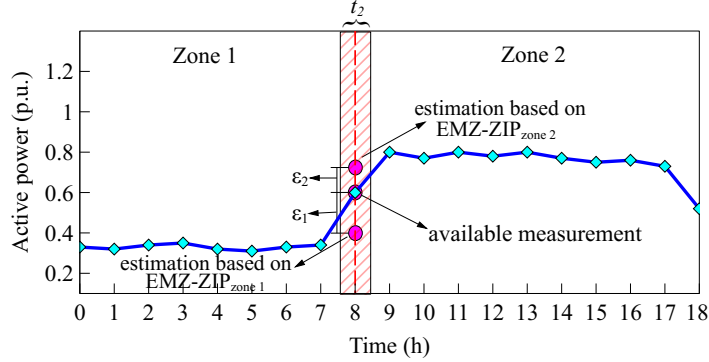
Figure 3.23 Zone transitions

More structural changes in the SPSP behavior can be managed by the Analysis 1 and 2 blocks presented in Figure 3.1. This is a key aspect of the proposal that allows for more robust and efficient management in the transitions between zones. Next, at run time t_4 the EMS optimization problem is solved. If the optimization problem converges it follows to t_5, otherwise the previous operating setpoints are kept. In this run time (i.e., t_5) the valid operating setpoints are sent to the local controllers of dispatchable units in the MG. Specifically, the voltage references and the power generation references are sent using the communication links. It should be noted that full EMS procedure ($t_0 - t_5$), there is a time range by around several minutes (e.g., 10 minutes, 15 minutes, etc.). It should be noted that in cases of load perturbations (i.e., connection/disconnection), the local controllers react first to maintain the balance between generation and demand. Finally, at run time t_6 the EMS re-start its procedures and go back to t_1.

3.7 Implementation aspects

To implement the proposed methodology described in this chapter, the following aspects should be considered:

For stage A, based on the information obtained through semi-structured surveys, a relational database is created which includes the ZIP models of the devices that the SPSPs may include. For stage B, the information obtained through the surveys and the actual measurements of the external weather variables are used as input data for the zone classifier which is based on ANN and was implemented using the *Neural Networks Toolbox* of MATLAB® [202]. Then the zones classifier

module identifies the zones and for each of them an extended TV-ZIP model is established with the SPSP devices can be active. Through this procedure the EMZ-ZIP model is developed.

For the EMZ-ZIP model parameter identification procedure (stage C), measurements obtained through an SPSP simulator, and the proposed GO strategy were used. The former was implemented in MATLAB®/Simulink® considering the constructive and operational characteristics of an actual SPSP (see Annexed E.6), whereas the latter was implemented using the *Global Optimization Toolbox* of MATLAB® [203].

For stage D, the EMS optimization routine integrating the EMZ-ZIP model was implemented in CVX, a package for specifying and solving convex programs [204], [205] considering the information generated in the previous stages and the technical characteristics of the MG. Whereas the MG-EMS operation is executed in stage E. For this purpose, the MG and Supervisory Control and Data Acquisition (SCADA) are modeled in MATLAB®/Simulink® using the Simscape™ Electrical™ Specialized Power Systems blocks [206] which simulates the actual operation of an MG. The time domain simulations are 1 millisecond while the EMS optimization routine is executed every 10 minutes, while the other routines, for example, the detection of changes in the scheduling of productive activities, are executed every time a new measurement arrives from the SCADA.

Finally, once the MG and SCADA models, databases and others were implemented, the actual operation of the MG was simulated on a computer with the following characteristics: HP ENVY 27 All-in-One, Intel® Core™ i7-4790T @2.70 GHz, 12.0 GB RAM.

3.8 Extensions

In this section, some feasible extensions to the proposed methodology are discussed.

Firstly, it should be noted that ramping and reserves constraints are not part of the EMS formulation in (49)-(61). Regarding ramping constraints, DGs in MGs generally have fast start-up, shut-down, and ramp characteristics in the order of a few minutes [26]. Diesel units in particular accept load rapidly, with start times to full load as fast as 10 seconds and ramp-up time from 25% percent to 100% of load in as little as 5 seconds [207].

Concerning system reserves, they are required to deal with forecast errors, e.g., from renewable generation. These reserves can be modeled as a percentage of the expected renewable generation and demand [208]. For example, a 35% of the forecasted hourly peak demand [209] can be added to (52). Alternatively, probabilistic approaches using interval predictions can be incorporated in the proposed EMS optimization problem for more accurate estimation of system's reserves [210].

Despite the above, both ramping and reserves constraints can be included in the EMS formulation presented in Section 3.5.2, for example, following the EMS model presented in [26]. In addition, uncertainties in the renewables forecast can significantly affect dispatch decisions in the MG. Nevertheless, the analysis of the effect of uncertainties in renewable energy and demand forecasting is beyond the scope of this study. With this aim, a model predictive control [26], [211], robust [212] or stochastic approaches [213] can be used.

Secondly, as mentioned above, the system considered in this work for the development of the EMS mathematical model is assumed to be balanced. Nevertheless, MGs usually have unbalanced characteristics. Thus, according to [41], under certain loading conditions, phase unbalances can lead to deviations of the optimal dispatch strategy or the inability of the system to meet reactive power requirements. In addition, in an unbalanced configuration, the same load will produce higher system losses as compared to a balanced configuration, and when voltage-dependent load models are considered, higher voltage in one of the phases will lead to higher power absorbed.

In this context, the methodology proposed in this work presents some limitations to consider phase unbalances. For example, the EMZ-ZIP model considers the loads to be equally distributed in each phase, which may lead to an under or over estimation of the SPSPs consumption when voltage asymmetries exist.

Notwithstanding the above, the methodology proposed in this work can be extended to represent the case of an unbalanced system. For this purpose, it would be necessary to consider the following extensions based on the methodology presented in Section 3.

- To develop an estimation model for the per phase assignment of loads in the MG.
- To incorporate a per phase description and database for the proposed EMZ-ZIP model.
- To extend the EMS mathematical model to include the details of an unbalanced three-phase system, for example, considering the EMS model presented in [41].

It should be noted that, the balanced MG system, where the loads are assumed to be evenly shared among the phases, represents a less critical scenario in terms of system losses, voltage variations, and reactive power requirements. Therefore, by considering an unbalanced representation, we would expect a better result in terms of a more accurate estimation of the SPSPs consumption, leading to better decision making by the EMS. In other words, the results of this work may be a conservative estimation of the capabilities of the proposed methodology.

3.9 Summary

This chapter describes the proposed methodology for modeling SPSPs and their integration into an EMS. The methodology includes the development of a database containing the ZIP parameters of the devices that may belong to an SPSP. Then, the procedure for the development of the EMZ-ZIP model is presented. First, the extended TV-ZIP model that considers a flexible component and the parameters stored in the database of the devices that can belong to an SPSP is developed. Secondly, the zoning procedure is described for which it is key to consider the external weather variables that can influence the electrical behavior of SPSPs. Once the EMZ-ZIP model has been built, a GO strategy is proposed in which the results of the McCormick's relaxations are used to obtain the starting points for estimating the EMZ-ZIP parameters. Next, the integration of the EMZ-ZIP to an EMS approach is proposed. For this purpose, to ensure that the operation of the MG is within the limits of bus voltages, among others, a convex EMS with network constraints is considered. Then, the BAM is used to develop a convex approximation of the EMZ-ZIP to achieve an effective integration of the model to the EMS. Finally, this chapter also described some feasible extensions for the proposed methodology and the most relevant aspects for the implementation of the models, databases and routines that comprise the proposed methodology.

4 Case Study, Results and Discussion

This thesis proposes a methodology for modeling SPSPs and integrating them into an EMS for a MG. In this sense, this chapter presents the application of the proposed methodology to a case study. First, Section 4.1 presents an overview of the case study considered to apply the proposed methodology. Second, Section 4.2 presents the development of the EMZ-ZIP model and the estimation of its parameters. Third, Section 4.3 presents the results and analysis of the simulations of the energy management performed by the EMS (integrating the EMZ-ZIP model) during the operation of the MG. Next, Section 4.4 shows the results and analysis of two complementary performance cases to evaluate the functionality of the proposed methodology. The analysis of the computational time required for the EMS to reach convergence is presented in Section 4.5. Finally, Section 4.6 presents the discussion of the results obtained by applying the methodology proposed in this work to the case study under consideration.

4.1 Case study details

The methodology for modeling SPSPs and their integration into an EMS for a MG is tested and validated in a case study. This consists of a 9-bus test system, which has the characteristics of a low-voltage MG, specifically the low X/R ratio [90]. The 9-bus system was selected because its topology is similar to the actual isolated MGs installed in Chile (e.g., [97], [214]). Figure 4.1 shows an overview of the MG of the case study. The reference values of the lengths and the X and R values of the MG feeders were taken from [214]. As can be seen in Figure 4.1, the MG comprises two diesel generators (DGU), two transformers, a PV generator connected to the system through an inverter and three consumption centers.

Additionally, as can be seen in Figure 4.1, an SPSP was connected to the MG at bus 6, which in this case is a solar drying process. This process consists of a processing and drying center for fruits and other vegetables (see Annexed B) for which it includes an electric heater, an electric fan, and some auxiliary equipment. The productive process is continuous process the drying period depending primarily on the air-drying temperature, and humidity [215]. Because it is an SPSP, it mainly takes advantage of solar radiation to increase the internal temperature of the dryer. However, during periods of poor solar contribution (e.g., sunrise, sunset, night, cloudy days, among others) the electric heater is used to maintain a temperature for the drying process. In addition, the electric fan is activated primarily during periods of high solar contribution to regulate the process temperature. Besides, the auxiliary electric equipment (e.g., office devices, lighting, among others) are used in the offices of the SPSP for the administrative activities of the process. These administrative activities are typically carried out from 9:00 a.m. to 6:00 p.m. (18h) The SPSP electric consumption measurements are collected at the coupling point, as indicated in Figure 4.1.

As previously described, the modeling of the MG and the SPSP of the case study was implemented in MATLAB®/Simulink® using the Simscape™ Electrical™ Specialized Power Systems blocks. Details of the models and parameter values of the MG elements of the case study are presented in Annexed E.
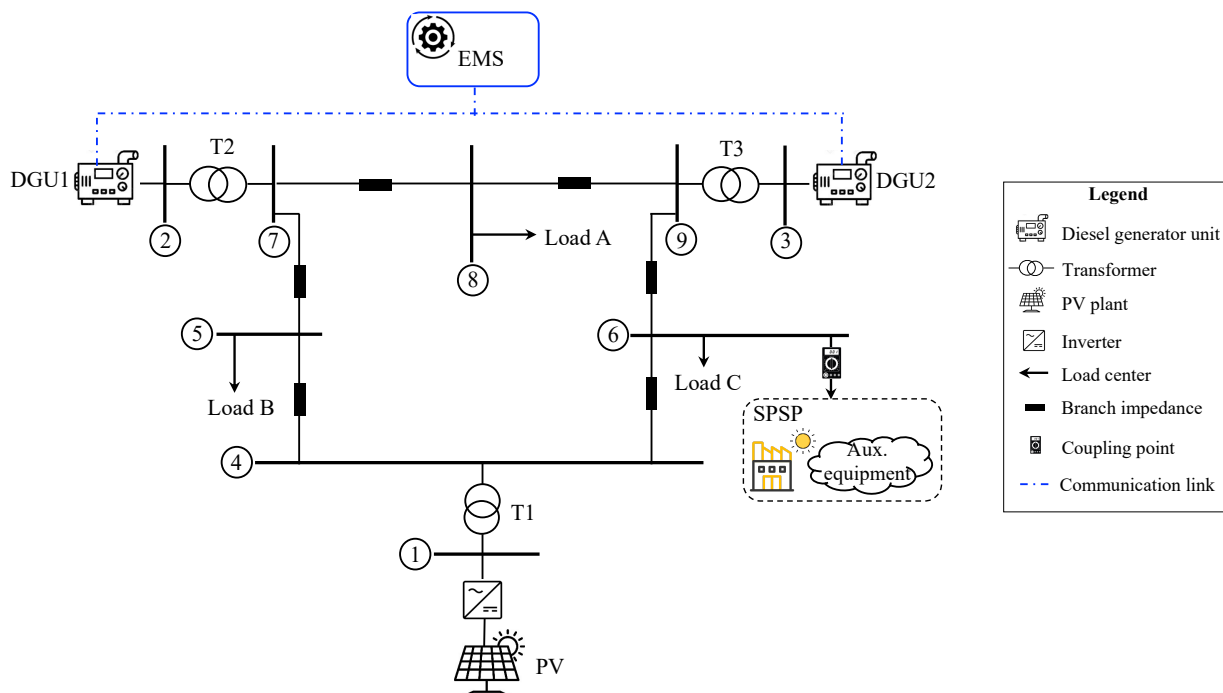
Figure 4.1 Overview of the MG system including an SPSP

4.2 Development of the EMZ-ZIP load model for the case study

Once the test MG and the SPSP have been defined, the first stage of the proposed methodology (see Section 3) consists of the development of the database containing the ZIP models of the devices that an SPSP may have. As mentioned in the previous section, the case study includes a solar drying productive process. Then, from the semi-structured survey of the SPSP process operators, the devices comprising the SPSP and the time of energy use are determined.

Table 4.1 shows the semi-structured survey and information collected for the solar drying process. Next, a relational database is established for this productive process which contains the ZIP models of the electrical devices mentioned above. The ZIP parameters of these devices are taken from [33]. For example, the ZIP parameters for the heater are $\alpha_{1,heater} = 0.92, \alpha_{2,heater} = 0.1, \alpha_{3,heater} = -0.02$, whereas for the fan they are $\alpha_{1,fan} = 0.26, \alpha_{2,fan} = 0.9, \alpha_{3,fan} = -0.16$. In addition, the P_o parameter values (i.e., nominal power) for the heater, the electric fan, and auxiliary equipment are listed in Table 4.1.

75

Table 4.1 Information of the SPSP's electrical devices and their time of use of energy obtained through the semi-structured survey.

	Type of device	Nominal power (W)	Nominal voltaje (V)	Quantity	Time of use of energy (⊠ = on, ▨ = off)																							
					1	2	3	4	5	6	7	8	9	10	11	12	13	14	15	16	17	18	19	20	21	22	23	24
Solar dryer SPSP	Heater	2,000	220	1	on	on	on	on	on	on	on	on	off	off	off	off	off	off	off	off	off	on	on	on	on	on	on	on
	Fan	610	220	1	off	off	off	off	off	off	off	off	on	on	on	on	on	on	on	on	on	on	on	on	off	off	off	off
	Aux. eq.	420 - 800	220	n/a	on	on	on	on	on	on	on	on	on	on	on	on	on	on	on	on	on	on	on	on	on	on	on	on

The next stage of the proposed methodology consists of developing the extended TV-ZIP model of the SPSP under study. In this sense, by considering the ZIP load models of the electric devices that belong to the drying process (see Table 4.1) and utilizing the procedure described in Section 3.3.1, the extended TV-ZIP model for the active power is expressed as follows:

$$P(k) = ZIP_{flex}\left(\tilde{V}(k)\right) + \delta_1(k)ZIP_{heater}\left(\tilde{V}(k)\right) + \delta_2(k)ZIP_{fan}\left(\tilde{V}(k)\right) \tag{91}$$

$$\sum_{\omega=1}^{2} \delta_\omega(k) \leq 1 \tag{92}$$

$$ZIP_{flex}\left(\tilde{V}(k)\right) = P_{flex}(k)\left(\tilde{\alpha}_1(k)\tilde{V}^2(k) + \tilde{\alpha}_2(k)\tilde{V}(k) + \tilde{\alpha}_3(k)\right) \tag{93}$$

Note that because auxiliary equipment can be turned on or off at any instant (influenced by, for example, people's behavior), the flexible component of the extended TV-ZIP model will capture and represent their electrical behavior.

The next step in the proposed methodology is the zoning of the extended TV-ZIP model. For this purpose, the procedure described in Section 3.3.2 is considered. First, the measurement data of the variables of interest for the solar drying process are obtained, which are mainly solar radiation, ambient temperature, relative humidity, and time. On the one hand, the data of these variables are the inputs for the ANN-based zones identifier, and they are actual measurements that were taken from [216]. On the other hand, the time of use of energy information obtained through the semi-structured survey (see Table 4.1) is used to develop the output vector for the ANN training.

The ANN approach used in this work is a MLP with a sigmoidal activation function and the training process was performed using the Levenberg-Marquardt algorithm. The ANN architecture is defined following the method described in Section 3.3.2; thus, the ANN consists of an input layer, a hidden layer with 8 neurons and an output layer as shown in Figure 4.2.
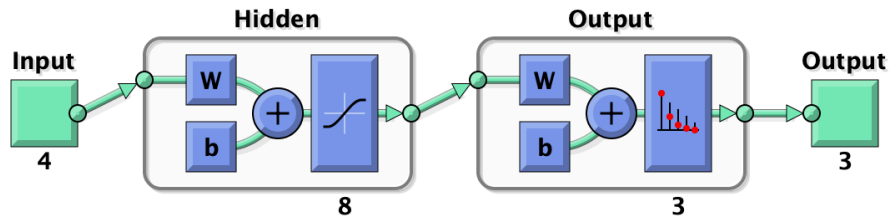
Figure 4.2 ANN architecture

For the zone identification procedure, solar radiation, ambient temperature, relative humidity data measured every 10 minutes for 54 days and time information (i.e., an input 1296 x 4 matrix), and an output vector of 1296 are used. Then, 70% of the data set was used for training, 15% for validation and 15% for testing. With the trained model, a second data set of 188 samples (i.e., 48 hours) was used to perform zone identification. Figure 4.3 shows the plots of the second data set used by the zone classifier and the results of the identified zones.
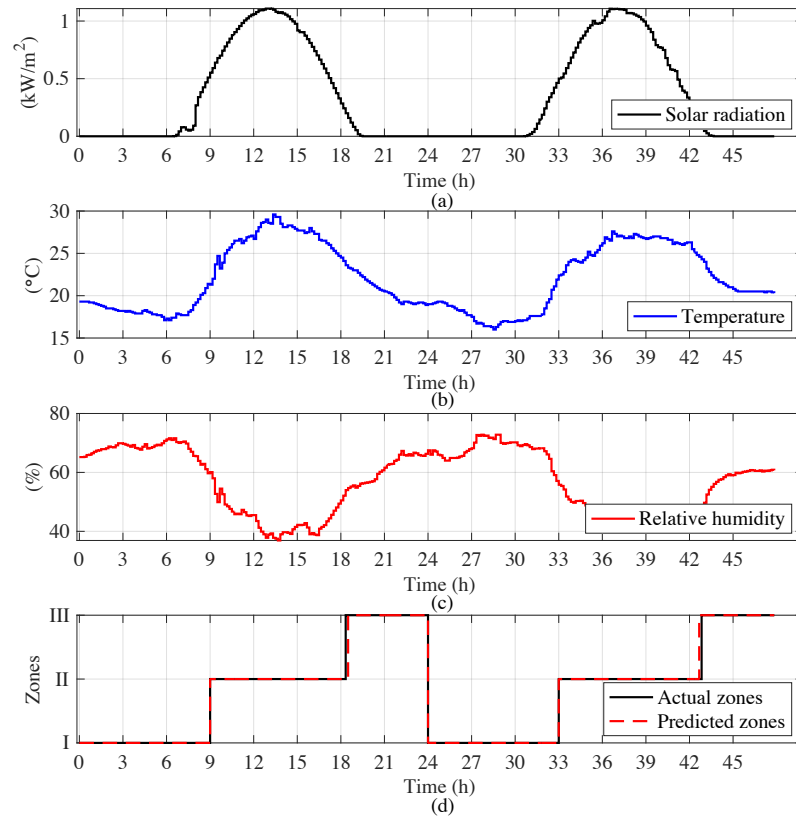
Figure 4.3 (a) Solar irradiation, (b) ambient temperature, (c) relative humidity, and (d) actual and predicted zones

Considering the time of use of energy information obtained from the semi-structured survey (see Table 4.1), it can be established that the heater may be turned on in zones I and III, the electric fan can be activated mainly in zone III, and the auxiliary equipment may be active at any time, i.e., in all zones. Then, using the expressions in (91)-(93), an extended TV-ZIP is established for each identified zone for which parameter identification is carried out. Table 4.2 summarizes the details of the active devices and the parameters to be identified in each zone.

Table 4.2 Active devices and parameters to be identified in each zone

Zone	Active devices	Parameters
I	Heater + auxiliary equipment	$P_{flex}(k), \tilde{\alpha}_1(k), \tilde{\alpha}_2(k), \tilde{\alpha}_3(k), \delta_1(k)$
II	Electric fan + auxiliary equipment	$P_{flex}(k), \tilde{\alpha}_1(k), \tilde{\alpha}_2(k), \tilde{\alpha}_3(k), \delta_2(k)$
III	Heater + auxiliary equipment	$P_{flex}(k), \tilde{\alpha}_1(k), \tilde{\alpha}_2(k), \tilde{\alpha}_3(k), \delta_1(k)$

Parameter identification is performed considering the procedure proposed in Section 3.4, specifically the optimization problem in (16)-(22) and the GO-MK strategy. In addition, parameter identification is carried out for every 10 minutes of a representative day, i.e., 144 discrete time steps. Moreover, the input data (i.e., voltage and power measurements) required for parameter identification were obtained from a simulator of the solar drying productive process (see Annexed E.6). Measurements collected every 10 minutes for 8 days are considered, i.e., 1152 samples of which the measurements of 7 days are used for parameter identification and the measurements of the remaining day are considered to validate the parameter identification result. Figure 4.4 displays the results of the active power estimated using the EMZ-ZIP model and the evolution of the identified parameters.
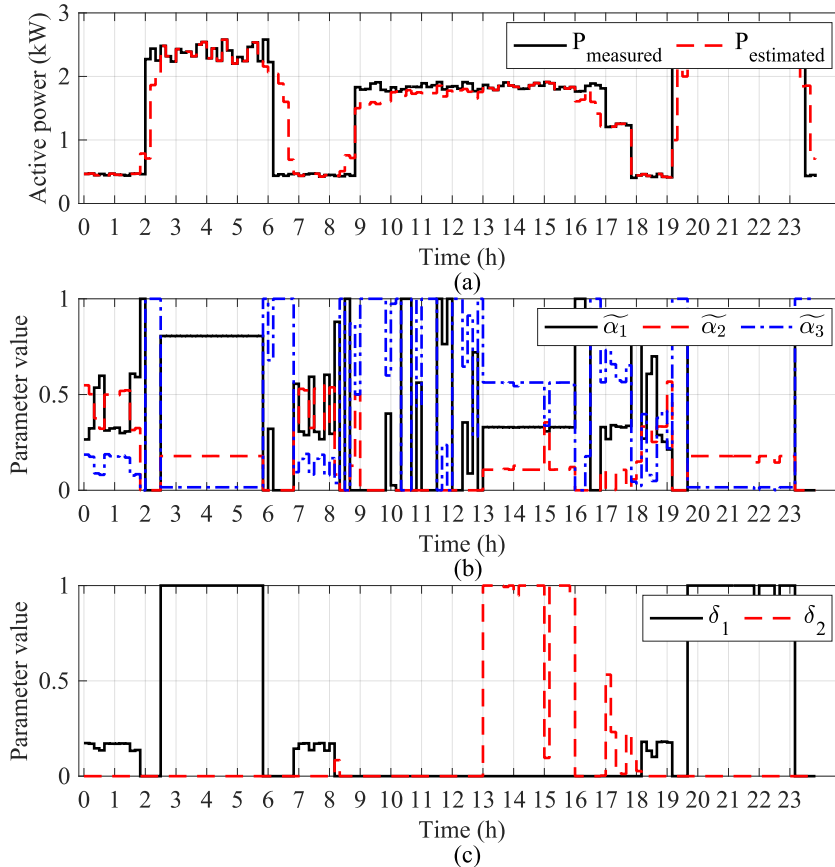
Figure 4.4 (a) Measured and estimated active power, (b) evolution of the parameters $\tilde{\alpha}_1(k), \tilde{\alpha}_2(k), \tilde{\alpha}_3(k)$ identified using the EMZ-ZIP, and (c) evolution of the parameters $\delta_1(k), \delta_2(k)$ identified using the EMZ-ZIP load model

As illustrated by Figure 4.4(a), the EMZ-ZIP model can properly estimate new values of active power for the validation period (i.e., 1 day). Figure 4.4(b) shows the evolution of the parameters the capture the sensitivity of the SPSP loads to voltage variations (i.e., $\tilde{\alpha}_1(k), \tilde{\alpha}_2(k), \tilde{\alpha}_3(k)$). Moreover, Figure 4.4(c) illustrates the evolution identified parameters $\delta_1(k)$ and $\delta_2(k)$ which represent the contribution of the heater and electric fan to total load consumption, respectively. Additionally, to assess the quality of the EMZ-ZIP, a residual analysis was performed. Figure 7 depicts the results of the residual analysis.
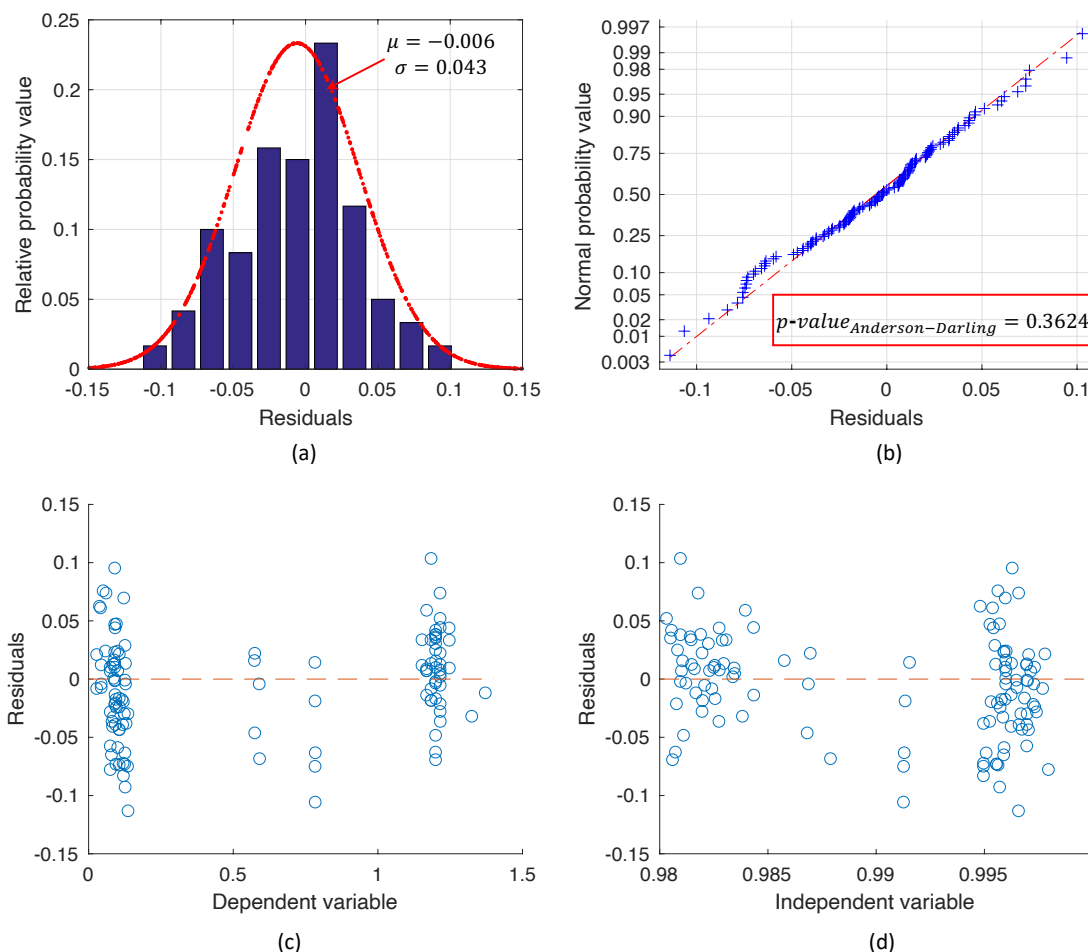
Figure 4.5 (a) Histogram of residuals, (b) normal probability plot, (c) residuals vs. dependent variable plot, and (d) residuals vs. independent variable plot

It can be observed from Figure 4.5(a) and Figure 4.5(b) that the residuals are normally distributed ($\mu = 0.0018, \sigma = 0.041$). Nevertheless, some deviations int the tails can be observed. So, we applied the Anderson-Darling normality test [217] where the resulting $p-value = 0.07$ confirms that the residuals are normally distributed. From the results in Figure 4.5(c) and Figure 4.5(d), it is evident that the residuals have no dependence with the dependent variable and the independent variable. These results reveal that the EMZ-ZIP load model can adequately represent the relationship between the dependent variable and the independent variable, i.e., power consumption of the SPSP and voltage, respectively.

Table 4.3 shows the type of programming model, size (number of decision variables), computational time and percentage time improvement to identify the parameters of the representative (i.e., 144 discrete time steps) of the TV-ZIP and the EMZ-ZIP models considering the GO and the GO-MK strategy (see Section 3.4). It should be noted that the GO approach employs a random starting point; thus, to determine the computational time, we performed 25 experiments with random points following a uniform distribution and averaged the times obtained.

Table 4.3 Type of programming model, size, computational time, and percentage time improvement for the TV-ZIP and the EMZ-ZIP

Load model	Strategy	Type of programming model	Size (number of decision variables)	Time (s)	Time improvement (%)
TV-ZIP	GO	NLP	576	179.33	-
	GO-MK	LP+NLP	1584	155.65	15.21
EMZ-ZIP	GO	NLP	720	354.75	-
	GO-MK	LP+NLP	1872	270.43	31.17

As can be seen in Table 4.3, the GO approach solves an NLP type problem, while the resulting problem for the GO-MK strategy is LP+NLP due to the use of the MK result as a starting point for the GO method. In general, the optimization problem solved by the GO-MK strategy presents more variables because it first solves the problem with the MK relaxation. However, the GO-MK method presents a lower computational time than the GO with random starting point. For example, for the TV-ZIP model and for the EMZ-ZIP model there is an improvement in computational time of about 15% and 31%, respectively. This is an expected result for two main reasons. First, although the MK result is suboptimal, it is close to the global optimum; therefore, the GO method requires less time to reach the best solution. Second, the McCormik's relaxations optimization model is a LP type which does not considerably increase the computational burden because it can be solved in polynomial time [179].

Considering the GO-MK strategy, the number of variables of the EMZ-ZIP is relatively larger (1872) than the TV-ZIP model (1584) because of the EMZ-ZIP model structure (see Section 3.3). Therefore, it takes more time to estimate the parameters of the EMZ-ZIP model. In average, it takes 1.08 seconds and 1.87 seconds to estimate the set of parameters for each time step k for the TV-ZIP and the EMZ-ZIP model, respectively. Then, the total time span incurred to estimate the parameters of the EMZ-ZIP model for a representative day (i.e., 144 discrete time steps) is within a reasonable computational time (around 4.5 minutes), making it suitable for practical applications.

4.3   Operation of MG-EMS

Once the EMZ-ZIP parameters have been identified, the MG operation can be performed (stage E of the proposed methodology, see Section 3.1). The time domain of the MG operation simulation

is 1 millisecond, while the EMS minimizes the operational costs of the MG (using the optimization problem described in Section 3.5.2) based on available generation and expected demand, and then sends operating setpoints every 10 minutes to the dispatchable units. In addition, the primary control of voltage and frequency are based on local control strategies implemented at each generation unit (see Annexed E).

Since the MG includes a PV generation unit (see Figure 4.1), its power injection was obtained using the model described in Annexed E.5 and a solar radiation profile taken from [216]. The expected power consumption in the EMS is obtained through the already identified parameters of the EMZ-ZIP (in the case of the SPSP), while the power consumption of the other loads in the system are obtained in a similar way because they are modeled as voltage-sensitive loads.

One day of operation (i.e., 24 hours) was considered to analyze the operation of the MG-EMS. In addition, to analyze the performance of the MG operation when representing the SPSP consumption with different load models, three cases were considered: i) EMS including a CP model (in this case a persistence model[a] [218] was used), ii) EMS considering a TV-ZIP to represent the SPSP, and iii) the EMZ-ZIP model as integral part into the EMS. For comparison purposes, the following performance indicators were considered: i) simulated system operating costs and expected EMS operating costs (in Chilean pesos or CLP), ii) reference and operating voltages at the generation buses, iii) and the estimated power consumption of the SPSP in the EMS. It should be noted that the same PV power generation profile was considered for the three cases of load representation models, i.e., CP, TV-ZIP and EMZ-ZIP. Figure 4.6 shows the evolution of the simulated system operating costs and the expected costs obtained from the EMS for the analysis period (i.e., 1 day) and for the three cases of load representation, and the relative error between the costs obtained with the CP representation vs. the other two models.

---

[a] The persistence model consists of using the power consumption measurement of the previous time step to determine the operating setpoints for the next time step, i.e., $P(k) = P(k-1)$.
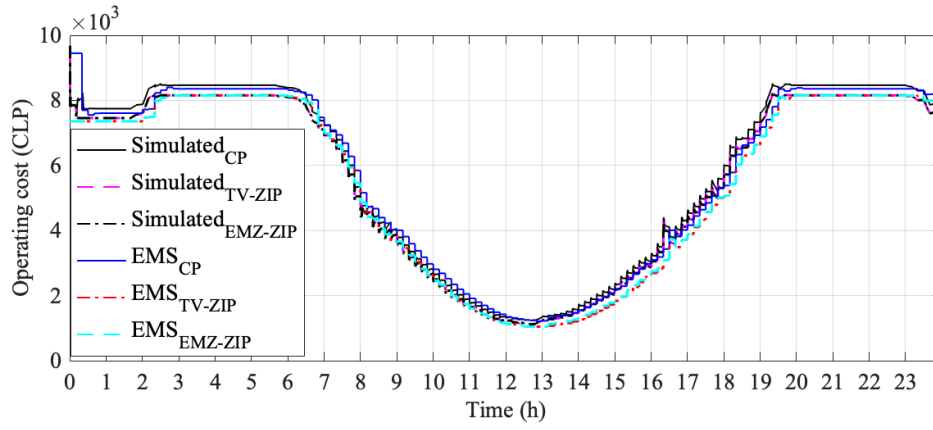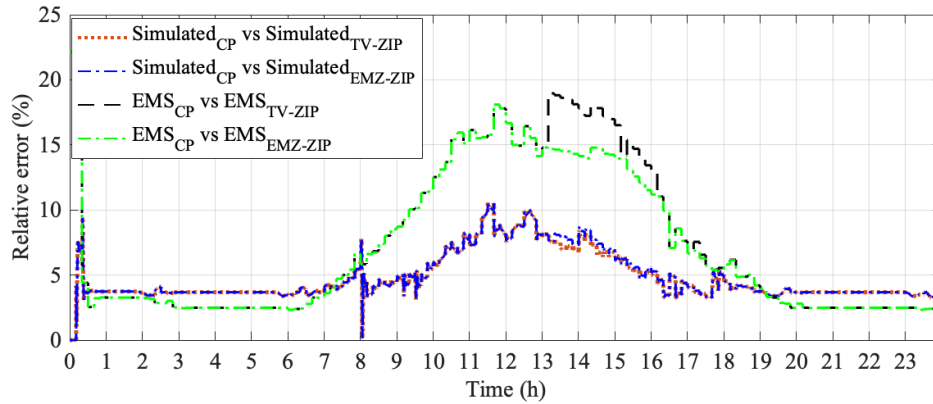
Figure 4.6 (a) Simulated system operating costs and estimated costs obtained from the EMS for the three cases (i.e., CP, TV-ZIP and EMZ-ZIP), (b) evolution of the relative error between the costs obtained with the CP model vs. TV-ZIP and EMZ-ZIP

Table 4.4 presents a summary of simulated operating costs for the three SPSP load representation cases. The summary includes the following: total operating cost (Total), minimum cost (Min), maximum cost (Max), average total operating cost for the evaluation day (Avg.), average operating cost reduction considering the CP model as base case (Avg. red.), and the minimum, maximum and standard deviation (Std.) of the average operating cost reduction. Table 4.5 shows the summary of the operating costs obtained from the EMS for the three cases, considering the same indicators. And Table 4.6 presents a summary of the difference (relative percentage error) between the simulated operating costs and those obtained from the EMS for each case of representation of the SPSP load.

Table 4.4 Summary of simulated operating costs

Load model	Total (CLP)	Min (CLP)	Max (CLP)	Avg. (CLP)	Avg. red. (%)	Min (%)	Max (%)	Std.
CP	3.927e6	1.232e3	9.677e3	5.843e3	-	-	-	-
TV-ZIP	3.768e6	1.112e3	9.677e3	5.606e3	4.762	0	10.564	1.774
EMZ-ZIP	3.767e6	1.112e3	9.677e3	5.605e3	**4.800**	0	10.564	1.824

Table 4.5 Summary of operating costs obtained from the EMS

Load model	Total (CLP)	Min (CLP)	Max (CLP)	Avg. (CLP)	Avg. red. (%)	Min (%)	Max (%)	Std.
CP	3.885e6	1.216e3	9.449e3	5.780e3	-	-	-	-
TV-ZIP	3.689e6	1.044e3	8.149e3	5.489e3	**7.447**	2.328	22.142	5.885
EMZ-ZIP	3.695e6	1.044e3	8.149e3	5.497e3	7.075	2.328	22.142	5.349

Table 4.6 Summary of the difference between the simulated operating costs and those obtained from the EMS for the three cases of load representation

Load model	Avg. (%)	Min (%)	Max (%)
CP	4.280	0.0024	25.811
TV-ZIP	4.769	0.0053	27.356
EMZ-ZIP	**4.361**	0.0049	29.356

The results of actual MG operating costs in Table 4.4 show that considering load representations that capture the sensitivity of the loads to voltage variations results in a considerable reduction in total MG operating costs, by about 5% in the case of EMZ-ZIP. This result is explained by the fact that when considering voltage sensitive loads, the EMS with an AC approach will try to minimize the voltage at the load buses to reduce the power consumption; thus, reducing the operating costs, and consequently the voltages will be close to the minimum allowed value [133]. This same trend was observed in the operating costs obtained from the EMS (see Table 4.5). Nevertheless, in this case, the highest reduction in operating costs (7.447%) is obtained with the TV-ZIP model. Further, the results in Table 4.6 show that the smallest difference between the actual operating costs and the operating costs estimated from the EMS is obtained with the EMZ-ZIP model (4.361%). This can be explained because the EMZ-ZIP model better captures the dependence of the SPSP loads on voltage (see Section 2.3.3); therefore, it better represents the SPSP power consumption.

Figure 4.7(a) shows the results of the reference and generated power of the diesel generators, and the power generation profile of the PV unit. Figure 4.7(b) shows the power consumption profile of the SPSP simulated in the system and obtained from the EMS using the CP load model. In addition, Figure 4.8(a), Figure 4.8(b), Figure 4.9(a) and Figure 4.9(b) show similar results but considering the TV-ZIP model (Figure 4.8) and the EMZ-ZIP model (Figure 4.9).

Figure 4.7 (a) Reference and generated power of the diesel generators, and the power generation profile of the PV unit, (b) power consumption profile of the SPSP simulated and obtained from the EMS using the CP model

Figure 4.8 (a) Reference and generated power of the diesel generators, and the power generation profile of the PV unit, (b) power consumption profile of the SPSP simulated and obtained from the EMS using the TV-ZIP load model

Figure 4.9 (a) Reference and generated power of the diesel generators, and the power generation profile of the PV unit, (b) power consumption profile of the SPSP simulated and obtained from the EMS using the EMZ-ZIP load model

Table 4.7 presents a summary of the results of the relative percentage error of the SPSP power consumption between simulated and obtained from the EMS using each of the load models, i.e., CP, TV-ZIP and EMZ-ZIP. The results include the average error (Avg.), minimum (Min), maximum (Max) and standard deviation (Std.).

Table 4.7 Summary of the results of the relative percentage error of the SPSP power consumption between simulated and obtained from the EMS using each load

Load model	Avg. (%)	Min (%)	Max (%)	Std.
CP	12.515	1.269e-7	294.419	32.923
TV-ZIP	12.691	0.0011	305.529	30.994
EMZ-ZIP	**11.973**	0.0013	305.259	31.607

As can be seen in Figure 4.7(a), Figure 4.8(a) and Figure 4.9(a) the local controllers of the diesel generators are able to follow the power operating setpoints sent from the EMS. In addition, it is observed that the diesel generators decrease their power generation when the PV unit injects its energy production to the system. Thus, there is not a significant difference between the actual operating costs and the operating costs obtained from the EMS. Moreover, in the period between 13:00 and 16:00 there is a fan switch-on. Then, comparing Figure 4.8(b) and Figure 4.9(b) it can be observed that the TV-ZIP model is not able to represent the switching on of another device in the same zone which leads to a higher estimation error than the EMZ-ZIP model. Further, the results in Table 4.7 reveal that when considering the EMZ-ZIP model to represent the power consumption of the SPSP, the average error between the simulated and estimated consumption of the SPSP is slightly lower (11.973%) compared to the other load models. This is because the EMZ-ZIP model better captures the dependence of the SPSP loads on voltage variations which leads to a decrease in the error.

85

Figure 4.10(a) displays the results of the reference and operating voltages at the generation buses of the system, and Figure 4.10 (b) shows the operating voltages at the MG load buses when the SPSP load is represented with a CP model. Besides, Figure 4.11(a), Figure 4.11(b), Figure 4.12(a) and Figure 4.12 (b) depict similar results but when the SPSP power consumption is represented through a TV-ZIP model (Figure 4.11) and using the EMZ-ZIP model (Figure 4.12). Table 4.8 presents a summary of the results of the relative percentage error between voltage references and bus voltages at generation buses.
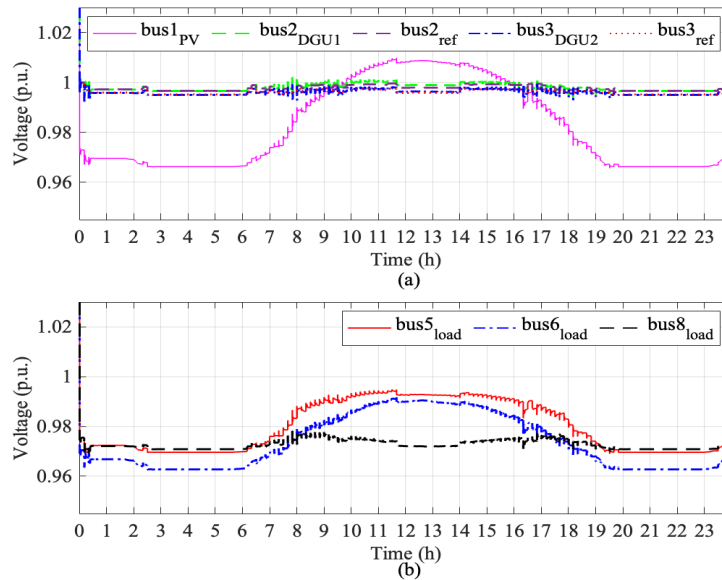
Figure 4.10 (a) Reference and operating voltages at the generation buses of the system, (b) operating voltages at the load buses of the MG when the SPSP power consumption is represented through a CP model
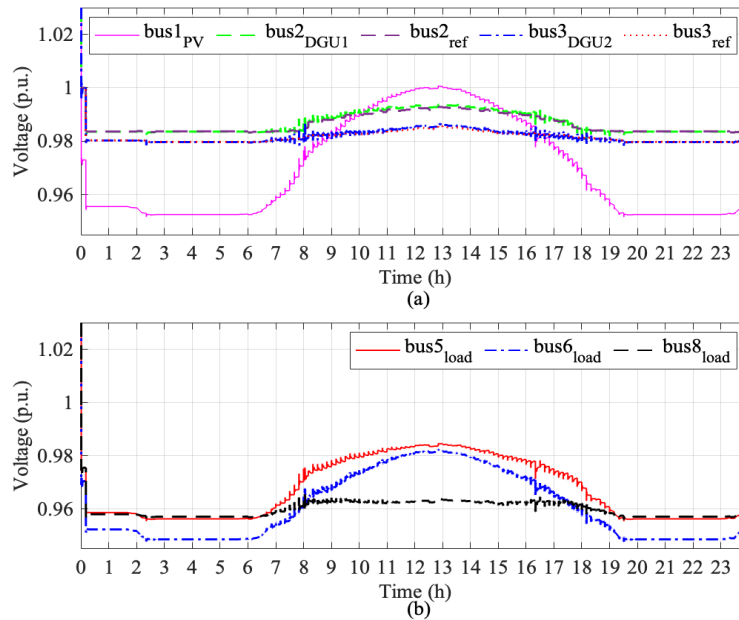
Figure 4.11 (a) Reference and operating voltages at the generation buses of the system, (b) operating voltages at the load buses of the MG when the SPSP power consumption is represented through a TV-ZIP model

86
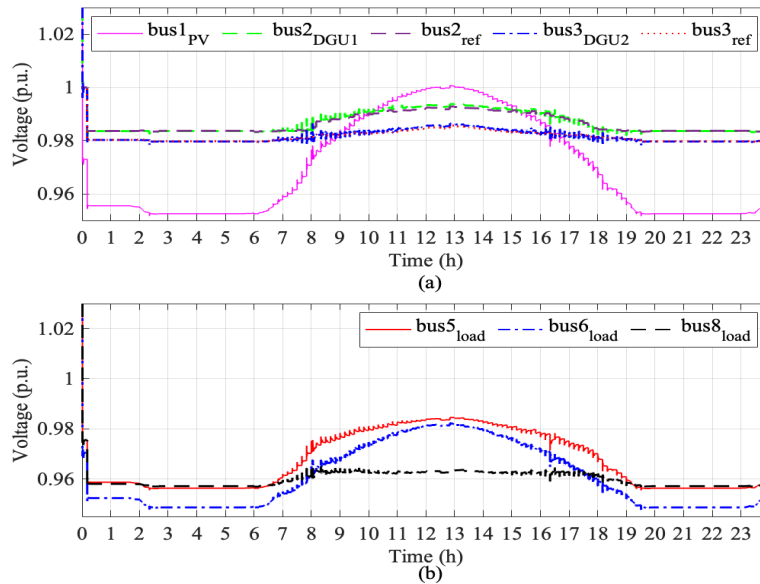
Figure 4.12 (a) Reference and operating voltages at the generation buses of the system, (b) operating voltages at the load buses of the MG when the SPSP power consumption is represented through the EMZ-ZIP load model

Table 4.8 Summary of the results of the relative percentage error between voltage references and bus voltages at generation buses

	DGU1			DGU2		
Load model	**Avg. (%)**	**Min (%)**	**Max (%)**	**Avg. (%)**	**Min (%)**	**Max (%)**
CP	0.0436	1.225e-5	9.249	0.0324	2.015e-5	8.629
TV-ZIP	0.0426	1.582e-5	9.249	0.0340	4.709e-5	8.629
EMZ-ZIP	**0.0425**	**2.365e-5**	9.249	**0.0339**	**6.178e-5**	8.629

Figure 4.13 depicts the simulated operating frequency of the MG when the SPSP power consumption is represented through the CP, TV-ZIP and EMZ-ZIP model. Table 4.9 presents a summary of the results of the simulated operating frequency of the MG when the SPSP power consumption is represented through the CP, TV-ZIP and EMZ-ZIP model. The results include the average frequency (Avg.), minimum (Min), maximum (Max) and standard deviation (Std.).

Figure 4.13 Simulated operating frequency of the MG when the power consumption of the SPSP is represented through the CP, TV-ZIP and EMZ-ZIP model

87

Table 4.9 Summary of the results of the simulated operating frequency of the MG when the SPSP power consumption is represented through the CP, TV-ZIP and EMZ-ZIP model

Load model	Avg. (Hz)	Min (Hz)	Max (Hz)	Std. (Hz)
CP	49.67	48.22	51.80	0.27
TV-ZIP	49.70	48.31	51.09	0.24
EMZ-ZIP	49.71	48.33	51.08	0.23

Overall, the results shown in Figure 4.10, Figure 4.11 and Figure 4.11 show that with the operating setpoints sent from the EMS, the voltages at the generation and load buses of the MG are under normal operating levels for the three cases of SPSP load representation (CP, TV-ZIP and EMZ-ZIP). However, comparing Figure 4.10(a), Figure 4.11(a) and Figure 4.12(a) shows that the reference voltages sent by the EMS remain close to 1.00 p.u. when the SPSP consumption is represented through a CP model. This is an expected result because this type of model does not consider the dependence of the power consumption on the voltage. In contrast, as previously mentioned, when voltage-dependent load models (i.e., TV-ZIP or EMZ-ZIP) are considered, the EMS will try to keep the voltages at the load buses to the minimum allowed value to decrease the load consumption; hence, minimizing the operating costs. Nevertheless, using the EMZ-ZIP model results in a slightly smaller difference between the simulated and reference voltages sent from the EMS (see Table 4.8). Finally, considering the results of Figure 4.13 and Table 4.9 it is observed that the average operating frequency is closer to the nominal frequency (50 Hz) when the SPSP is represented using the EMZ-ZIP than the CP model. Surprisingly, the operating frequency results using the TV-ZIP are similar to the EMZ-ZIP. This can be explained by the time-variant characteristic of the TV-ZIP model that makes it better than the conventional ZIP model.

4.4   Practical performance aspects

From the results presented in the previous section, the advantage of considering voltage-dependent loads to represent the loads, especially of the SPSP, was evident. However, the results showed slight differences between the EMZ-ZIP model and the TV-ZIP model. In this sense, to further analyze the performance of the two models, we designed two additional cases of MG operation that are expected in practice, which are: i) change in the scheduling of the SPSP production activities, and ii) variability in the solar radiation profile.

Case 1: In this case, we have assumed that there was a change in the scheduling of the SPSP production activities. More specifically, we consider moving the morning work shift to an earlier time because more products need to be produced. Therefore, in the new scheduling, the work shift starts at 8:00 a.m. instead of 9:00 a.m. In this context, one day of MG operation was simulated including the change in productive activities and keeping the MG operating parameters similar to the experiments performed in the previous section. This experiment was performed by representing the SPSP in the EMS through the TV-ZIP model and then using the EMZ-ZIP. Moreover, a three-hour analysis w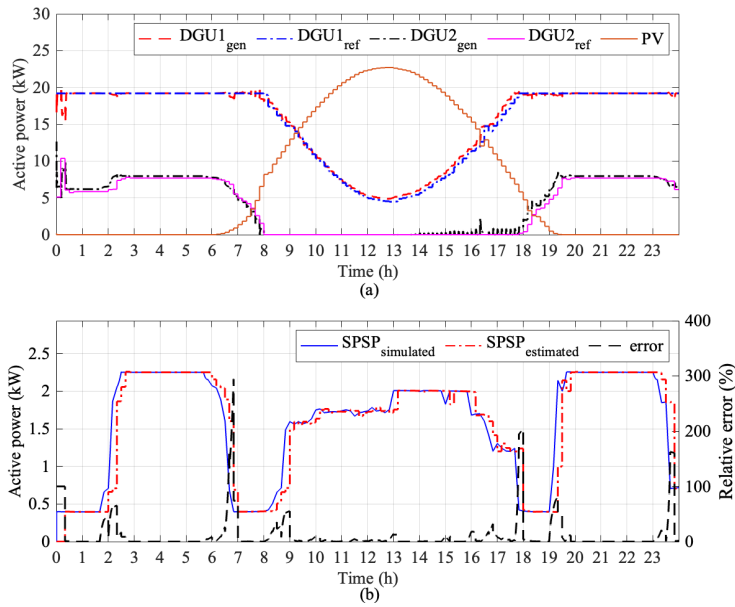indow from 7:00 a.m. to 10:00 a.m. was considered. Figure 4.14 depicts the reference and generated power of the diesel generators, and the power generation profile of the PV

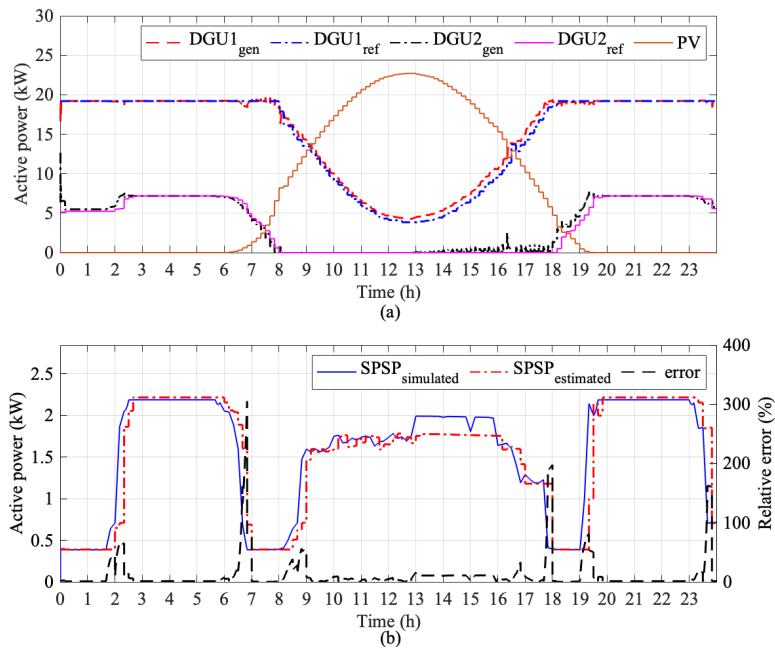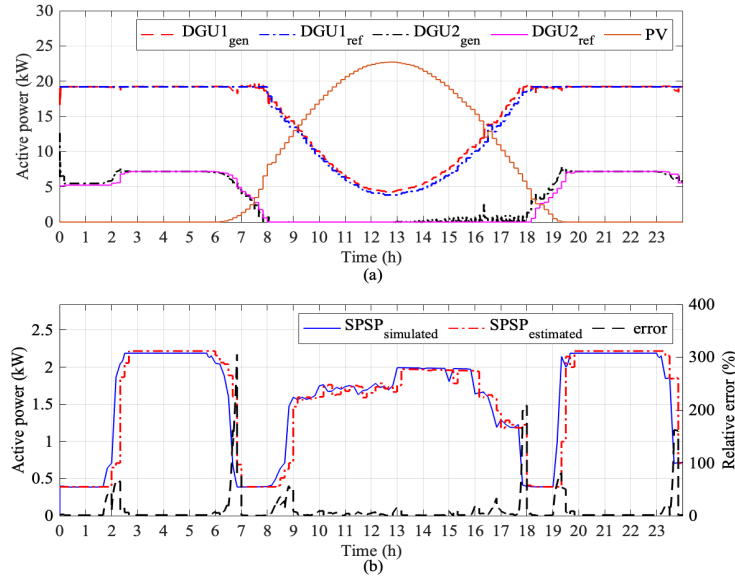unit, the power consumption profile of the SPSP simulated and obtained from the EMS using the TV-ZIP load model, and the zoom plot of the three-hour period. Figure 4.15 shows the same results but in this case the SPSP was represented using the EMZ-ZIP model. Table 4.10 presents a summary of the results of the relative percentage error of the SPSP power consumption between simulated and obtained from the EMS using each of the load models considered in this case, i.e., TV-ZIP and EMZ-ZIP. Table 4.11 shows a summary of the difference between simulated operating costs and those obtained from the EMS for the whole operating day. Table 4.12 summarizes the results of the relative percentage error of the SPSP power consumption between simulated and obtained from the EMS using each load model for the three-hour analysis window. Table 4.13 gives a summary of the difference between operating the actual MG operating costs and the costs obtained from the EMS for the whole operating day. Figure 4.16 shows the simulated operating frequency of the MG when the power consumption of the SPSP is represented through the TV-ZIP and EMZ-ZIP model for the three-hour analysis window. Table 4.14 presents a summary of the simulated operating frequency results such as average frequency (Avg.), minimum (Min), maximum (Max) and standard deviation (Std.).
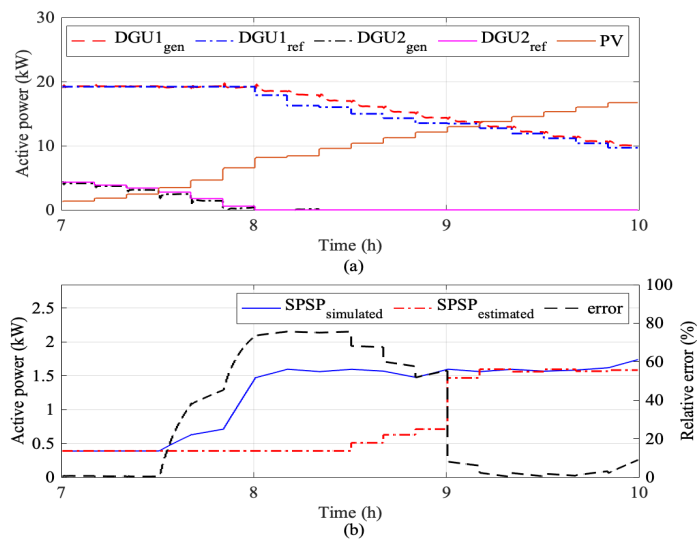
Figure 4.14 (a) Reference and generated power of the diesel generators, and the power generation profile of the PV unit, (b) power consumption profile of the SPSP simulated and estimated in the EMS using the TV-ZIP for the three-hour period

89
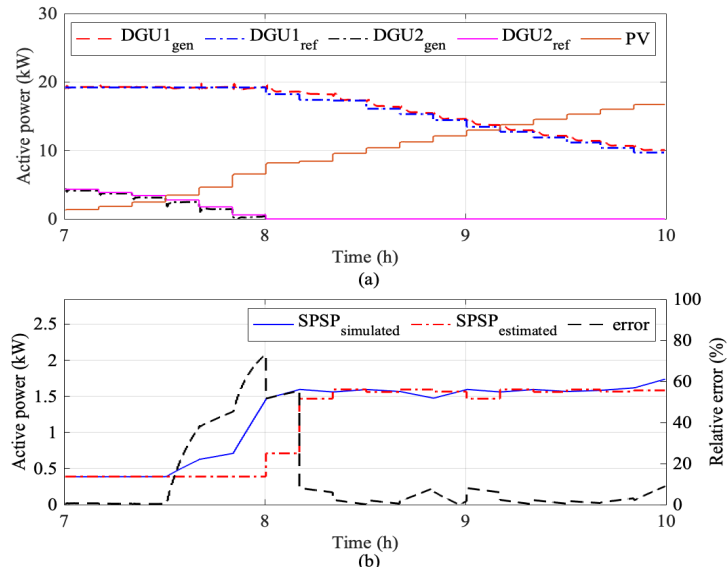
Figure 4.15 (a) Reference and generated power of the diesel generators, and the power generation profile of the PV unit, (b) power consumption profile of the SPSP simulated and estimated in the EMS using the EMZ-ZIP for the three-hour period

Table 4.10 Summary of the results of the relative percentage error of the SPSP power consumption between simulated and obtained from the EMS using each load model for the whole operating day

Load model	Avg. (%)	Min (%)	Max (%)	Std.
TV-ZIP	15.215	0.0011	305.529	32.898
EMZ-ZIP	**12.189**	0.0013	305.259	31.845

Table 4.11 Summary of the difference between simulated operating costs and those obtained from the EMS for the whole operating day

Load model	Avg. (%)	Min (%)	Max (%)
TV-ZIP	4.794	0.0053	27.356
EMZ-ZIP	**4.285**	0.0049	27.355

Table 4.12 Summary of the results of the relative percentage error of the SPSP power consumption between simulated and obtained from the EMS using each load model for the three-hour analysis window

Load model	Avg. (%)	Min (%)	Max (%)	Std.
TV-ZIP	45.205	0.154	75.634	28.586
EMZ-ZIP	**17.198**	0.086	73.038	21.967

Table 4.13 Summary of the difference between simulated operating costs and those obtained from the EMS for the three-hour analysis window

Load model	Avg. (%)	Min (%)	Max (%)
TV-ZIP	3.720	0.141	10.267
EMZ-ZIP	**2.511**	0.271	8.115

90
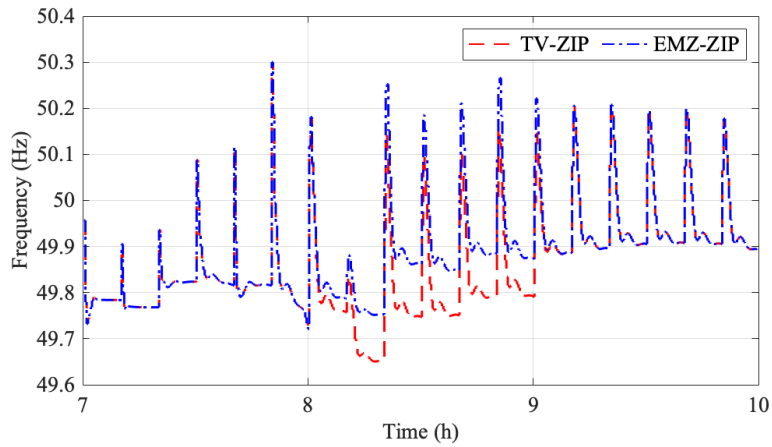
Figure 4.16 Simulated operating frequency of the MG when the power consumption of the SPSP is represented through the TV-ZIP and EMZ-ZIP model for the three-hour analysis window

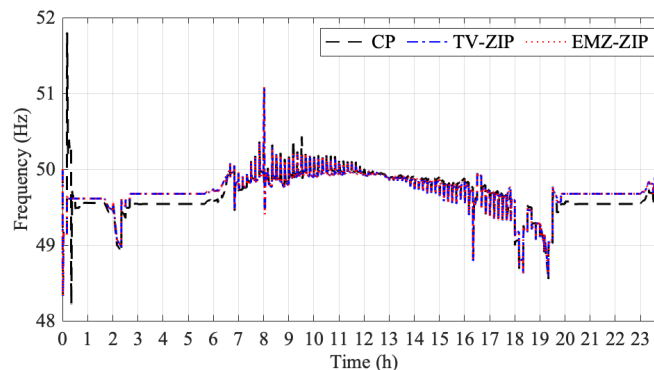Table 4.14 Summary of the results of the simulated operating frequency of the MG when the SPSP power consumption is represented through the TV-ZIP and EMZ-ZIP model for the three-hour analysis window

Load model	Avg. (Hz)	Min (Hz)	Max (Hz)	Std.
TV-ZIP	49.86	49.65	50.30	0.112
EMZ-ZIP	49.89	49.72	50.30	0.108

As can be seen in Figure 4.14(b), the TV-ZIP model was not able to identify the change in the scheduling of production activities; therefore, it presents a cumulative average error of about 45% in the analysis window (see Table 4.12). In contrast, the EMZ-ZIP model presents a lower cumulative error in the analysis window, specifically 17.198%. This is because the EMS in its routines includes a zone transition analysis (see Section 3.6). Then, in the case of the change in the scheduling of production activities, it can use the EMZ-ZIP zoning to advance the operating zone (see Figure 4.15(b)). Therefore, this feature presented by the EMZ-ZIP model contributes to reduce the SPSP consumption estimation error both in the analysis window (see Table 4.12) and in the whole operating day (see Table 4.10) which leads to reduce the error between the actual operating costs of the MG and those expected from the EMS which in this case is 2.511% as shown in Table 4.13. Finally, considering the results of Figure 4.16 and Table 4.14 it can be observed that the average operating frequency is closer to the nominal frequency (50 Hz) when the SPSP is represented using the EMZ-ZIP than the TV-ZIP model. In addition, the average operating frequency of the system in the period where the scheduling change occurs is closer to the nominal frequency (50 Hz) when using the EMZ-ZIP model. This is because of the zone transition analysis strategy of the EMZ-ZIP.

Case 2: In practical operating scenarios, some variability in the solar resource is expected, for example, due to cloudy days. In this sense, a random variable with uniform distribution was added to the original solar radiation profile. In addition, to evaluate the performance of the two models

(i.e., TV-ZIP and EMZ-ZIP) in representing the SPSP consumption under these variability conditions, a sensitivity analysis was performed. This consisted of adding the random variable with 10%, 20% or 30% of the value of each solar radiation profile measurement. The sensitivity analysis focused mainly on the performance of each model to represent the SPSP consumption and the difference between the actual operating costs and those obtained from the EMS. Figure 4.17(a) shows the results of the reference and generated power of the diesel generators, and the power generation profile of the PV unit and Figure 4.17(b) shows the power consumption profile of the SPSP simulated in the system and obtained from the EMS using the CP load model for 30% variability in the solar radiation profile. Figure 4.18 shows the same results but in this case the SPSP was represented using the EMZ-ZIP model. Table 4.15 presents a summary of the relative percentage error of the SPSP power consumption between simulated and obtained from the EMS for the sensitivity analysis, while Table 4.16 summarizes the relative percentage error between the simulated operating costs and those obtained from the EMS. The base case results correspond to those previously obtained with the original solar radiation profile.
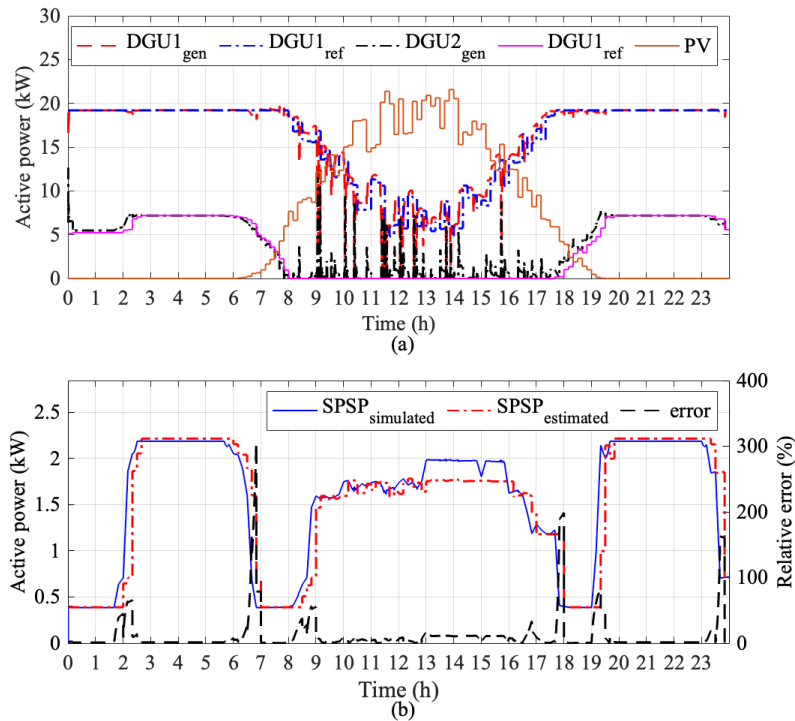
Figure 4.17 (a) Reference and generated power of the diesel generators, and the power generation profile of the PV unit, and (b) power consumption profile of the SPSP simulated and obtained from the EMS using the TV-ZIP load model for 30% variability in the solar radiation profile
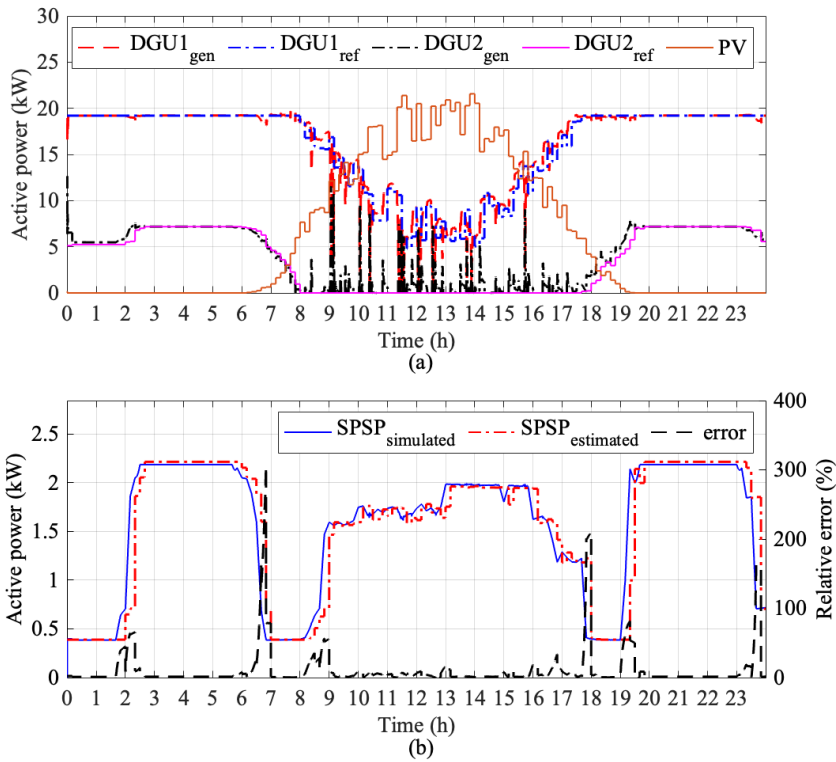
Figure 4.18 (a) Reference and generated power of the diesel generators, and the power generation profile of the PV unit, and (b) power consumption profile of the SPSP simulated and obtained from the EMS using the EMZ-ZIP load model for 30% variability in the solar radiation profile

Table 4.15 Summary of the sensitivity analysis results: relative percentage error of the SPSP power consumption between simulated and obtained from the EMS

Solar radiation var.	Load model	Avg. (%)	Min (%)	Max (%)
Base case	TV-ZIP	4.769	0.0053	27.356
	EMZ-ZIP	4.361	0.0049	29.356
10%	TV-ZIP	5.468	0.0015	47.181
	EMZ-ZIP	5.255	0.0019	47.182
20%	TV-ZIP	7.310	0.0030	85.175
	EMZ-ZIP	7.175	0.0024	85.175
30%	TV-ZIP	8.484	0.0039	139.314
	EMZ-ZIP	8.425	0.0039	139.311

Table 4.16 Summary of the sensitivity analysis results: relative percentage error between the simulated operating costs and those obtained from the EMS

Solar radiation var.	Load model	Avg. (%)	Min (%)	Max (%)
Base case	TV-ZIP	12.691	0.0011	305.529
	EMZ-ZIP	11.973	0.0013	305.259
10%	TV-ZIP	12.722	0.0028	305.309
	EMZ-ZIP	12.001	0.0082	305.309
20%	TV-ZIP	12.733	0.0019	305.356
	EMZ-ZIP	12.022	0.0085	305.356
30%	ZIP	12.746	0.0010	305.300
	EMZ-ZIP	12.039	0.0030	305.300

Overall, the results in Figure 4.17(a) and Figure 4.18(a) show that the variability in the solar radiation profile influences the operating setpoints sent from the EMS, since in certain periods the reference power of the DGU1 increases or decreases to cope with such variability. In addition, the local controllers are able to follow the power references sent from the EMS. However, DGU2 must generate power at certain times to maintain the balance between generation and demand, which is considerably affected by the variability of the solar radiation profile.

In addition, as expected, the variability in the solar resource considerably influences the performance of the load models when estimating SPSP consumption. This is evident in Table 4.15 since the error between the simulated and estimated power with the TV-ZIP model increases from 4.769% in the base case to 8.484% when the variability is 30%. Similarly, the error between the simulated and estimated power with the EMZ-ZIP model increases from 4.361% to 8.425%. This increase in the SPSP power consumption estimation error affects the expected costs in the EMS vs. the actual operating costs of the MG. However, in all scenarios of solar profile variability the EMZ-ZIP load model presents a lower error than the TV-ZIP model (see Table 4.16).

4.5   EMS computational performance

Table 4.17 shows the computing time required to reach convergence for each case presented above (i.e., operation of MG-EMS, change in planning of production activities and solar radiation variability) and for each model. We ran the computational experiment for each case and for each load model during a 24-hour period. We then averaged the time taken by the EMS each time it solves the optimization problem, these averages are illustrated in Table 4.17. Note that the EMS runs every 10 minutes. Thus, it runs 144 times over a 24-hour period. Table 4.17 shows that, in all the studied cases, the convergence time of the EMS that integrates the EMZ-ZIP model is almost the same as the CP and the TV-ZIP in all cases. This implies that, although the proposed approach is more elaborate, it does not significantly increase the solver time. Therefore, making it feasible for practical applications where the proposed approach can be implemented on a typical computer

used in rural MGs. It should be noted that no convergence problems were observed in all numerical exercises performed with the programmed EMS routines.

Table 4.17 Average time taken by the EMS to reach convergence for each case and for each load model

Case	Load model	Avg. time (sec)
Operation of MG-EMS	CP	1.988
	TV-ZIP	2.039
	EMZ-ZIP	2.043
Change in the scheduling of the SPSP production activities	TV-ZIP	1.865
	EMZ-ZIP	2.025
Solar radiation variability	TV-ZIP	2.202
	EMZ-ZIP	2.001

4.6   Discussion

In this chapter, a case study is presented in which the proposed methodology is applied to model SPSPs and integrate them into an EMS approach for the operation of a MG. To evaluate the performance of the EMZ-ZIP model, it is compared with two other alternatives (i.e., CP model and TV-ZIP) to represent the power consumption of the SPSP. The actual MG operating costs, the expected costs from the EMS, the SPSP power consumption simulated and obtained from the EMS, and the voltage levels at the generation and load buses are considered as performance indicators.

Firstly, using the MK result as a starting point for the GO method achieves better performance from a computational time point of view. This is because two main reasons: i) although the MK result is suboptimal, it is close to the global optimum; therefore, the GO method requires less time to reach the best solution, and ii) the McCormik's relaxations optimization model is a LP type which does not considerably increase the computational burden because it can be solved in polynomial time [179]. In addition, the number of variables of the EMZ-ZIP is relatively larger than the TV-ZIP model because of the EMZ-ZIP model structure (see Section 3.3). Therefore, it takes more time to estimate the parameters of the EMZ-ZIP model. Nevertheless, the total time span incurred to estimate the parameters of the EMZ-ZIP model for a representative day (i.e., 144 discrete time steps) is within a reasonable computational time, making it suitable for practical applications.

Secondly, the reduction of operating costs is evidenced by considering voltage-dependent load models. In this sense, using the proposed EMZ-ZIP model, the highest reduction in actual operating costs is achieved and the lowest relative error between the actual operating costs and the expected costs in the EMS. In addition, the ability of the EMZ-ZIP model to deal with considerable changes in the SPSP consumption profile due to a change in the scheduling of production activities is

remarkable both in the estimation of SPSP consumption and the operating frequency of the MG. Further, the sensitivity analysis, specifically the variability in the solar radiation profile evidence the robustness of the EMS when considering the EMZ-ZIP model to represent the productive process consumption. More specifically, despite the expected increase in the SPSP consumption estimation error and between the actual operating costs and those expected from the EMS, using the EMZ-ZIP model resulted in slight lower errors. In summary, these results reveal that the EMZ-ZIP model has a better performance compared to the other two considered alternatives to represent the complex electrical behavior of the SPSPs.

Finally, it should be noted that the benefits of the proposed EMZ-ZIP model versus the existing TV-ZIP model are relatively small. A comparative summary is presented in the following Table 4.18.

Table 4.18 Comparative summary of the results obtained using the EMZ-ZIP and the TV-ZIP models

	Description	EMZ-ZIP	TV-ZIP
Operation of MG-EMS	Relative error of the SPSP power consumption between simulated and obtained from the EMS (%)	12.0	12.7
	Difference between simulated operating costs and those obtained from the EMS (%)	4.4	4.8
	Average reduction in MG operating costs (%)	4.8	4.8
Change in the scheduling of the SPSP production activities	Relative error of the SPSP power consumption between simulated and obtained from the EMS for the three-hour analysis window (%)	17.2	45.2
	Difference between simulated operating costs and those obtained from the EMS for the three-hour analysis window (%)	2.5	3.7
	Relative error of the SPSP power consumption between simulated and obtained from the EMS for the whole operating day (%)	12.2	15.2
	Difference between simulated operating costs and those obtained from the EMS for the whole operating day (%)	4.3	4.8
Solar radiation variability	Average relative error of the SPSP power consumption between simulated and obtained from the EMS for a 10% in solar radiation variability (%)	5.3	5.5
	Average relative error between the simulated operating costs and those obtained from the EMS for a 10% in solar radiation variability (%)	12.0	12.7

The EMZ-ZIP approach dominates the overall performance indexes (costs and prediction errors) with values between 2.5% and 17.2%. Thus, the additional benefits seem to be relatively small for a proposal that is more complex than the TV-ZIP one. Nevertheless, the EMZ-ZIP approach also involves the zone definition and transition strategies where the benefits obtained in reducing the SPSP consumption estimation error are much more relevant (17.2%) than the TV-ZIP (45.2%). Moreover, it should be noted that the proposed zone definition strategy is not feasible for the conventional TV-ZIP approach. This is because the zone definition requires the information collected from surveys and ZIP model databases, which are part of the EMZ-ZIP proposal. Furthermore, as described above, the increased complexity of the EMZ-ZIP is manageable from the perspective of computational requirements and convergence.

It should be noted that, although the differences in percentages between the results of the EMZ-ZIP and TV-ZIP models are relatively small, achieving a decrease in the operating costs of MGs installed in remote locations would directly imply an increase in the autonomy of such MGs. This is because the fossil fuel-based generation units would be used in a better way. Therefore, it is expected that fuel consumption will be lower leading to an increase in the autonomy of the MGs and a reduction in other associated costs such as fuel logistics and transportation.

5 Conclusions and Future work

5.1 Conclusions

In this thesis, a methodology for modeling the SPSPs that include electrical devices and their integration into an EMS for an MG has been proposed. The voltage-dependence and the complex electrical consumption of the SPSPs was addressed through a novel extended multi-zone ZIP load model. This model employs information of the electrical devices that the SPSPs may include and the time of use of energy of these devices obtained through semi-structured surveys. With this information, first, a relational database is created that includes the ZIP models of the devices that may have SPSPs. Second, an extended ZIP model is developed combining a flexible ZIP component and the ZIP models of the devices that belong to an SPSP. Then, through a zoning procedure and using the information obtained from the surveys, the zones and the devices that may be active in each zone are identified. This is useful primarily for two reasons: i) it reduces the complexity for parameter identification and ii) it improves the representation of the sensitivity of the SPSP loads to voltage variations. Next, based on a BAM approach an integration of the EMZ-ZIP model to an EMS for the operation of an MG was proposed.

The semi-structured survey plays a key role in collecting information regarding the structure of the SPSP, i.e., the electrical devices it may include and their time of use of energy. Further, with the information of the SPSP structure, it is feasible to create a database which contains the ZIP models of the devices that the SPSP may contain. It should be noted that this database is the main source of information for all stages of the methodology presented in Section 3. Moreover, the time of use of energy information was used to analyze the influence of external weather variables on the operation of the SPSP devices and to determine the operation zones used in the training stage of the ANN.

The GO strategy showed excellent performance in dealing with non-convexities due to the product of the bilinear terms of the flexible component of the EMZ-ZIP model. In addition, when using the result of the McCormick's relaxations as a starting point for GO, the size (i.e., number of decision variables) of the resulting GO-MK problem increases significantly. Nevertheless, the computational time required to estimate the model parameters is considerably reduced compared to using a random starting point. This is due to two main reasons. First, although the MK result is suboptimal, it is close to the global optimum; therefore, the GO method requires less time to reach the best solution. Second, the McCormik's relaxations optimization model is a LP type which does not considerably increase the computational burden because it can be solved in polynomial time.

The benefits of considering physical representation models to capture the voltage dependence of the SPSP loads was evidenced. This is because by considering the voltage effect, a considerable reduction of the actual MG operating costs was obtained, especially when considering the EMZ-ZIP model, while the bus voltages remain within normal operating ranges. These results are explained by the fact that when considering voltage sensitive load models as an integral part of an AC-based EMS approach, it will try to decrease the voltage at the load buses close to the minimum allowed value to reduce the power consumption; hence, minimizing the operating costs [133].

Overall, the EMZ-ZIP approach dominates performance indexes such as costs and prediction errors. Thus, the additional benefits seem to be relatively small for a proposal that is more complex than the TV-ZIP model. Nevertheless, the EMZ-ZIP approach also involves the zone definition and transition strategies where the benefits obtained in reducing the SPSP consumption estimation error are much more relevant than the TV-ZIP. This is an important feature when considering practical operating scenarios, e.g., change in the scheduling of SPSPs production activities. Moreover, it should be noted that the proposed zone definition strategy is not feasible for the conventional TV-ZIP approach. This is because the zone definition requires the information collected from surveys and ZIP model databases, which are part of the EMZ-ZIP proposal. Furthermore, the increased complexity of the EMZ-ZIP is manageable from the perspective of computational requirements and convergence to solve the parameter estimation problem and the EMS optimization problem by integrating the EMZ-ZIP model.

Finally, our results provide compelling evidence for modeling the SPSPs through an EMZ-ZIP load model to provide technical and economic benefits to the MG. Therefore, this work indicates the advantages gained from extending and zoning the TV-ZIP load model to represent the complicated electrical behavior of SPSPs, which is influenced by voltage variations and external weather variables.

5.2 Future work

Although the proposed methodology for modeling the SPSPs and their integration into an EMS for a MG is novel, future work will focus on the following aspects:

- In this work we considered the electricity consumption measurements of the SPSPs, however, some may include DG which leads to the measurements being the net demand. This may affect the structure of the proposed load model, the zoning procedure, and the parameter identification procedure. Therefore, further work is planned on this topic. For example, the approach to include DG in the load models presented in [219] may be used.

- Although analysis blocks 1 and 2 (see Section 3) are described methodologically, they were not fully addressed in this thesis. In this sense, future work will focus on developing these blocks of analysis and incorporating them into the proposed methodology.

- The complete development of the aforementioned analysis blocks will lead to a complex interaction between the blocks and mainly the zone classifier because the commands indicating the re-execution of certain stages of the proposed methodology would be modified. Therefore, a further analysis of this interaction should be conducted.

- Phase unbalances are relevant and impactful in MGs because they can lead to deviations of the optimal dispatch strategy or the inability of the system to meet reactive power requirements [41]. Therefore, a further analysis of these conditions considering SPSPs as part of the system should be studied.

- Uncertainty in the renewables forecast can significantly affect dispatch decisions in the MG. Therefore, future work will focus on analyzing strategies to deal with uncertainty, e.g., model predictive control [26], among others.

- Finally, the proposed methodology can be applied in other contexts such as industrial plants, which are connected to the main grid as part of an overall distribution EMS considering industrial flexibility mechanisms. Preliminary results of these extensions are presented in Annexed F.

Bibliography

[1] United Nations, "Sustainable Development Goals." [Online]. Available: https://sdgs.un.org/es/goals. [Accessed: 19-Nov-2021].

[2] Ministerio de Energía, "Energía 2050: Política Energética de Chile." [Online]. Available: https://www.energia.gob.cl/sites/default/files/energia_2050_-_politica_energetica_de_chile.pdf. [Accessed: 09-Jun-2020].

[3] G. Jimenez-Estevez, R. Palma-Behnke, R. R. Latorre, and L. Moran, "Heat and Dust: The Solar Energy Challenge in Chile," *IEEE Power Energy Mag.*, vol. 13, no. 2, pp. 71–77, 2015.

[4] Ministerio de Energía, "Anuario Estadístico de Energía 2018." [Online]. Available: https://www.cne.cl/wp-content/uploads/2019/04/Anuario-CNE-2018.pdf. [Accessed: 09-Jun-2020].

[5] Revista Electricidad, "Generación eléctrica: 17 proyectos entrarán en operación en 2020," 2019. [Online]. Available: https://www.revistaei.cl/2019/12/23/generacion-electrica-17-proyectos-entraran-en-operacion-en-2020/#. [Accessed: 09-Jun-2020].

[6] P. Ramirez-Del-Barrio *et al.*, "Sustainable development through the use of solar energy for productive processes: The Ayllu Solar Project," in *2017 IEEE Global Humanitarian Technology Conference (GHTC)*, 2017, pp. 1–8.

[7] A. M. Adil and Y. Ko, "Socio-technical evolution of Decentralized Energy Systems: A critical review and implications for urban planning and policy," *Renew. Sustain. Energy Rev.*, vol. 57, pp. 1025–1037, 2016.

[8] BayWa r.e., "White paper: Grid parity and the solar renaissance", May, 2019.

[9] E. Wood, "Navigant Counts 126 New Microgrid Projects & Other News from Ameresco, Demand Energy and UET".

[10] N. Hatziargyriou, *Microgrid: architectures and control*, 1st ed. Wiley-IEEE Press, 2014.

[11] J. Barrientos, J. D. López, and F. Valencia, "A Novel Stochastic-Programming-Based Energy Management System to Promote Self-Consumption in Industrial Processes," *Energies*, vol. 11, no. 2. 2018.

[12] Z. Liu, J. Yang, W. Jiang, C. Wei, P. Zhang, and J. Xu, "Research on Optimized Energy Scheduling of Rural Microgrid," *Applied Sciences*, vol. 9, no. 21. 2019.

[13] M. S. U. R. Mahadi, R. Alam, and D. Fernández, "Designing a solar microgrid system for powering an off-grid fish hatchery and nearby households in Bangladesh," *AIP Conf. Proc.*, vol. 1980, no. 1, 2018.

[14] G. Mohy-ud-din, D. H. Vu, K. M. Muttaqi, and D. Sutanto, "An Integrated Energy

Management Approach for the Economic Operation of Industrial Microgrids Under Uncertainty of Renewable Energy," *IEEE Trans. Ind. Appl.*, vol. 56, no. 2, pp. 1062–1073, 2020.

[15] J. Barrientos, J. D. López, and F. Valencia, "Adaptive Energy Management System for Self-consumption in Productive Processes," in *Applied Computer Sciences in Engineering*, 2018, pp. 16–27.

[16] A. Arif, Z. Wang, J. Wang, B. Mather, H. Bashualdo, and D. Zhao, "Load Modeling—A Review," *IEEE Trans. Smart Grid*, vol. 9, no. 6, pp. 5986–5999, 2018.

[17] H. Shayeghi, E. Shahryari, M. Moradzadeh, and P. Siano, "A Survey on Microgrid Energy Management Considering Flexible Energy Sources," *Energies*, vol. 12, no. 11. 2019.

[18] F. Valencia, J. Collado, D. Sáez, and L. G. Marín, "Robust Energy Management System for a Microgrid Based on a Fuzzy Prediction Interval Model," *IEEE Trans. Smart Grid*, vol. 7, no. 3, pp. 1486–1494, 2016.

[19] D. Sáez, F. Ávila, D. Olivares, C. Cañizares, and L. Marín, "Fuzzy Prediction Interval Models for Forecasting Renewable Resources and Loads in Microgrids," *IEEE Trans. Smart Grid*, vol. 6, no. 2, pp. 548–556, 2015.

[20] F. Valencia, D. Sáez, J. Collado, F. Ávila, A. Marquez, and J. J. Espinosa, "Robust Energy Management System Based on Interval Fuzzy Models," *IEEE Trans. Control Syst. Technol.*, vol. 24, no. 1, pp. 140–157, 2016.

[21] H. Chitsaz, H. Shaker, H. Zareipour, D. Wood, and N. Amjady, "Short-term electricity load forecasting of buildings in microgrids," *Energy Build.*, vol. 99, pp. 50–60, 2015.

[22] L. Hernández, C. Baladrón, J. M. Aguiar, B. Carro, A. Sánchez-Esguevillas, and J. Lloret, "Artificial neural networks for short-term load forecasting in microgrids environment," *Energy*, vol. 75, pp. 252–264, 2014.

[23] C. W. Lou and M. C. Dong, "A novel random fuzzy neural networks for tackling uncertainties of electric load forecasting," *Int. J. Electr. Power Energy Syst.*, vol. 73, pp. 34–44, 2015.

[24] A. K. Singh, Ibraheem, S. Khatoon, M. Muazzam, and D. K. Chaturvedi, "Load forecasting techniques and methodologies: A review," in *2012 2nd International Conference on Power, Control and Embedded Systems*, 2012, pp. 1–10.

[25] B. Yildiz, J. I. Bilbao, and A. B. Sproul, "A review and analysis of regression and machine learning models on commercial building electricity load forecasting," *Renew. Sustain. Energy Rev.*, vol. 73, pp. 1104–1122, 2017.

[26] B. V Solanki, A. Raghurajan, K. Bhattacharya, and C. A. Cañizares, "Including Smart Loads for Optimal Demand Response in Integrated Energy Management Systems for Isolated

Microgrids," *IEEE Trans. Smart Grid*, vol. 8, no. 4, pp. 1739–1748, 2017.

[27] A. Adadi and M. Berrada, "Peeking Inside the Black-Box: A Survey on Explainable Artificial Intelligence (XAI)," *IEEE Access*, vol. 6, pp. 52138–52160, 2018.

[28] S. Chatzivasileiadis, A. Venzke, J. Stiasny, and G. Misyris, "Machine Learning in Power Systems: Is It Time to Trust It?," *IEEE Power Energy Mag.*, vol. 20, no. 3, pp. 32–41, 2022.

[29] B. Lepri, N. Oliver, E. Letouzé, A. Pentland, and P. Vinck, "Fair, Transparent, and Accountable Algorithmic Decision-making Processes," *Philos. Technol.*, vol. 31, no. 4, pp. 611–627, 2018.

[30] S. Park, J. Moon, and E. Hwang, "Explainable Anomaly Detection for District Heating Based on Shapley Additive Explanations," in *2020 International Conference on Data Mining Workshops (ICDMW)*, 2020, pp. 762–765.

[31] J. Moon, S. Park, S. Rho, and E. Hwang, "Interpretable Short-Term Electrical Load Forecasting Scheme Using Cubist," *Comput. Intell. Neurosci.*, vol. 2022, p. 6892995, 2022.

[32] M. Sadeghi and G. A. sarvi, "Determination of ZIP parameters with least squares optimization method," in *2009 IEEE Electrical Power & Energy Conference (EPEC)*, 2009, pp. 1–6.

[33] A. Bokhari *et al.*, "Experimental Determination of the ZIP Coefficients for Modern Residential, Commercial, and Industrial Loads," *IEEE Trans. Power Deliv.*, vol. 29, no. 3, pp. 1372–1381, 2014.

[34] M. Bircan, A. Durusu, B. Kekezoglu, O. Elma, and U. S. Selamogullari, "Experimental determination of ZIP coefficients for residential appliances and ZIP model based appliance identification: The case of YTU Smart Home," *Electr. Power Syst. Res.*, vol. 179, p. 106070, 2020.

[35] M. Leinakse, G. Andreesen, P. Tani, and J. Kilter, "Estimation of Exponential and ZIP Load Model of Aggregated Load with Distributed Generation," in *2021 IEEE 62nd International Scientific Conference on Power and Electrical Engineering of Riga Technical University (RTUCON)*, 2021, pp. 1–6.

[36] U. Eminoglu and M. H. Hocaoglu, "A new power flow method for radial distribution systems including voltage dependent load models," *Electr. Power Syst. Res.*, vol. 76, no. 1, pp. 106–114, 2005.

[37] J. Milanović, K. Yamashita, S. Martinez, S. Djokić, and L. Korunović, "International industry practice on power system load modelling," in *2014 IEEE PES General Meeting | Conference & Exposition*, 2014, p. 1.

[38] C. Wang, Z. Wang, J. Wang, and D. Zhao, "SVM-Based Parameter Identification for Composite ZIP and Electronic Load Modeling," *IEEE Trans. Power Syst.*, vol. 34, no. 1, pp.

182–193, 2019.

[39]   A. M. A. Haidar, K. M. Muttaqi, and M. H. Haque, "Multistage time-variant electric vehicle load modelling for capturing accurate electric vehicle behaviour and electric vehicle impact on electricity distribution grids," *IET Gener. Transm. Distrib.*, vol. 9, no. 16, pp. 2705–2716, 2015.

[40]   D. Espín-Sarzosa, R. Palma-Behnke, and O. Núñez-Mata, "Energy Management Systems for Microgrids: Main Existing Trends in Centralized Control Architectures," *Energies*, vol. 13, no. 3. 2020.

[41]   D. E. Olivares, C. A. Cañizares, and M. Kazerani, "A Centralized Energy Management System for Isolated Microgrids," *IEEE Trans. Smart Grid*, vol. 5, no. 4, pp. 1864–1875, 2014.

[42]   GIZ, "Productive Use of Energy – PRODUSE: Measuring Impacts of Electrification on Small and Micro-Enterprises in Sub-Saharan Africa," Eschborn, Germany, 2013.

[43]   S. Fan, D. Nyange, and N. Rao, "Public Investment and Poverty Reduction in Tanzania: Evidence from Household Survey Data," Washington, DC, DSGD Discussion Paper No. 18, 2005.

[44]   Asian Development Bank, "Assessing the Impact of Transport and Energy Infrastructure on Poverty Reduction," Mandaluyong, 2005.

[45]   T. Bernard, M. Torero, and A. Teffera, "Welfare impact of Rural Electrification, 'Short term' evidence from Ethiopia: A Report for the Ethiopian Electric Power Corporation and the World Bank," 2009.

[46]   A. L. Kooijman-van Dijk, "The role of energy in creating opportunities for income generation in the Indian Himalayas," *Energy Policy*, vol. 41, pp. 529–536, 2012.

[47]   A. Brüderle, B. Attigah, and M. Bodenbender, "Productive Use of Energy – PRODUSE: A Manual for Electrification Practitioners," Eschborn, 2011.

[48]   L. Mayer-Tasch, "Promoting Productive Use of Energy in the Framework of Energy Access Programmes." Addis Abeba, 2013.

[49]   S. Booth, X. Li, I. Baring-Gould, D. Kollanyi, A. Bharadwaj, and P. Weston, "Productive Use of Energy in African Micro-Grids: Technical and Business Considerations," United States, 2018.

[50]   J. Terrapon-Pfaff, M.-C. Gröne, C. Dienst, and W. Ortiz, "Productive use of energy – Pathway to development? Reviewing the outcomes and impacts of small-scale energy projects in the global south," *Renew. Sustain. Energy Rev.*, vol. 96, pp. 198–209, 2018.

[51]   World Bank Group, "The Welfare Impact of Rural Electrification: A Reassessment of the Costs and Benefits," Washington, DC, USA, 2008.

[52] R. Román *et al.*, *La fuerza del Sol*, 1st Editio. Santiago, Chile: BigBang Productora de Contenidos, 2017.

[53] G. Frick and J. Hirschmann, "Theory and experience with solar stills in Chile," *Sol. Energy*, vol. 14, no. 4, pp. 405–413, 1973.

[54] H. Rodríguez, "Barrier removal for rural electrification with renewable energies," Santiago, Chile, HR/251-2012/PNUD-GEF, 2012.

[55] Ministerio de Energía, "Ley 20.698: Propicia la ampliación de la matriz energética mediante fuentes renovables no convencionales (Support for power system expansion with renewable systems)." Congreso Nacional de Chile (National Congress of Chile), Santiago, Chile, 2013.

[56] J. Haas *et al.*, "Sunset or sunrise? Understanding the barriers and options for the massive deployment of solar technologies in Chile," *Energy Policy*, vol. 112, pp. 399–414, 2018.

[57] World Bank Group, "SOLARGIS," 2021. [Online]. Available: https://solargis.com/maps-and-gis-data/download/world. [Accessed: 02-Dec-2021].

[58] Comisión Nacional de Energía, "Energía Abierta," *Capacidad instalada*, 2021. [Online]. Available: http://energiaabierta.cl/visualizaciones/capacidad-instalada/. [Accessed: 09-Dec-2021].

[59] Comisón Nacional de Energía, "Anuario estadístico de energía 2019," *Anuario Sector Energético*, 2019. .

[60] G. A. Jimenez-Estevez, R. Palma-Behnke, D. Ortiz-Villalba, O. N. Mata, and C. S. Montes, "It Takes a Village: Social SCADA and Approaches to Community Engagement in Isolated Microgrids," *IEEE Power Energy Mag.*, vol. 12, no. 4, pp. 60–69, 2014.

[61] Comisión Nacional de Energía, "Reporte Mensual ERNC," Santiago, Chile, 2017.

[62] S. Feron, H. Heinrichs, and R. R. Cordero, "Sustainability of rural electrification programs based on off-grid photovoltaic (PV) systems in Chile," *Energy. Sustain. Soc.*, vol. 6, no. 1, p. 32, 2016.

[63] GreenLabUC, "Estimación de Parámetros para Cuantificación de Beneficios Sociales y Externalidades en Proyectos de Energización," Santiago, Chile, 2012.

[64] P. Ramírez-Del-Barrio, F. Valencia, A. Marconi-Vargas, I. Polanco-Lobos, and P. Mendoza-Araya, "An alpaca fiber processing solution based on Solar energy for an isolated location in Chile following a co-construction approach," in *2017 IEEE Mexican Humanitarian Technology Conference (MHTC)*, 2017, pp. 130–136.

[65] United Nations, "Promoting the Use of Electric Water Pumps for Irrigation in Sudan," *Promoting the Use of Electric Water Pumps for Irrigation in Sudan*, 2021. [Online]. Available: https://sustainabledevelopment.un.org/partnership/?p=30762. [Accessed: 17-Dec-2021].

[66] S. Senthil Kumar, C. Bibin, K. Akash, K. Aravindan, M. Kishore, and G. Magesh, "Solar powered water pumping systems for irrigation: A comprehensive review on developments and prospects towards a green energy approach," *Mater. Today Proc.*, vol. 33, pp. 303–307, 2020.

[67] D. L. Fenton, G. H. Abernathy, G. A. Krivokapich, and J. V Otts, "Operation and evaluation of the Willard solar thermal power irrigation system," *Sol. Energy*, vol. 32, no. 6, pp. 735–751, 1984.

[68] S. S. Chandel, M. Nagaraju Naik, and R. Chandel, "Review of solar photovoltaic water pumping system technology for irrigation and community drinking water supplies," *Renew. Sustain. Energy Rev.*, vol. 49, pp. 1084–1099, 2015.

[69] J. Velasco, "Cosecha de energía fotovoltaica para uso en riego," *Cosecha de energía fotovoltaica para uso en riego*, 2017. [Online]. Available: https://www.redagricola.com/cl/cosecha-energia-fotovoltaica-uso-riego/. [Accessed: 17-Dec-2021].

[70] R. Carbone, C. De Capua, and R. Morello, "Photovoltaic systems for powering greenhouses," in *2011 International Conference on Clean Electrical Power (ICCEP)*, 2011, pp. 474–479.

[71] T. Alinejad, M. Yaghoubi, and A. Vadiee, "Thermo-environomic assessment of an integrated greenhouse with an adjustable solar photovoltaic blind system," *Renew. Energy*, vol. 156, pp. 1–13, 2020.

[72] A. Vadiee and V. Martin, "Energy management in horticultural applications through the closed greenhouse concept, state of the art," *Renew. Sustain. Energy Rev.*, vol. 16, no. 7, pp. 5087–5100, 2012.

[73] M. Green and D. Schwarz, "Solar Drying Technology for Food Preservation," Jan. 2001.

[74] M. A. Aravindh and A. Sreekumar, "Solar Drying—A Sustainable Way of Food Processing," in *Green Energy and Technology*, A. Sharma and S. Kar, Eds. New Delhi: Springer, 2015, pp. 27–46.

[75] J. Meruane and M. Morales, "The northern river shrimp Cryphiops caementarius (Decapoda, Palaemonidae), research chronology between 1958 and 2008, II: Aquaculture research and development in Northern Chile," *Crustaceana*, vol. 86, pp. 1452–1467, Nov. 2013.

[76] C. Ferreccio and A. M. Sancha, "Arsenic exposure and its impact on health in Chile," *J. Health. Popul. Nutr.*, vol. 24, no. 2, pp. 164–175, 2006.

[77] V. Silva-Pinto, B. Arrianza, and V. Standen, "Evaluación de la frecuencia de espina bífida oculta y su posible relación con el arsénico ambiental en una muestra prehispánica de la Quebrada de Camarones, norte de Chile," *Rev. Med. Chil.*, vol. 138, no. 4, pp. 461–469, 2010.

[78]   SERC-Chile, "Ayllu Solar," *What is Ayllu Solar?*, 2021. [Online]. Available: https://ayllusolar.cl/en/iniciative/. [Accessed: 10-Dec-2021].

[79]   C. Tirado Echavarria, A. Cortés, M. Carretero, and F. Bozinovic, "Does the presence of livestock alter the trophic behaviour of sympatric populations of wild camelids Vicugna vicugna Molina 1782 and Lama guanicoe Müller 1976 (Artiodactyla: Camelidae)? Evidence from Central Andes," *Gayana*, vol. 80, pp. 29–39, Mar. 2016.

[80]   S. Schmid, "The value chain of alpaca fiber in Peru, an economic analysis," ETH Zürich, 2006.

[81]   B. Lasseter, "Microgrids [distributed power generation]," in *2001 IEEE Power Engineering Society Winter Meeting. Conference Proceedings (Cat. No.01CH37194)*, 2001, vol. 1, pp. 146–149 vol.1.

[82]   R. H. Lasseter, "MicroGrids," in *2002 IEEE Power Engineering Society Winter Meeting. Conference Proceedings (Cat. No.02CH37309)*, 2002, vol. 1, pp. 305–308 vol.1.

[83]   H. Shayeghi and M. Alilou, "3 - Distributed generation and microgrids," E. B. T.-H. R. E. S. and M. Kabalci, Ed. Academic Press, 2021, pp. 73–102.

[84]   T. S. Ustun, C. Ozansoy, and A. Zayegh, "Recent developments in microgrids and example cases around the world—A review," *Renew. Sustain. Energy Rev.*, vol. 15, no. 8, pp. 4030–4041, 2011.

[85]   A. H. Hubble and T. S. Ustun, "Scaling renewable energy based microgrids in underserved communities: Latin America, South Asia, and Sub-Saharan Africa," in *2016 IEEE PES PowerAfrica*, 2016, pp. 134–138.

[86]   C. Bustos and D. Watts, "Novel methodology for microgrids in isolated communities: Electricity cost-coverage trade-off with 3-stage technology mix, dispatch & configuration optimizations," *Appl. Energy*, vol. 195, pp. 204–221, 2017.

[87]   M. Castilla *et al.*, "The growing state of distributed generation and microgrids in the Ibero-American region: A view from the RIGMEI network," in *2014 IEEE PES Transmission & Distribution Conference and Exposition - Latin America (PES T&D-LA)*, 2014, pp. 1–6.

[88]   C. Strunck, C. Rehtanz, D. Espín-Sarzosa, and R. Palma-Behnke, "Control Possibilities for Community Microgrids Considering Small Production Processes and its Benefits to the Whole System," in *2020 IEEE PES Transmission & Distribution Conference and Exhibition - Latin America (T&D LA)*, 2020, pp. 1–6.

[89]   R. Palma-Behnke *et al.*, "Lowering Electricity Access Barriers by Means of Participative Processes Applied to Microgrid Solutions: The Chilean Case," *Proc. IEEE*, vol. 107, no. 9, pp. 1857–1871, 2019.

[90]   D. E. Olivares *et al.*, "Trends in Microgrid Control," *IEEE Trans. Smart Grid*, vol. 5, no. 4,

pp. 1905–1919, 2014.

[91] F. Mumtaz and I. S. Bayram, "Planning, Operation, and Protection of Microgrids: An Overview," *Energy Procedia*, vol. 107, pp. 94–100, 2017.

[92] S. Chandak and P. Rout, "Seamless transition of microgrid between islanded and grid-connected mode of operation," *IET Energy Syst. Integr.*, Jan. 2021.

[93] S. D'silva, M. Shadmand, S. Bayhan, and H. Abu-Rub, "Towards Grid of Microgrids: Seamless Transition between Grid-Connected and Islanded Modes of Operation," *IEEE Open J. Ind. Electron. Soc.*, vol. 1, pp. 66–81, 2020.

[94] A. Bidram and A. Davoudi, "Hierarchical Structure of Microgrids Control System," *IEEE Trans. Smart Grid*, vol. 3, no. 4, pp. 1963–1976, 2012.

[95] A. Anvari-Moghaddam, H. Abdi, B. Mohammadi-Ivatloo, and N. Hatziargyriou, *Microgrids: Advances in Operation, Control, and Protection*. Springer International Publishing, 2021.

[96] G. Liu, T. B. Ollis, B. Xiao, X. Zhang, and K. Tomsovic, "Community Microgrid Scheduling Considering Network Operational Constraints and Building Thermal Dynamics," *Energies*, vol. 10, no. 10. 2017.

[97] R. Palma-Behnke *et al.*, "A Microgrid Energy Management System Based on the Rolling Horizon Strategy," *IEEE Trans. Smart Grid*, vol. 4, no. 2, pp. 996–1006, 2013.

[98] Y. Han, K. Zhang, H. Li, E. A. A. Coelho, and J. M. Guerrero, "MAS-Based Distributed Coordinated Control and Optimization in Microgrid and Microgrid Clusters: A Comprehensive Overview," *IEEE Trans. Power Electron.*, vol. 33, no. 8, pp. 6488–6508, 2018.

[99] E. Espina, J. Llanos, C. Burgos-Mellado, R. Cárdenas-Dobson, M. Martínez-Gómez, and D. Sáez, "Distributed Control Strategies for Microgrids: An Overview," *IEEE Access*, vol. 8, pp. 193412–193448, 2020.

[100] K. Sakurama and M. Miura, "Communication-Based Decentralized Demand Response for Smart Microgrids," *IEEE Trans. Ind. Electron.*, vol. 64, no. 6, pp. 5192–5202, 2017.

[101] M. Saleh, Y. Esa, M. E. Hariri, and A. Mohamed, "Impact of Information and Communication Technology Limitations on Microgrid Operation," *Energies*, vol. 12, no. 15. 2019.

[102] D. Y. Yamashita, I. Vechiu, and J.-P. Gaubert, "A review of hierarchical control for building microgrids," *Renew. Sustain. Energy Rev.*, vol. 118, p. 109523, 2020.

[103] T. A. Papadopoulos, E. N. Tzanidakis, P. N. Papadopoulos, P. Crolla, G. K. Papagiannis, and G. M. Burt, "Aggregate load modeling in microgrids using online measurements," in *MedPower 2014*, 2014, pp. 1–8.

[104] G. E. P. Box, G. M. Jenkins, and H. Day, *Time Series Analysis: Forecasting and Control*. Holden-Day, 1976.

[105] C. Kuster, Y. Rezgui, and M. Mourshed, "Electrical load forecasting models: A critical systematic review," *Sustain. Cities Soc.*, vol. 35, pp. 257–270, 2017.

[106] Y. Zhai, *Time Series Forecasting Competition Among Three Sophisticated Paradigms*. University of North Carolina at Wilmington, 2005.

[107] E. H. K. Fung, Y. K. Wong, H. F. Ho, and M. P. Mignolet, "Modelling and prediction of machining errors using ARMAX and NARMAX structures," *Appl. Math. Model.*, vol. 27, no. 8, pp. 611–627, 2003.

[108] B. Wang, N. Tai, H. Zhai, J. Ye, J. Zhu, and L. Qi, "A new ARMAX model based on evolutionary algorithm and particle swarm optimization for short-term load forecasting," *Electr. Power Syst. Res.*, vol. 78, no. 10, pp. 1679–1685, 2008.

[109] M. A. Hammad, B. Jereb, B. Rosi, and D. Dragan, "Methods and Models for Electric Load Forecasting: A Comprehensive Review," *Logist. Sustain. Transp.*, vol. 11, pp. 51–76, Feb. 2020.

[110] M. Paliwal and U. A. Kumar, "Neural networks and statistical techniques: A review of applications," *Expert Syst. Appl.*, vol. 36, no. 1, pp. 2–17, 2009.

[111] L. Hernandez, C. Baladrón, J. M. Aguiar, B. Carro, A. J. Sanchez-Esguevillas, and J. Lloret, "Short-Term Load Forecasting for Microgrids Based on Artificial Neural Networks," *Energies*, vol. 6, no. 3. 2013.

[112] W.-C. Hong, "Electric load forecasting by support vector model," *Appl. Math. Model.*, vol. 33, no. 5, pp. 2444–2454, 2009.

[113] K. Zor, O. Timur, and A. Teke, "A state-of-the-art review of artificial intelligence techniques for short-term electric load forecasting," in *2017 6th International Youth Conference on Energy (IYCE)*, 2017, pp. 1–7.

[114] S. R. Abbas and M. Arif, "Electric Load Forecasting Using Support Vector Machines Optimized by Genetic Algorithm," in *2006 IEEE International Multitopic Conference*, 2006, pp. 395–399.

[115] S. Fan and L. Chen, "Short-term load forecasting based on an adaptive hybrid method," *IEEE Trans. Power Syst.*, vol. 21, no. 1, pp. 392–401, 2006.

[116] G. kaur and M. Singh, "Electric Load and Solar Irradiance Forecasting in Microgrid using High Order MIMO Fuzzy Logic Approach," *Int. J. Adv. Eng. Res. Sci.*, vol. 6, pp. 329–336, Jan. 2019.

[117] M. Faysal, M. Islam, M. Murad, M. Islam, and M. Amin, "Electrical Load Forecasting Using Fuzzy System," *J. Comput. Commun.*, vol. 7, no. 9, pp. 27–37, 2019.

[118] T. Hong and P. Wang, "Fuzzy interaction regression for short term load forecasting," *Fuzzy Optim. Decis. Mak.*, vol. 13, Mar. 2014.

[119] R. Mamlook, O. Badran, and E. Abdulhadi, "A fuzzy inference model for short-term load forecasting," *Energy Policy*, vol. 37, no. 4, pp. 1239–1248, 2009.

[120] V. N. Coelho *et al.*, "A self-adaptive evolutionary fuzzy model for load forecasting problems on smart grid environment," *Appl. Energy*, vol. 169, pp. 567–584, 2016.

[121] T. Faulwasser, A. Engelmann, T. Mühlpfordt, and V. Hagenmeyer, *Optimal Power Flow: An Introduction to Predictive, Distributed and Stochastic Control Challenges*. 2018.

[122] Z. Yuan, "Convex Optimal Power Flow Based on Second-Order Cone Programming: Models, Algorithms and Applications," Universidad Pontificia Comillas, 2018.

[123] A. Sani Hassan, L. Cipcigan, and N. Jenkins, "Impact of optimised distributed energy resources on local grid constraints," *Energy*, vol. 142, pp. 878–895, 2018.

[124] A. McIlvenna, "Exploring Optimization Techniques for an Existing Microgrid and the Unit Commitment with AC Optimal Power Flow Problem," University of Tennessee, 2019.

[125] A. Venzke, S. Chatzivasileiadis, and D. K. Molzahn, "Inexact convex relaxations for AC optimal power flow: Towards AC feasibility," *Electr. Power Syst. Res.*, vol. 187, p. 106480, 2020.

[126] S. Salinas, M. Li, P. Li, and Y. Fu, "Dynamic Energy Management for the Smart Grid With Distributed Energy Resources," *IEEE Trans. Smart Grid*, vol. 4, no. 4, pp. 2139–2151, 2013.

[127] Y. Huang, S. Mao, and R. M. Nelms, "Adaptive Electricity Scheduling in Microgrids," *IEEE Trans. Smart Grid*, vol. 5, no. 1, pp. 270–281, 2014.

[128] S. Sun, M. Dong, and B. Liang, "Joint supply, demand, and energy storage management towards microgrid cost minimization," in *2014 IEEE International Conference on Smart Grid Communications (SmartGridComm)*, 2014, pp. 109–114.

[129] W. Shi, N. Li, C. Chu, and R. Gadh, "Real-Time Energy Management in Microgrids," *IEEE Trans. Smart Grid*, vol. 8, no. 1, pp. 228–238, 2017.

[130] G. Liu, T. Jiang, T. B. Ollis, X. Zhang, and K. Tomsovic, "Distributed energy management for community microgrids considering network operational constraints and building thermal dynamics," *Appl. Energy*, vol. 239, pp. 83–95, 2019.

[131] A. Paudel, M. Khorasany, and H. B. Gooi, "Decentralized Local Energy Trading in Microgrids With Voltage Management," *IEEE Trans. Ind. Informatics*, vol. 17, no. 2, pp. 1111–1121, 2021.

[132] S. Mashayekh, M. Stadler, G. Cardoso, and M. Heleno, "A mixed integer linear programming approach for optimal DER portfolio, sizing, and placement in multi-energy

microgrids," *Appl. Energy*, vol. 187, pp. 154–168, 2017.

[133] B. V Solanki, C. A. Cañizares, and K. Bhattacharya, "Practical Energy Management Systems for Isolated Microgrids," *IEEE Trans. Smart Grid*, vol. 10, no. 5, pp. 4762–4775, 2019.

[134] M. Jereminov, B. Hooi, A. Pandey, H. Song, C. Faloutsos, and L. Pileggi, "Impact of Load Models on Power Flow Optimization," in *2019 IEEE Power & Energy Society General Meeting (PESGM)*, 2019, pp. 1–5.

[135] A. Dwyer, R. E. Nielsen, J. Stangl, and N. S. Markushevich, "Load to voltage dependency tests at B.C. Hydro," *IEEE Trans. Power Syst.*, vol. 10, no. 2, pp. 709–715, 1995.

[136] M. Farrokhabadi, C. A. Cañizares, and K. Bhattacharya, "Frequency Control in Isolated/Islanded Microgrids Through Voltage Regulation," *IEEE Trans. Smart Grid*, vol. 8, no. 3, pp. 1185–1194, 2017.

[137] EPRI, "Measurement-Based Load Modeling," Tech. rep. 1014402, Palo Alto, CA, 2006.

[138] A. Perez Tellez, "Modelling aggregate loads in power systems," Electric Power and Energy Systems, School of Electrical Engineering (EES), KTH, 2017.

[139] K. P. Schneider, J. C. Fuller, and D. P. Chassin, "Multi-State Load Models for Distribution System Analysis," *IEEE Trans. Power Syst.*, vol. 26, no. 4, pp. 2425–2433, 2011.

[140] F. K. Tuffner, K. P. Schneider, J. Hansen, and M. A. Elizondo, "Modeling Load Dynamics to Support Resiliency-Based Operations in Low-Inertia Microgrids," *IEEE Trans. Smart Grid*, vol. 10, no. 3, pp. 2726–2737, 2019.

[141] D. Espín-Sarzosa, R. Palma-Behnke, and F. Valencia, "Modeling of Small Productive Processes for the Operation of a Microgrid," *Energies*, vol. 14, no. 14. 2021.

[142] K. P. Burnham and D. R. Anderson, *Model Selection and Multimodel Inference: A Practical Information-Theoretic Approach*. Springer New York, 2003.

[143] G. Li and J. Shi, "On comparing three artificial neural networks for wind speed forecasting," *Appl. Energy*, vol. 87, no. 7, pp. 2313–2320, 2010.

[144] M. S. Hossan, H. M. M. Maruf, and B. Chowdhury, "Comparison of the ZIP load model and the exponential load model for CVR factor evaluation," in *2017 IEEE Power & Energy Society General Meeting*, 2017, pp. 1–5.

[145] J. R. Martí, H. Ahmadi, and L. Bashualdo, "Linear Power-Flow Formulation Based on a Voltage-Dependent Load Model," *IEEE Trans. Power Deliv.*, vol. 28, no. 3, pp. 1682–1690, 2013.

[146] Z. Wang and J. Wang, "Time-Varying Stochastic Assessment of Conservation Voltage Reduction Based on Load Modeling," *IEEE Trans. Power Syst.*, vol. 29, no. 5, pp. 2321–

2328, 2014.

[147] M. Sharifzadeh, A. Sikinioti-Lock, and N. Shah, "Machine-learning methods for integrated renewable power generation: A comparative study of artificial neural networks, support vector regression, and Gaussian Process Regression," *Renew. Sustain. Energy Rev.*, vol. 108, pp. 513–538, 2019.

[148] J. Llanos *et al.*, "Load estimation for microgrid planning based on a self-organizing map methodology," *Appl. Soft Comput.*, vol. 53, pp. 323–335, 2017.

[149] S. Dreiseitl and L. Ohno-Machado, "Logistic regression and artificial neural network classification models: a methodology review," *J. Biomed. Inform.*, vol. 35, no. 5, pp. 352–359, 2002.

[150] R. Linder, J. Geier, and M. Kölliker, "Artificial neural networks, classification trees and regression: Which method for which customer base?," *J. Database Mark. Cust. Strateg. Manag.*, vol. 11, no. 4, pp. 344–356, 2004.

[151] A. V. Olgac and B. Karlik, "Performance Analysis of Various Activation Functions in Generalized MLP Architectures of Neural Networks," *Int. J. Artif. Intell. Expert Syst.*, vol. 1, no. 4, 2010.

[152] S. Narayan, "The generalized sigmoid activation function: Competitive supervised learning," *Inf. Sci. (Ny).*, vol. 99, no. 1, pp. 69–82, 1997.

[153] Z. Cömert and A. Kocamaz, "A Study of Artificial Neural Network Training Algorithms for Classification of Cardiotocography Signals," *J. Sci. Technol.*, vol. 7, no. 2, pp. 93–103, 2017.

[154] N. Khan, D. Gaurav, and T. Kandl, "Performance Evaluation of Levenberg-Marquardt Technique in Error Reduction for Diabetes Condition Classification," *Procedia Comput. Sci.*, vol. 18, pp. 2629–2637, 2013.

[155] Y.-C. Du and A. Stephanus, "Levenberg-Marquardt Neural Network Algorithm for Degree of Arteriovenous Fistula Stenosis Classification Using a Dual Optical Photoplethysmography Sensor," *Sensors*, vol. 18, no. 7. 2018.

[156] D. J. Fonseca, D. O. Navaresse, and G. P. Moynihan, "Simulation metamodeling through artificial neural networks," *Eng. Appl. Artif. Intell.*, vol. 16, no. 3, pp. 177–183, 2003.

[157] F. Bre, J. M. Gimenez, and V. D. Fachinotti, "Prediction of wind pressure coefficients on building surfaces using artificial neural networks," *Energy Build.*, vol. 158, pp. 1429–1441, 2018.

[158] F. Bolger and G. Wright, "Assessing the quality of expert judgment: Issues and analysis," *Decis. Support Syst.*, vol. 11, no. 1, pp. 1–24, 1994.

[159] B. K. Lad and M. S. Kulkarni, "A parameter estimation method for machine tool reliability

analysis using expert judgement," *Int. J. Data Anal. Tech. Strateg.*, vol. 2, no. 2, pp. 155–169, Jan. 2010.

[160] M. L. Johnson and L. M. B. T.-M. in E. Faunt, "Parameter estimation by least-squares methods," in *Numerical Computer Methods*, vol. 210, Academic Press, 1992, pp. 1–37.

[161] P. Ju and E. Handschin, "Identifiability of load models [power systems]," *IEE Proc. - Gener. Transm. Distrib.*, vol. 144, no. 1, pp. 45–49, 1997.

[162] M. Cococcioni and L. Fiaschi, "The Big-M method with the numerical infinite M," *Optim. Lett.*, 2020.

[163] L. Liberti and N. Maculan, *Global Optimization: From Theory to Implementation*, 1st Edition. Boston: Springer, Boston, MA, 2006.

[164] F. A. Al-Khayyal, "Jointly constrained bilinear programs and related problems: An overview," *Comput. Math. with Appl.*, vol. 19, no. 11, pp. 53–62, 1990.

[165] G. P. Mccormick, "Computability of global solutions to factorable nonconvex programs: Part I -- Convex underestimating problems," *Math. Program. Ser. A B*, vol. 10, no. 1, pp. 147–175, 1976.

[166] J. K. Scott, M. D. Stuber, and P. I. Barton, "Generalized McCormick relaxations," *J. Glob. Optim.*, vol. 51, no. 4, pp. 569–606, 2011.

[167] H. Nagarajan, M. Lu, S. Wang, R. Bent, and K. Sundar, "An adaptive, multivariate partitioning algorithm for global optimization of nonconvex programs," *J. Glob. Optim.*, vol. 74, no. 4, pp. 639–675, 2019.

[168] J. Teles, P. Castro, and H. Matos, *A New Method for the Global Optimization of Nonlinear Problems with Bilinear Terms*. 2011.

[169] M. Locatelli and F. Schoen, "(Global) Optimization: Historical notes and recent developments," *EURO J. Comput. Optim.*, vol. 9, p. 100012, 2021.

[170] S. Kolodziej, P. M. Castro, and I. E. Grossmann, "Global optimization of bilinear programs with a multiparametric disaggregation technique," *J. Glob. Optim.*, vol. 57, no. 4, pp. 1039–1063, 2013.

[171] L. Liberti, P. Milano, P. Zza, and L. Vinci, "Introduction to global optimization," Mar. 2006.

[172] G. Rangaiah, *Stochastic Global Optimization: Techniques and Applications in Chemical Engineering*. World Scientific, 2010.

[173] A. Zhigljavsky and A. Žilinskas, *Stochastic Global Optimization*, 1st Editio. Springer, Boston, MA, 2008.

[174] Z. Ugray, L. Lasdon, J. Plummer, F. Glover, J. Kelly, and R. Martí, "Scatter Search and Local NLP Solvers: A Multistart Framework for Global Optimization," *INFORMS J.*

Comput., vol. 19, no. 3, pp. 328–340, Jul. 2007.

[175] M. Dourado, J. F. Meireles, and A. M. A. C. Rocah, "A global optimization approach applied to structural dynamic updating," in *Lecture Notes in Computer Science*, 2014, p. 16.

[176] T. Goel and N. Stander, "Adaptive simulated annealing for global optimization in LS-OPT," in *Proceedings of the 7th European LS-DYNA conference*, 2009, pp. 1–8.

[177] L. Meng, *Hierarchical Control for Optimal and Distributed Operation of Microgrid Systems*, Ph.D. thes. Department of Energy Technology, Aalborg University, 2015.

[178] K. Vugrin, "On the Effects of Noise on Parameter Identification Optimization Problems," Virginia Tech, 2005.

[179] G. B. Dantzig, "Linear Programming," *Oper. Res.*, vol. 50, no. 1, pp. 42–47, Feb. 2002.

[180] J. A. Taylor, *Convex Optimization of Power Systems*. Cambridge: Cambridge University Press, 2015.

[181] F. U. Nazir, B. C. Pal, and R. A. Jabr, "Approximate Load Models for Conic OPF Solvers," *IEEE Trans. Power Syst.*, vol. 36, no. 1, pp. 549–552, 2021.

[182] M. Elsied, A. Oukaour, H. Gualous, R. Hassan, and A. Amin, "An advanced energy management of microgrid system based on genetic algorithm," in *2014 IEEE 23rd International Symposium on Industrial Electronics (ISIE)*, 2014, pp. 2541–2547.

[183] U. B. Tayab, F. Yang, M. El-Hendawi, and J. Lu, "Energy Management System for a Grid-Connected Microgrid with Photovoltaic and Battery Energy Storage System," in *2018 Australian & New Zealand Control Conference (ANZCC)*, 2018, pp. 141–144.

[184] M. F. Roslan, M. A. Hannan, P. Jern Ker, R. A. Begum, T. M. Indra Mahlia, and Z. Y. Dong, "Scheduling controller for microgrids energy management system using optimization algorithm in achieving cost saving and emission reduction," *Appl. Energy*, vol. 292, p. 116883, 2021.

[185] U. B. Tayab, J. Lu, F. Yang, T. S. AlGarni, and M. Kashif, "Energy management system for microgrids using weighted salp swarm algorithm and hybrid forecasting approach," *Renew. Energy*, vol. 180, pp. 467–481, 2021.

[186] V. V. S. N. Murty and A. Kumar, "Multi-objective energy management in microgrids with hybrid energy sources and battery energy storage systems," *Prot. Control Mod. Power Syst.*, vol. 5, no. 1, p. 2, 2020.

[187] M. F. Zia, E. Elbouchikhi, M. Benbouzid, and J. M. Guerrero, "Energy Management System for an Islanded Microgrid With Convex Relaxation," *IEEE Trans. Ind. Appl.*, vol. 55, no. 6, pp. 7175–7185, 2019.

[188] M. J. Dolan, E. M. Davidson, G. W. Ault, F. Coffele, I. Kockar, and J. R. McDonald, "Using

optimal power flow for management of power flows in active distribution networks within thermal constraints," in *2009 44th International Universities Power Engineering Conference (UPEC)*, 2009, pp. 1–5.

[189] J. J. Grainger, W. D. Stevenson, and G. W. Chang, *Power Systems Analysis*. McGraw-Hill Education, 2016.

[190] R. A. Jabr, "A Conic Quadratic Format for the Load Flow Equations of Meshed Networks," *IEEE Trans. Power Syst.*, vol. 22, no. 4, pp. 2285–2286, 2007.

[191] M. S. Javadi, C. S. Gouveia, L. M. Carvalho, and R. Silva, "Optimal Power Flow Solution for Distribution Networks using Quadratically Constrained Programming and McCormick Relaxation Technique," in *2021 IEEE International Conference on Environment and Electrical Engineering and 2021 IEEE Industrial and Commercial Power Systems Europe (EEEIC / I&CPS Europe)*, 2021, pp. 1–6.

[192] Z. Q. Wu, "Loss and Branch Power Flow Allocation Based on Topological Method," *Electr. Power Components Syst.*, vol. 30, no. 11, pp. 1179–1193, Nov. 2002.

[193] R. A. Jabr, "Radial distribution load flow using conic programming," *IEEE Trans. Power Syst.*, vol. 21, no. 3, pp. 1458–1459, 2006.

[194] C. Shah and R. Wies, "Algorithms for Optimal Power Flow in Isolated Distribution Networks Using Different Battery Energy Storage Models," in *2020 IEEE Power & Energy Society Innovative Smart Grid Technologies Conference (ISGT)*, 2020, pp. 1–5.

[195] S. Boyd, S. P. Boyd, L. Vandenberghe, and C. U. Press, *Convex Optimization*. Cambridge University Press, 2004.

[196] B. Kocuk, S. Dey, and X. Sun, "Strong SOCP Relaxations for the Optimal Power Flow Problem," *Oper. Res.*, vol. 64, May 2016.

[197] M. S. Lobo, L. Vandenberghe, S. Boyd, and H. Lebret, "Applications of second-order cone programming," *Linear Algebra Appl.*, vol. 284, no. 1, pp. 193–228, 1998.

[198] F. Valencia and A. Marquez, "An Economic Robust Programming Approach for the Design of Energy Management Systems," in *Power Quality in Future Electrical Power Systems*, 1st ed., S. H. E. A. A. Ahmed F. Zobaa, Ed. 2017, pp. 359–377.

[199] O. Núñez-Mata, R. Palma-Behnke, F. Valencia, A. Urrutia-Molina, P. Mendoza-Araya, and G. Jiménez-Estévez, "Coupling an adaptive protection system with an energy management system for microgrids," *Electr. J.*, vol. 32, no. 10, p. 106675, 2019.

[200] J. Marchgraber and W. Gawlik, "Investigation of Black-Starting and Islanding Capabilities of a Battery Energy Storage System Supplying a Microgrid Consisting of Wind Turbines, Impedance- and Motor-Loads," *Energies*, vol. 13, no. 19. 2020.

[201] W. J. Praiselin and J. B. Edward, "Integrated renewable energy sources with droop control

techniques-based microgrid operation," in *Woodhead Publishing Series in Energy*, A. H. Fathima, N. Prabaharan, K. Palanisamy, A. Kalam, S. Mekhilef, and J. J. B. T.-H.-R. E. S. in M. Justo, Eds. Woodhead Publishing, 2018, pp. 39–60.

[202] The Math Works Inc., "Neural Network Toolbox." MA, USA.

[203] The MathWorks Inc., "Global Optimization Toolbox." Massachusetts, Unites States, 2020.

[204] M. Grant and S. Boyd, "CVX: Matlab software for disciplined convex programming, version 2.0 beta." 2013.

[205] M. Grant and S. Boyd, "Graph implementations for nonsmooth convex programs, Recent Advances in Learning and Control (a tribute to M. Vidyasagar)," in *Lecture Notes in Control and Information Sciences*, V. Blondel, S. Boyd, and H. Kimura, Eds. Springer, 2008, pp. 95–110.

[206] The MathWorks Inc., "MATLAB and Simulink Release 2020a." Massachusetts, Unites States, 2020.

[207] S. Francois-Xavier and T. Craig, "Hybrid Microgrids: The Time Is Now.," *Microgrids that Combine Renewable Energy with Diesel or Gas Generator Sets and Energy Storage Capabilities Can Deliver Clean, Cost-effective Electricity to Remote Locations with Limited or No Access to Reliable Utility Power.*, 2016. [Online]. Available: https://www.petersonpower.com/white-paper/hybrid-microgrids-time-now. [Accessed: 10-Jun-2022].

[208] S. Córdova, C. Cañizares, Á. Lorca, and D. E. Olivares, "An Energy Management System With Short-Term Fluctuation Reserves and Battery Degradation for Isolated Microgrids," *IEEE Trans. Smart Grid*, vol. 12, no. 6, pp. 4668–4680, 2021.

[209] S. Talari, M. Yazdaninejad, and M.-R. Haghifam, "Stochastic-based scheduling of the microgrid operation including wind turbines, photovoltaic cells, energy storages and responsive loads," *IET Gener. Transm. Distrib.*, vol. 9, no. 12, pp. 1498–1509, Sep. 2015.

[210] A. Zakariazadeh, S. Jadid, and P. Siano, "Smart microgrid energy and reserve scheduling with demand response using stochastic optimization," *Int. J. Electr. Power Energy Syst.*, vol. 63, pp. 523–533, 2014.

[211] J. Cheng, D. Duan, X. Cheng, L. Yang, and S. Cui, "Probabilistic Microgrid Energy Management with Interval Predictions," *Energies*, vol. 13, no. 12. 2020.

[212] Y. Xiang, J. Liu, and Y. Liu, "Robust Energy Management of Microgrid With Uncertain Renewable Generation and Load," *IEEE Trans. Smart Grid*, vol. 7, no. 2, pp. 1034–1043, 2016.

[213] D. E. Olivares, J. D. Lara, C. A. Cañizares, and M. Kazerani, "Stochastic-Predictive Energy Management System for Isolated Microgrids," *IEEE Trans. Smart Grid*, vol. 6, no. 6, pp.

2681–2693, 2015.

[214] O. Núñez-Mata, R. Palma-Behnke, F. Valencia, P. Mendoza-Araya, and G. Jiménez-Estévez, "Adaptive Protection System for Microgrids Based on a Robust Optimization Strategy," *Energies*, vol. 11, no. 2. 2018.

[215] C.-G. Jorge de Jesús, C. T. Margarita, C.-T. Beatriz, L.-Z. Francisco Román, M.-P. Gerardo Alberto, and V.-G. Carlos Jesahel, "Improvements and Evaluation on Bitter Orange Leaves (Citrus aurantium L.) Solar Drying in Humid Climates," *Sustainability*, vol. 13, no. 16. 2021.

[216] A. Molina, M. Falvey, and R. Rondanelli, "A solar radiation database for Chile," *Sci. Rep.*, vol. 7, no. 1, p. 14823, 2017.

[217] N. Mohd Razali and Y. Bee Wah, "Power comparisons of Shapiro-Wilk, Kolmogorov-Smirnov, Lilliefors and Anderson-Darling tests," *J. Stat. Model. Anal.*, vol. 2, no. 1, pp. 21–33, 2011.

[218] C. F. M. Coimbra and H. T. C. Pedro, *Stochastic-Learning Methods*. Elsevier, 2013.

[219] A. Samadi, L. Söder, E. Shayesteh, and R. Eriksson, "Static Equivalent of Distribution Grids With High Penetration of PV Systems," *IEEE Trans. Smart Grid*, vol. 6, no. 4, pp. 1763–1774, 2015.

[220] Ayllu-Solar, "Solar Energy: Sustainable Development for Arica & Parinacota Semi-annual Y4Q2 Report," no. May 2015, 2018.

[221] T. M. I. Natick, "Synchronous Machine pu Standard." [Online]. Available: https://www.mathworks.com/help/physmod/sps/powersys/ref/synchronousmachinepustandard.html. [Accessed: 27-Sep-2021].

[222] P. Kundur, *Power System Stability And Control*. New York: McGraw-Hill, 1994.

[223] "IEEE Recommended Practice for Excitation System Models for Power System Stability Studies," *IEEE Std 421.5-1992*. pp. 1–56, 1992.

[224] The-MathWorks-Inc.-Natick, "Three-Phase Transformer (Two Windings)." [Online]. Available: https://www.mathworks.com/help/physmod/sps/powersys/ref/threephasetransformerthreewindings.html. [Accessed: 27-Sep-2021].

[225] The-MathWorks-Inc.-Natick, "Three-Phase Parallel RLC Load." [Online]. Available: https://www.mathworks.com/help/physmod/sps/powersys/ref/threephaseparallelrlcload.html. [Accessed: 27-Sep-2021].

[226] L. F. N. Lourenço, R. M. Monaro, M. B. C. Salles, J. R. Cardoso, and L. Quéval, "Evaluation of the Reactive Power Support Capability and Associated Technical Costs of Photovoltaic Farms' Operation," *Energies*, vol. 11, no. 6. 2018.

[227] M. Y. Worku, M. A. Hassan, and M. A. Abido, "Real Time Energy Management and Control of Renewable Energy based Microgrid in Grid Connected and Island Modes," *Energies*, vol. 12, no. 2. 2019.

[228] D. Yunus A. Cengel and A. J. Ghajar, *Heat and Mass Transfer: Fundamentals and Applications*. McGraw-Hill Education, 2014.

[229] J. Espinoza, "Innovación en el deshidratado solar," *Ingeniare. Rev. Chil. Ing.*, vol. 24, pp. 72–80, 2016.

[230] Ayllu-Solar, "Container deshidratador solar 'ContEnerSol,'" Viña del Mar.

[231] S. Bischof, H. Trittenbach, M. Vollmer, D. Werle, T. Blank, and K. Böhm, "HIPE: An Energy-Status-Data Set from Industrial Production," in *Proceedings of the Ninth International Conference on Future Energy Systems*, 2018, pp. 599–603.

[232] "EPEX Spot Market Data." [Online]. Available: https://www.epexspot.com/en/market-data. [Accessed: 20-Nov-2021].

[233] S. Pfenninger and L. Staffell, "Renewables.ninja." [Online]. Available: https://www.renewables.ninja/. [Accessed: 20-Nov-2021].

ANNEXES

Annexed A List of acronyms

AC	Alternating Current
AI	Artificial Intelligence
AIC	Akaike's Information Criterion
ANN	Artificial Neural Network
ARIMA	Autoregressive Moving Average Model
ARMA	Autoregressive Moving Average Model
BAM	Binomial Approximation Method
BESS	Battery Energy Storage System
CLP	Chilean peso
CP	Constant power model
CST	Concentrating Solar Thermal
CVX	package for specifying and solving ConVeX programs
DC	Direct Current
DER	Distributed Energy Resources
DES	Decentralized Energy Systems
DG	Distributed Generation
DGU	Diesel Generator Unit
ED	Economic Dispatch
EMS	Energy Management System
EMZ-ZIP	Extended Multi-Zone ZIP Model
ESS	Energy Storage Systems
EV	Electric Vehicle
GA	Genetic Algorithms
GHI	Global Horizontal Irradiation
GIZ	Deutsche Gesellschaft für Internationale Zusammenarbeit
GO	Global Optimization
GPR	Gaussian Process Regression
HDI	Human Development Index
LM	Levenberg-Marquardt algorithm
LP	Linear Programming
LSTM	Long Short-Term Memory
MAE	Mean Absolute Error
MAPE	Mean Absolute Percentage Error
MAS	Multi-Agent System
MG	Microgrid
MILP	Mix-Integer Linear Programming
MK	McCormick approach

MLP	Multilayer Perceptron
MPP	Maximum Power Point
NCRE	Non-conventional Renewable Energy
NLP	Nonlinear Programming
OPF	Optimal Power Flow
PCC	Point of Common Coupling
PSO	Particle Swarm Optimization
PUE	Productive Use of Energy
PV	Photovoltaic
RMSE	Root Mean Squared Error
SA	Simulate Annealing
SARIMA	Seasonal Autoregressive Integrated Moving Average
SCOP	Second-Order Cone Programming
SERC	Solar Energy Research Center-Chile
SGD	Sustainable Development Goals
SOC	State of Charge
SOM	Self-organizing Maps
SPP	Small Productive Process
SPSP	Small Productive Solar Process
SVM	Support Vector Machine
SWH	Solar Water Heater
TAM	first-order Taylor series Approximation Method
TV-ZIP	Time-variant ZIP model
UC	Unit Commitment
VSC	Voltage Source Converter
ZIP	Constant impedance, constant current and constant power model

Annexed B The Ayllu Solar project

Due to its high solar energy potential, the Arica and Parinacota region was selected as a suitable location for the implementation of the Ayllu project. Besides, the main economic activities of this region are agriculture, mining, tourism, and trading. Thus, the introduction of productive use of solar energy projects in northern Chile constitutes a great opportunity for sustainable development of communities in such region. All small-scale projects of the Ayllu project use the solar energy as main source of energy to carry out their productive activities.

The key specific objectives of the Ayllu Solar [6] as follows:

- To create cost-effective, replicable, and scalable solar energy solutions in key areas for community development.
- To create human capital capabilities for the effective use and development of solar energy solutions through continuing education and skill-building tools with active engagement of the whole community.
- To ensure sustainability by developing effective solar energy solutions, business models, support network, community involvement and a proper institutional framework.

Figure 2.11 in Section 2.1.2 shows the Ayllu Solar small-scale projects (i.e., SPSPs) located in the Arica and Parinacota region. As can be seen in such figure, the Ayllu solar project comprises several initiatives, nevertheless, only the reference projects, i.e., those located in Caleta Vítor, Camarones and Visviri are described in more detail below.

Processing of agricultural products with solar energy [6]: This project has been implemented in the Caleta Vítor and Chaca valley, in the Arica commune. The main economic activity of community people is the agriculture. However, agriculture activities are developed in a traditional way, i.e., manually and do not consider packing, storage, or any other processing of the harvested products. Moreover, in this place, it is feasible to harvest crops most of the year, providing raw material (i.e., fruits and vegetables) regularly.

In this sense, there is a clear opportunity to take advantage of the solar energy to add value to the agricultural products produced. Accordingly, the project consisted of installing a solar dryer, packing and storage systems for fruits and vegetables harvested in Caleta Vítor and Valle del Chaca. Figure B.1 illustrates a general layout of the Caleta Vítor and Chaca valley SPSP. It includes the following subsystems: 1) PV generation system, 2) infrastructure (office, meeting room and processing room), 3) processing, sorting and calibration line, and 4) dehydration process line (solar dryer). Since this is a solar-based dehydration process, its behavior may be influenced by external weather variables, mainly solar radiation, ambient temperature, wind speed and relative humidity.

Figure B.1 General layout of the Caleta Vítor and Chaca Valley SPSP [78]

River shrimp farming [220]: This project has been implemented in the Camarones commune. This project aims to improve the socio-economic development of people of the people of the villages of Camarones, Maquita and Taltape through technological improvements in river shrimp and trout farming using a solar water treatment system. The technological improvement consists of the use of solar energy to improve the quality of the natural river water used in the cultivation of these aquatic species. The project also considers a PV generation system to supply the aquaculture system's electrical devices. Figure B.2 shows an overview of the aquaculture SPSP. As illustrated in Figure B.2, this project includes the following subsystems: 1) PV generation system, 2) solar water treatment system, and 3) water recirculation system that provides arsenic-free water. Similar to the SPSP described above, this aquaculture process is based on solar energy, thus, its electrical behavior can change due to the influence of external weather variables such as

solar radiation, ambient temperature, as well as endogenous variables such as the amount of dissolved chemicals in the treated water.
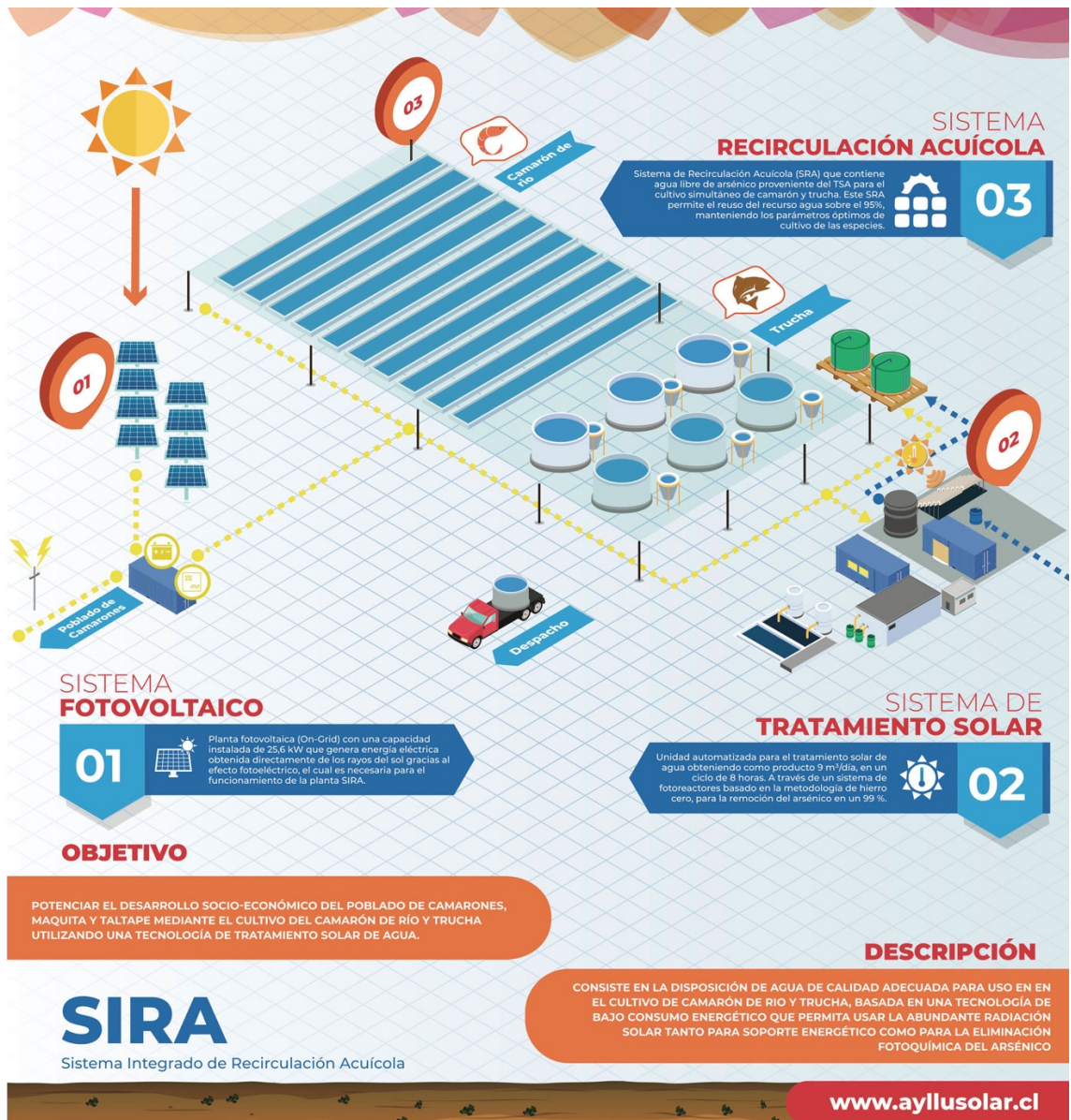

Figure B.2 General overview of the aquaculture SPSP installed in Camarones [78]

Camelid fiber collection and processing center [6]: This SPSP was established in the General Lagos jointly with the Visviri community where the main economic activity is the sale of camelid fiber. The work of shearing camelid fiber was usually done in the traditional way, in the same manner as it was done by their ancestors for several generations. However, adding value to the raw fiber produced in General Lagos and Visviri can help the people of these communities gain access to markets for the sale of the fiber. Therefore, the project consisted of implementing a camelid fiber collection and processing center. This center includes machinery that is powered by solar energy. Figure B.3 displays a general layout of the camelid fiber collection and processing center installed

123

in Visviri. It includes the following subsystems: 1) PV generation system, and 2) thermo-solar system for water heating for camelid fiber processing.

The climate in these places is cold semi-arid, with strong winds, high thermal oscillation, rainfall and thunderstorms in summer, snow in winter and a high solar radiation throughout the year. Therefore, these climatic conditions may influence the fiber processing process, for example, high relative humidity can affect fiber quality, while variation in ambient temperature can affect the thermo-solar process leading to varying process operating conditions. Consequently, it is worth considering the effect of these external weather variables when analyzing the electrical characteristics of this SPSP.
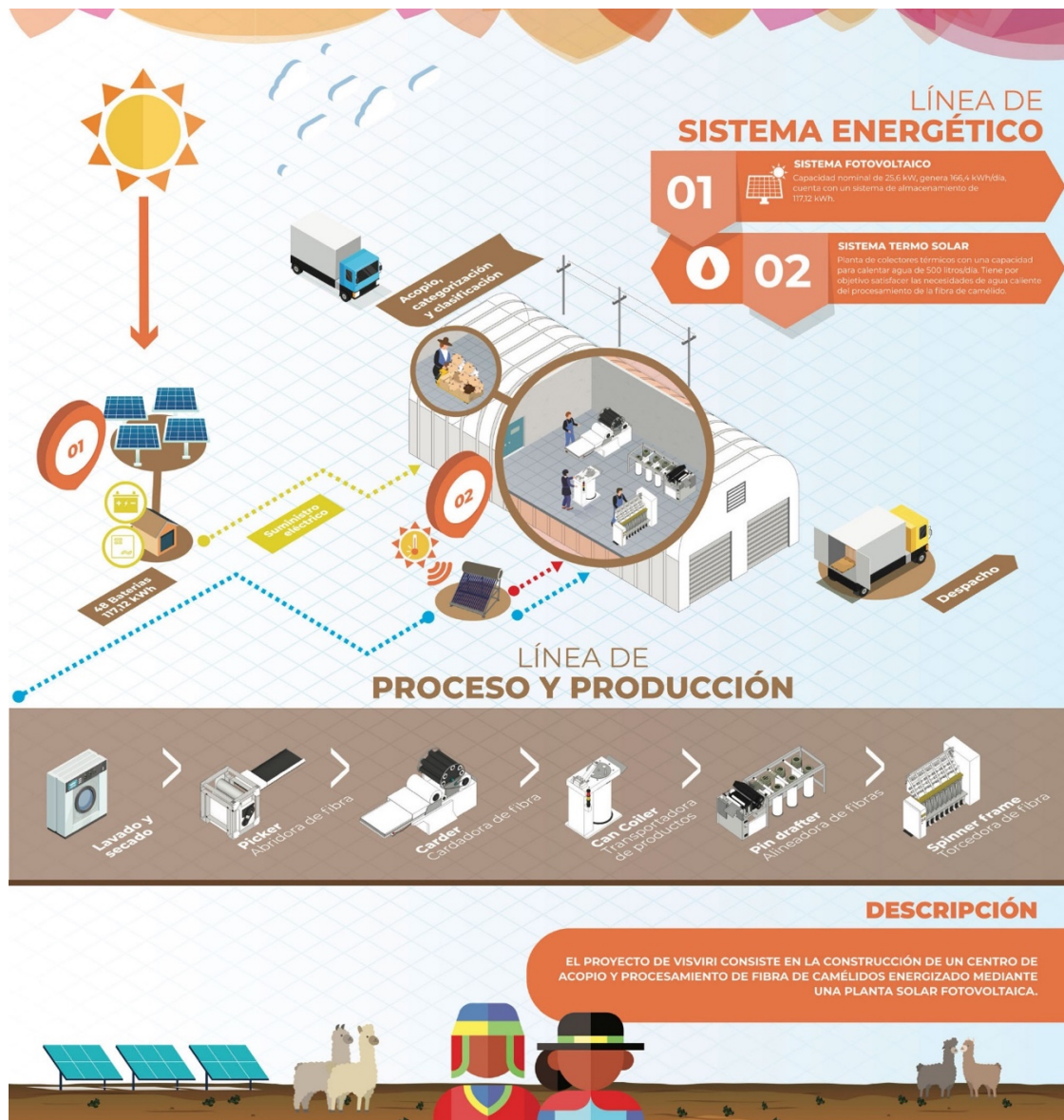

Figure B.3 General layout of the camelid fiber collection and processing center [78]

Annexed C Parameter identification through a convexification procedure

The authors in [141] proposed a procedure based on the convexification of the bilinear product through a transformation of variables to solve the minimization problem expressed in (16)-(22). Thus, such procedure is further described in this Section.

First, as previously mentioned, the parameter $P_{flex}(k)$ is non-identifiable [161]. Thus, to address this challenge, a splitting procedure is considered. More concretely, the minimization problem in (16)-(22) is broken-down into three stages.

In the first stage, the product between the variables $P_{flex}(k)$ and $\tilde{\alpha}_\varphi(k)$ ($\varphi \in \{1,2,3\}$) are replaced by auxiliary variables, thus

$$\Xi_\varphi(k) = P_{flex}(k)\tilde{\alpha}_\varphi(k), (\varphi \in \{1,2,3\}) \tag{94}$$

Then, the EMZ-ZIP load model in (17) becomes:

$$P(k) = \left(\Xi_1(k)\tilde{V}_d^2(k) + \Xi_2(k)\tilde{V}_d(k) + \Xi_3(k)\right) \\ + \sum_{\omega=1}^{\Omega_\psi} \delta_\omega(k)P_{0,\omega}\left(\alpha_{1,\omega}\tilde{V}_d^2(k) + \alpha_{2,\omega}\tilde{V}_d(k) + \alpha_{3,\omega}\right) \tag{95}$$

Next, replacing the expression (95) in (16)-(22), the resulting minimization problem is as follows:

$$\underset{\substack{\Xi_1(k),\Xi_2(k)\,\Xi_3(k), \\ \delta_\omega(k)}}{minimize} \sum_{d=1}^{D} \left(\vec{P}_d(k) - \hat{P}(k)\right)^2 \tag{96}$$

Subject to:

$$\hat{P}(k) = \left(\Xi_1(k)\tilde{V}_d^2(k) + \Xi_2(k)\tilde{V}_d(k) + \Xi_3(k)\right) \\ + \sum_{\omega=1}^{\Omega_j} \delta_\omega(k)P_{0,\omega}\left(\alpha_{1,\omega}\tilde{V}_d^2(k) + \alpha_{2,\omega}\tilde{V}_d(k) + \alpha_{3,\omega}\right) \tag{97}$$

$$\sum_{\omega=1}^{\Omega_j} \delta_\omega(k) = 1 \tag{98}$$

$$\Xi_1(k) + \Xi_2(k) + \Xi_3(k) = M \tag{99}$$

$$0 \le \delta_\omega(k) \le 1 \tag{100}$$

$$0 \le \Xi_1(k) + \Xi_2(k) + \Xi_3(k) \le M \tag{101}$$

Moreover, because $P_{flex}(k)$ is a non-identifiable parameter, the big-M method is utilized to bound the new set of variables $\Xi_\varphi(k)$ ($\varphi \in \{1,2,3\}$). The big-M value must be selected, large enough, but not too high to prevent the M value influencing the results of the optimization problem [162].

Once the variables $\Xi_\varphi(k)$ ($\varphi \in \{1,2,3\}$) and $\delta_\omega(k)$ ($\omega \in \{\Omega_\psi\}$) are identified, the original parameters $P_{flex}(k)$ and $\tilde{\alpha}_\varphi(k)$ ($\varphi \in \{1,2,3\}$) can be determined. For this purpose, the identified values of $\delta_\omega(k)$ are considered as fixed. Consequently, the original parameters (i.e., $P_{flex}(k)$ and $\tilde{\alpha}_\varphi(k)$) are identified in the second stage by using the minimization problem in (16)-(22) adding the constraints expressed in (102).

$$P_{flex}(k)\tilde{\alpha}_\varphi(k) \leq \Xi_\varphi, (\varphi \in \{1,2,3\}) \tag{102}$$

Finally, as previously mentioned $P_{flex}(k)$ is non-identifiable, hence, a correction on its identification is necessary. For this purpose, in the third stage the values already identified for $\delta_\omega(k)$ ($\omega \in \{\Omega_\psi\}$) and $\tilde{\alpha}_\varphi(k)$ ($\varphi \in \{1,2,3\}$) are taken as fixed. Therefore, the values of $P_{flex}(k)$ can be determined by solving the minimization problem (103)-(105).

$$\underset{P_{flex}(k)}{minimize} \sum_{d=1}^{D} \left(\vec{P}_d(k) - \hat{P}(k)\right)^2 \tag{103}$$

Subject to:

$$\hat{P}(k) = P_{flex}(k)\left(\tilde{\alpha}_1(k)\tilde{V}_d^2(k) + \tilde{\alpha}_2(k)\tilde{V}_d(k) + \tilde{\alpha}_3(k)\right)$$

$$+ \sum_{\omega=1}^{\Omega_\psi} \delta_\omega(k)P_{0,\omega}\left(\alpha_{1,\omega}\tilde{V}_d^2(k) + \alpha_{2,\omega}\tilde{V}_d(k) + \alpha_{3,\omega}\right) \tag{104}$$

$$0 \leq P_{flex}(k) \leq M \tag{105}$$

Note that the resulting minimization problems (96)-(101) and (103)-(105) are all convex and, thus, they have a global optimum, which can be numerically found in a finite number of steps [195] using different convex programming tools such as CVX [204], [205].

Annexed D Sensitivity analysis of the ZIP parameters for TAM and BAM

The sensitivity analysis consists of taking each parameter of the ZIP model and varying it by taking values from an interval (in this case between 0.01 and 1.00 with a fixed step of 0.01). It is important to note that, to fulfill that the sum of the ZIP parameters equals 1, the difference is equally distributed between the remaining two parameters. For example, if we consider that the parameter $\tilde{\alpha}_1$ will vary, the resulting expression is $\tilde{\alpha}_1 + \frac{\tilde{\alpha}_2}{2} + \frac{\tilde{\alpha}_3}{2} = 1$. Then, following the comparative analysis performed in Section 3.5.1, we varied the voltage between 0.85 p.u. and 1.15 p.u. with a step of 0.01 and analyze the relative error between the original ZIP model representation and each of the two approximation methods (i.e., TAM and BAM). Figure D.1, Figure D.2 and Figure D.3 show the results of the sensitivity analysis for the constant impedance, constant current and constant power parameters, respectively.
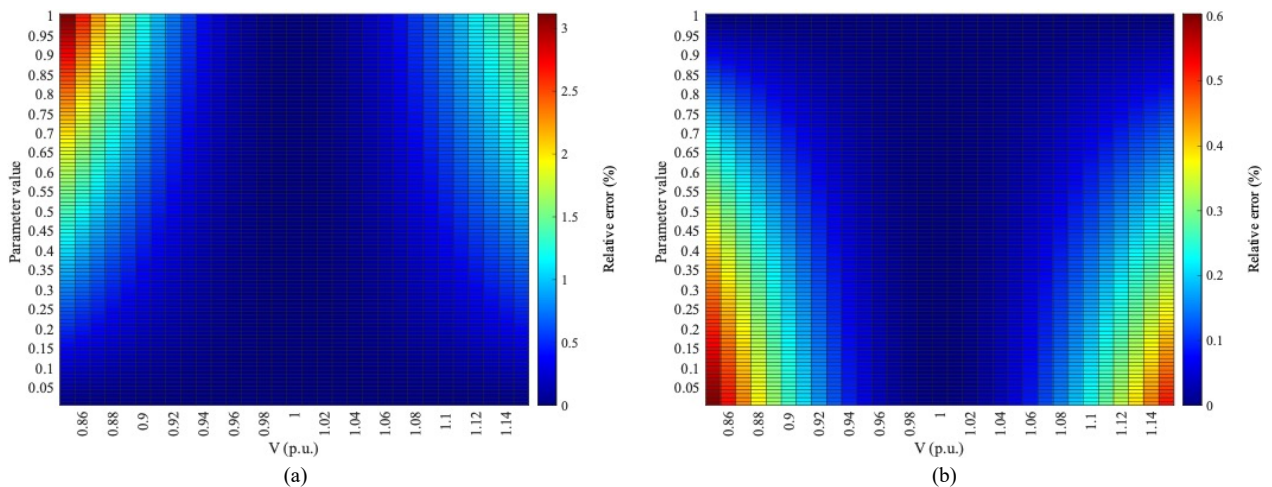

Figure D.1 Results of the sensitivity analysis for the constant impedance parameter: (a) TAM and (b) BAM
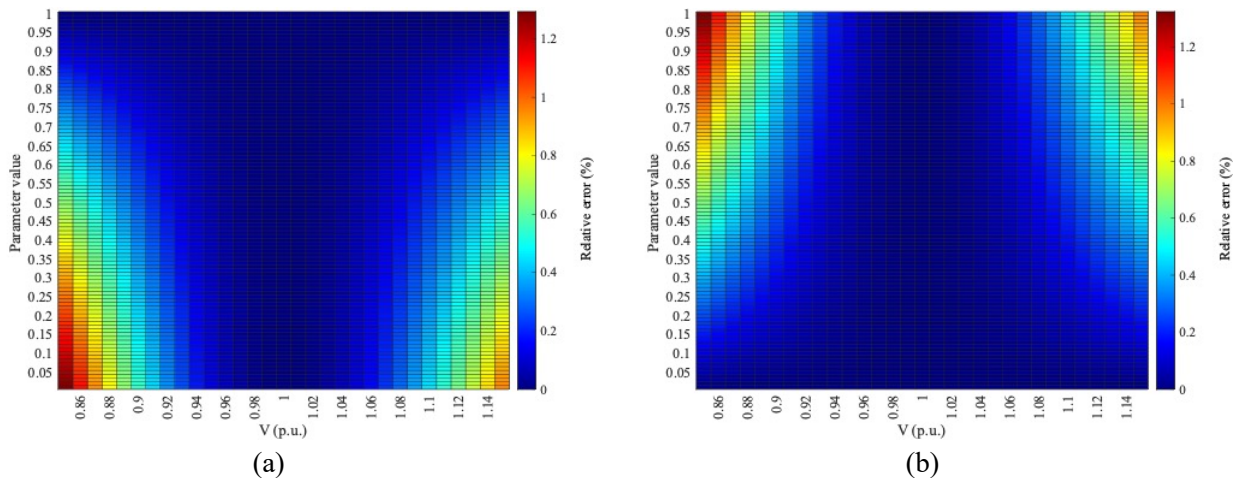

Figure D.2 Results of the sensitivity analysis for the constant current parameter: (a) TAM and (b) BAM
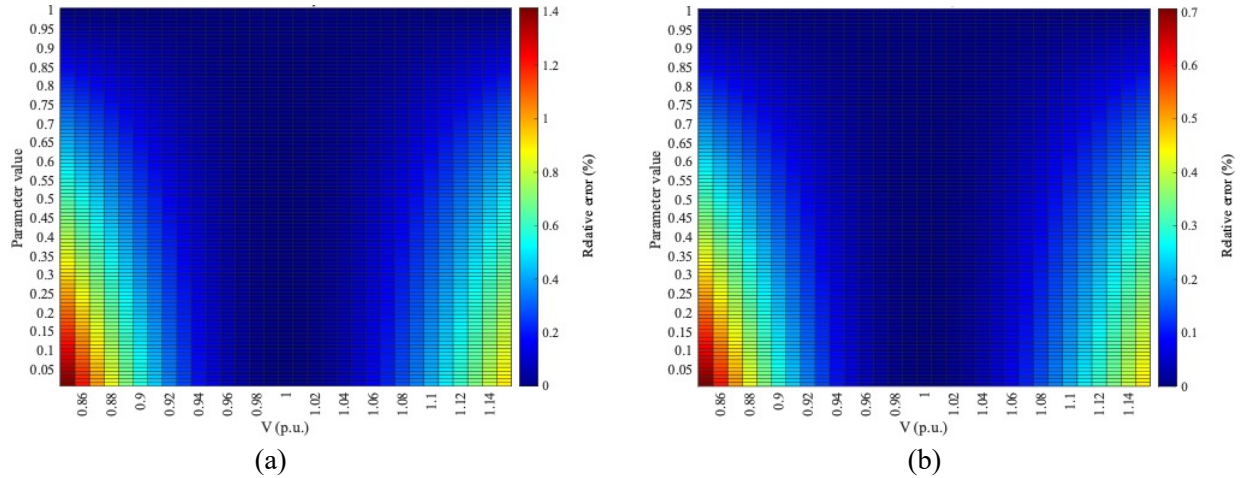
127

Figure D.3 Results of the sensitivity analysis for the constant power parameter: (a) TAM and (b) BAM

As can be seen from Figure D.1, Figure D.2 and Figure D.3, in general, the BAM exhibits a lower relative error than the TAM in all cases. For example, in the case of the constant power parameter the TAM presents a maximum error by around 3% while the BAM a maximum error by approximately 0.6%. Table D.1 presents a summary of the results of the sensitivity analysis for the three ZIP parameters (i.e., constant impedance, constant current and constant power) for TAM and BAM. For the summary, the maximum (Max), minimum (Min), average (Avg.), and standard deviation (Std.) of the relative errors for all cases and relative errors for voltages at the limits of the normal operating range, i.e., 0.90 p.u. and 1.10 p.u., were considered.

Table D.1 Summary of sensitivity analysis for constant impedance, constant current and constant power parameters for TAM and BAM

		Constant impedance		Constant current		Constant power	
		TAM	BAM	TAM	BAM	TAM	BAM
Overall	Min (%)	0.000	0.000	0.000	0.000	0.000	0.000
	Max (%)	3.114	0.603	1.293	1.324	1.413	0.706
	Avg. (%)	0.414	0.100	0.200	0.204	0.200	0.100
	Std. (%)	0.514	0.120	0.241	0.245	0.244	0.122
$V = 0.90$ p.u.	Min (%)	0.011	0.000	0.000	0.006	0.000	0.000
	Max (%)	1.235	0.261	0.547	0.556	0.578	0.289
	Avg. (%)	0.591	0.137	0.274	0.280	0.274	0.137
	Std. (%)	0.358	0.076	0.160	0.161	0.169	0.085
$V = 1.10$ p.u.	Min (%)	0.010	0.000	0.000	0.005	0.000	0.000
	Max (%)	0.826	0.235	0.448	0.455	0.429	0.215
	Avg. (%)	0.437	0.112	0.224	0.229	0.225	0.112
	Std. (%)	0.239	0.069	0.131	0.132	0.126	0.063

Can be seen from Table D.1 that considering the overall results, the BAM presents lower maximum, average and standard deviation relative error values than the TAM for the constant impedance and constant power parameters. However, the TAM presents a slight improvement when the results of the constant current parameter are analyzed. However, this improvement is approximately 0.005% and is therefore negligible. Therefore, the two approaches have practically the same relative error results for the constant current parameter. This same trend is repeated when analyzing the results for the voltage values at the limits of the normal operating range. Consequently, the BAM outperforms the TAM considering all the cases analyzed in the sensitivity analysis of the ZIP parameters.

Annexed E Models and parameter values of the MG elements for the case study

Annexed E1 Diesel generators

The diesel generator model comprises four main components, such as synchronous machine, an excitation system, a governor, and a diesel engine. The diesel generators are based on a three-phase salient pole synchronous machine. The electrical part of the machine is represented by a sixth-order state-space model [221]. Figure E.1 shows a simplified block diagram of a diesel generator and its main components. Table E.1 lists the synchronous machine parameters for the two diesel generators.
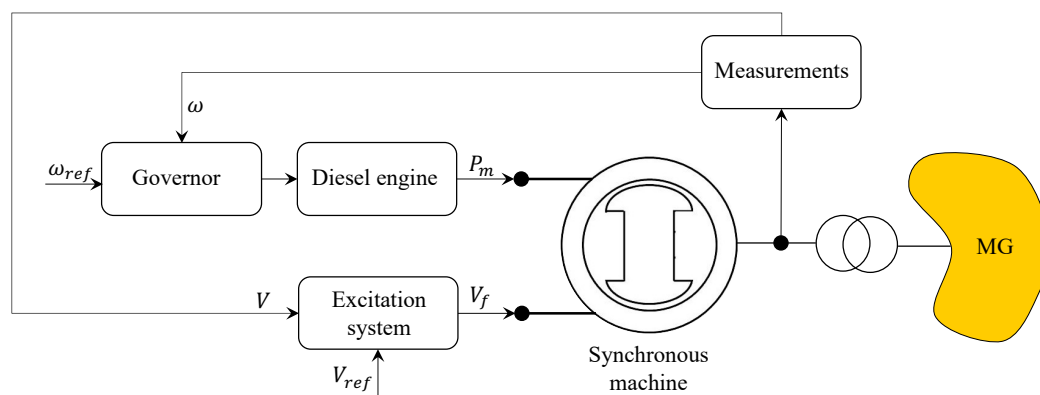

Figure E.1 Simplified block diagram of a diesel generator

Table E.1 Synchronous machine parameters

	DGU1	DGU2
Nominal power (kVA)	19.2	12.8
Nominal voltage (Vrms L-L)	220.0	220.0
Xd (p.u.)	1.966	2.057
Xd' (p.u.)	0.200	0.210
Xd'' (p.u.)	0.126	0.132
Tdo' (s)	4.484	4.489
Tdo'' (s)	0.068	0.068
Xq (p.u.)	0.977	1.022
Xq'' (p.u.)	0.225	0.236
Tqo'' (s)	0.100	0.100
Rs (p.u.)	0.061	0.078
Xl (p.u.)	0.079	0.083
H (s)	1.100	0.900

The excitation system of a diesel generator provides direct current to the synchronous machine field winding. Besides, the excitation system performs control functions of voltage and reactive power flow [222]. The excitation system are based on the IEEE type DC1A excitation system model (see Figure E.2) [223]. Table E.2 presents the exciter parameters for the two diesel generators.
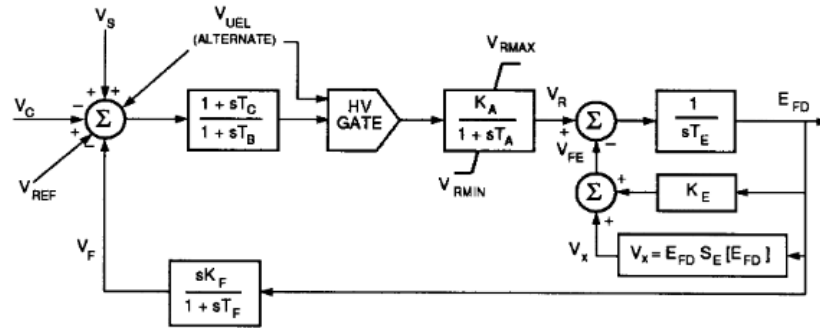
Figure E.2 Diesel generator excitation system block diagram [223]

Table E.2 Excitation system parameters

	DGU1	DGU2
Ka	400.0	400.0
Kf	0.030	0.030
Ta (s)	0.020	0.020
Tr (s)	0.020	0.020
Tf (s)	1.000	1.000
Vr min (p.u.)	-2.200	-2.200
Vr max (p.u.)	2.200	2.200

The governor of a diesel generator provides a mean of controlling power and frequency as function of the rotational speed of the diesel engine [222]. Figure E.3 depicts the diesel generator governor block diagram. Table E.3 lists the governor parameters for the two diesel generators.
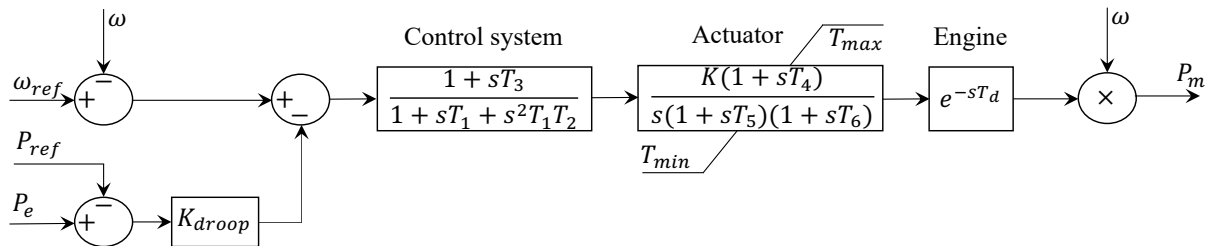

Figure E.3 Diesel generator governor block diagram

Table E.3 Diesel generator governor parameters

	DGU1	DGU2
T_1	0.628	3.927
T_2	0.395	15.421
T_3	0.200	0.200
T_4	0.250	0.250
T_5	0.009	0.009
T_6	0.038	0.038
T_d	0.024	0.024
K	0.395	1.696e3
K_{droop}	0.100	0.050

Annexed E2 Transformers

The transformer used in this work is a three-phase two-winding transformer. The transformer model is three-phase based on single-phase transformers with DY connection. More details of the mathematical model of the transformer can be found in [189], [224]. Table E.4 presents the parameters of the transformers considered in this work.

Table E.4 Transformer parameters

	T1	T2	T3
Nominal power (kVA)	25.0	25.0	25.0
Nominal primary voltage (Vrms L-L)	220.0	220.0	220.0
Nominal secondary voltage (Vrms L-L)	380.0	380.0	380.0
R1 (p.u.)	0.0015	0.0015	0.0015
L1 (p.u.)	0.0018	0.0018	0.0018
R2 (p.u.)	0.0009	0.0009	0.0009
L2 (p.u.)	0.0025	0.0025	0.0025
Rm (p.u.)	100.0	100.0	100.0
Lm (p.u.)	100.0	100.0	100.0

Annexed E3 Branches

As earlier mentioned, the MGs feeders are similar to those of distribution networks; therefore, they can be represented through a series impedance model. A detailed description of the model can be found in [189], [222]. Table E.5 presents the parameters of the MG branches shown in Figure 4.1.

Table E.5 Branch parameters

Branch		Length	R	X
From	**To**	**(km)**	**(ohm/km)**	**(ohm/km)**
4	5	0.20	1.01	0.2525
4	6	0.24	1.01	0.2525
5	7	0.25	1.01	0.2525
6	9	0.38	1.01	0.2525
7	8	0.48	1.01	0.2525
8	9	0.68	1.01	0.2525

Annexed E4 Loads

The MG loads, except for the SPSP load, are modeled as a balanced three-phase load. Besides, the active and reactive powers absorbed by the load are proportional to the square of the voltage applied at the load connection bus [225]. Table E.6 shows the nominal active and reactive powers of the system loads.

Table E.6 Load parameters

	Load A	Load B	Load C
Nominal active power (kVW)	8.33	9.80	6.86
Nominal reactive power (kVAr)	2.92	3.92	2.40

Annexed E5 PV plant

The PV plant model is based on a single-stage topology where only one DC/AC converter is used to interface the PV plant to the MG [226] (see Figure E.4). The DC/AC converter is modeled as a voltage source converter (VSC) which has a decoupled *d-q* controller [227]. The PV plant power generation is obtained by using the mathematical expression presented in (106) [97]. Besides, we have assumed that the PV plant is always operating at maximum power point (MPP). Further, the PV system is connected to the MG through a series RL filter. The single-stage PV system main parameters are summarized in Table E.7.
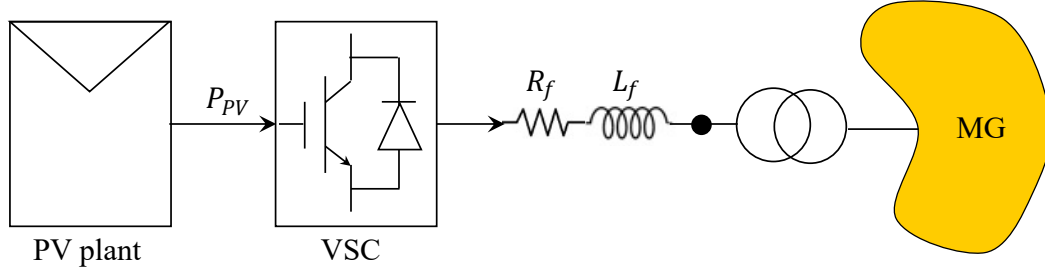

Figure E.4 Simplified scheme of a single-phase PV system

$$P_{PV}(k) = \eta_{PV} A_{PV} \Lambda(k) \tag{106}$$

where η_{PV} is the solar panel efficiency, A_{PV} denotes the total plant surface, and $\Lambda(k)$ represents the solar radiation.

Table E.7 Single-stage PV system parameters

η_{PV} (%)	16.48
A_{PV} (m^2)	121
R_f (ohm)	250
L_f (henry)	0.6631

Annexed E6 Solar drying productive process simulator

The solar drying productive process simulator comprises two main models, such as thermal model, and electrical model, which were implemented in MATLAB®/Simulink®. Figure E.5 shows a simplified scheme of the solar drying productive process simulator. As can be seen in Figure E.5, the thermal model and the electrical model are coupled through the commands (on/off) sent by the thermostats inside the thermal module.

On the one hand, the electrical module includes the following devices: i) an electric heater, ii) an electric fan, and iii) auxiliary equipment. These devices were implemented using the Simscape™ Electrical™ Specialized Power Systems blocks [206], and each device was represented through its ZIP load model. The ZIP parameters were taken from [33] and the nominal powers of the electric devices and other required parameters are presented in Table E.8.
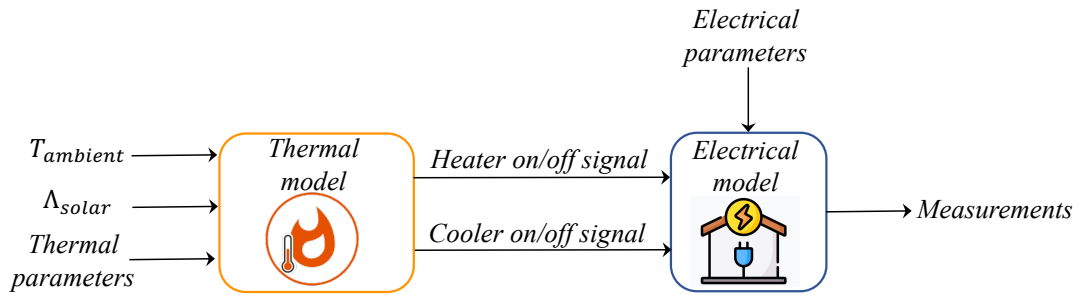
Figure E.5 Simplified scheme of the solar drying productive process simulator

On the other hand, the thermal model was implemented using the heat transfer equations described in [228]. For this purpose, the heat fluxes shown in Figure E.6 should be considered. Let $\dot{Q}_{solar}$ denote the heat flux contributed by solar radiation, $\dot{Q}_{heater}$ represents the heat flux contributed by the electric heater, $\dot{Q}_{fan}$ is the heat flux removed by the electric fan, and $\dot{Q}_{losses}$ are the heat losses through the dryer walls. Figure E.6 shows a simplified overview of the solar dryer and the heat fluxes involved. The heat transfer differential equations were implemented in MATLAB®/Simulink®, and the technical parameters of an actual solar dryer used in this type of productive process were used [229]. Figure E.7 shows some actual photos of the solar dryer. Table E.8 lists the general technical characteristics of the solar dryer, while Table E.9 presents the required parameters for the thermal model. Figure E.8 illustrates the operation of the solar dryer for two days. Figure E.8(a) shows the input data which in this case are the solar radiation and ambient temperature profiles. Figure E.8(b) displays the internal temperature profile of the solar dryer in which the influence of the solar input variables on the internal temperature can be seen. Finally, Figure E.8(c) depicts the electrical consumption profile of the dryer. As mentioned earlier, during periods of low solar radiation, the electrical heater is activated to maintain the working temperature range.
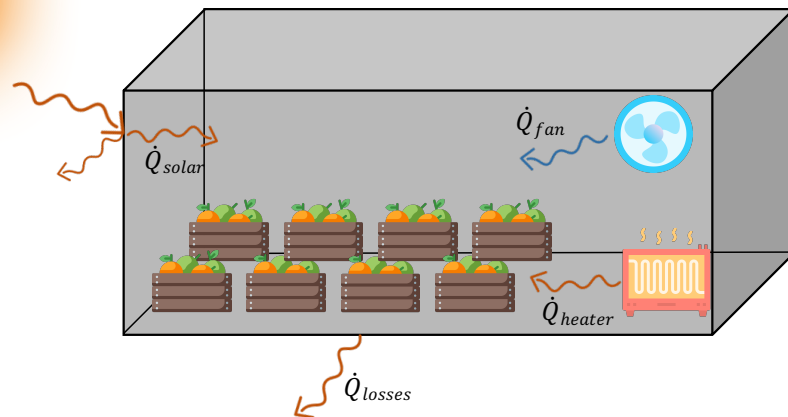

Figure E.6 Simplified overview of the solar dryer and its heat fluxes

Figure E.7 Actual photos of the solar dryer [230]

Table E.8 Technical characteristics of the solar dryer and electrical devices

Description	Technical characteristics (units)
Working temperature	~ 60 (ºC) – 70 (ºC)
Capacity	1,400 (kg) – 1,800 (kg)
Container	Length = 5.4 (m) Width = 2.2 (m) Height = 2.1 (m) Material: zinc
Thermal insulation	High-density polyurethane film Thickness = 0.04 (m)
Electric fan	Nominal active power = 610 (W) Frequency = 50 (Hz) Diameter = 0.45 (m)
Electric heater	Nominal active power = 2,000 (W) Frequency = 50 (Hz)

Table E.9 Thermal model parameters

Description	Value (units)
Temperature of hot air from heater	~ 250 (ºC)
Specific heat capacity of air at constant pressure	1005.4 (J/kg ºC)
Air mass flow rate through heater	58.5 (kg/h)
Density of air at sea level	1.225 (km/m^3)
Air mass flow rate through fan	315.62 (kg/h)
Dryer surface exposed to solar radiation	23.22 (m^2)
Solar radiation	Actual measurements[b] (W/m^2)
Absorptivity coefficient of the dryer walls	0.76
Emissivity coefficient of the dryer walls	0.60

---

[b] Actual measurements taken from [216]

Table E.9 Thermal model parameters (continued)

| Description	Value (units)
Boltzmann constant	5.67×10^{-8} (W/m^{2}K^4)
Equivalent thermal resistance of the dryer	7.13×10^{-6} (h ºC/J)
Mass of food	Depends on the product selected
Mass of the air inside the dryer	Depends on the mass food
Mass of food	Depends on the product selected
Specific heat capacity of food	Depends on the product selected
Ambient temperature	Actual measurements[2] (ºC)
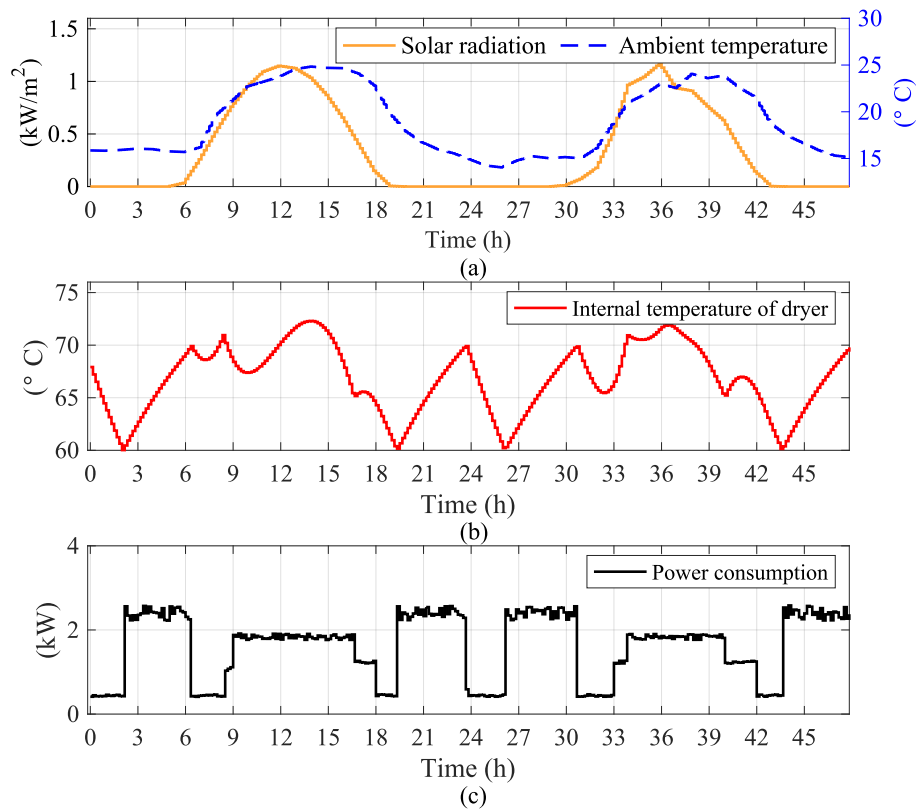
Figure E.8 (a) Solar radiation profile (left axis) and ambient temperature profile (right axis), (b) Internal temperature of dryer profile, and (c) dryer power consumption

Annexed F Case study of application of the proposed methodology to a small industrial grid in Germany[c]

As previously mentioned, the methodology proposed in this work was applied to a small electrical grid containing an industrial plant, which is installed at Karlsruhe Institute of Technology, Germany. The small electrical grid is connected to the main grid, and the industrial plant produces electronic systems for particle physics, battery systems, and medical applications in small batches, i.e., less than 1000 pieces. The productive process involves all processing steps from individual components to the final assembly [231]. It should be noted that, since there was no information on the specific devices that comprise the productive process, after performing the analysis with the zone identifier it was determined that this application case is best represented with one zone. Therefore, only the flexible component of the EMZ-ZIP model was considered to represent industrial consumption.

As mentioned above, in this application case, we used the flexible component of the EMZ-ZIP model presented in (12)-(15) to represent the industrial consumption. Then, the parameter identification procedure was performed by using the procedure described in Section 3.4. The energy management of the industrial grid was carried out considering the optimization problem presented in Section 3.5.2. However, since the industrial grid of this application case is connected to the main grid, the following objective function and balance equation were considered instead of the original ones.

$$\underset{P_{PCC}(k)}{minimize} \left(\sum_{k=1}^{K} C_{grid}(k) P_{PCC}(k) \right) \Delta_k \tag{107}$$

$$P_{PCC}(k) + P_{BESS}(k) + P_{PV}(k) = P_L\big(u_r(k)\big) + P^{loss}(k) \tag{108}$$

where, $C_{grid}(k)$ is the main grid electricity cost, $P_{PCC}(k)$ denotes the active power imported from the main grid, $P_{PV}(k)$ means the active power generated by the PV unit, $P_{BESS}(k)$ represents the active power injected/consumed by the BESS, and $P_L(u(k))$ denotes the industrial load represented through the TV-ZIP.

Figure F.1 depicts an overview of the topology of the industrial grid. It was modeled as a 4-buses radial distribution grid which is connected to the power distribution grid through the PCC at node 1 as illustrated in Figure F.1. Besides, the industrial grid includes a PV unit connected at bus

---

2, the industrial load is connected at node 3, and a BESS unit is installed at node 4. The colored arrows represent the different power flows within the industrial grid.
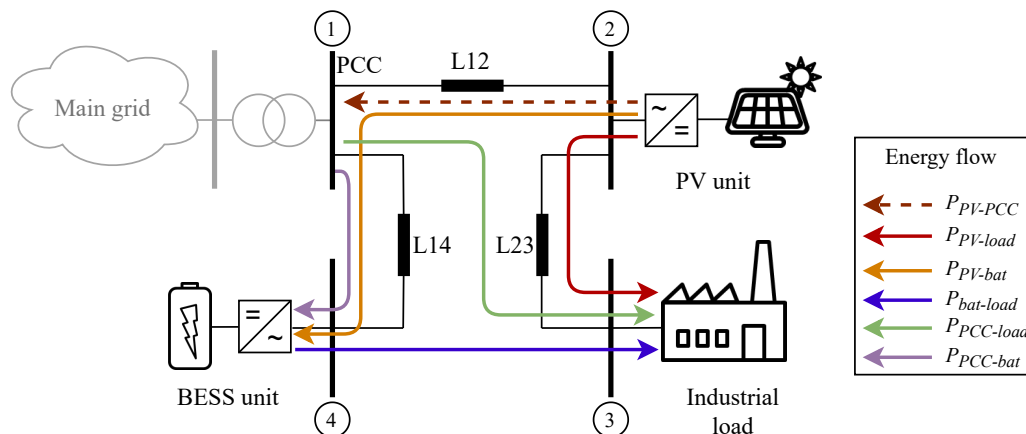

Figure F.1 Overview of the industrial grid topology

The active power measurements for the parameter identification procedure were taken from [231]. The BESS charging/discharging depends on the main grid electricity cost profile, which was obtained from [232]. The PV generation profile was taken from [233]. For this case study, we considered three operating cases:

Case 1: In this case, we assumed that the industrial load is represented through a CP, i.e., the effect of voltage is not considered. Furthermore, we have assumed that the BESS unit is not part of the system operation.

Case 2: In this case, we assumed that the industrial load is represented through a TV-ZIP, i.e., the effect of voltage on the load is considered. As previous case, we have assumed that the BESS unit is not part of the system operation.

Case 3: In this case, we assumed that the industrial load is represented through a TV-ZIP, i.e., the effect of voltage on the load is considered. Also, the BESS unit is part of the system operation; thus, it can purchase/sell energy from/to the grid. The BESS considers a mixed-integer linear model including SOC, efficiencies and maximum power for charging and discharging [194]. It should be noted that, for comparison purposes, the case 1 was considered as base case.

Figure F.2(a) shows the PV power generation profile (left axis) and the main grid electricity price profile (right axis). Figure F.2(b) displays the industrial consumption profile and the power at PCC for the three cases. Figure F.2(c) illustrates the results of the BESS operation, i.e., charging/discharging power profiles (left axis) and SOC profile (right axis), for the third case.

Table F.1 presents a summary of the results of energy imported from the main grid and total expenses for the three cases.
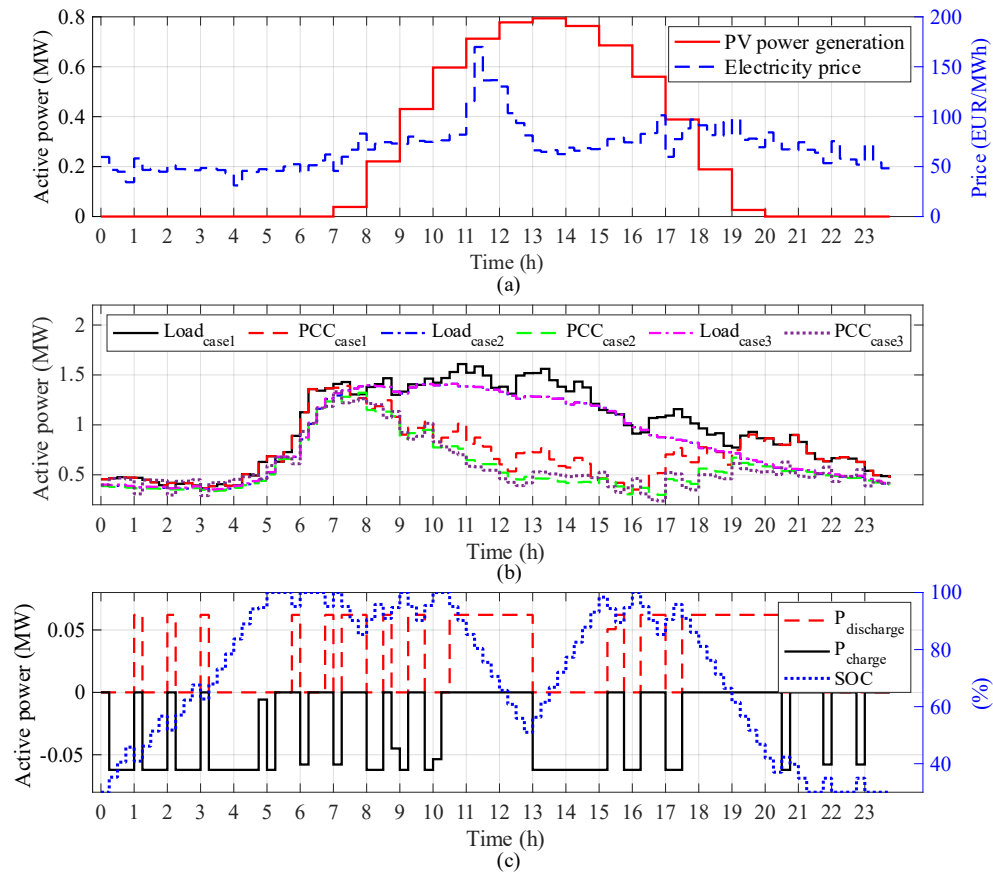

Figure F.2 (a) PV power generation profile (left axis) and the main grid electricity price profile (right axis), (b) industrial consumption profile and the power at PCC for the three cases, and (c) BESS charging/discharging power profiles (left axis) and SOC profile (right axis)

Table F.1 Summary of energy imported from the main grid and total expenses

Case	Total energy purchased (MWh)	% Reduction	Total expenses (EUR)	% Reduction
1	17.09	-	1209.12	-
2	13.90	18.66	979.49	18.99
3	14.09	17.55	971.22	19.68

Discussion: Considering the voltage effect on the industrial load in a considerable reduction in total energy purchased, about 19% in the case 2. This is because when considering voltage sensitive load models, the AC-based EMS will try to reduce the voltage close to the minimum allowed value at the load bus to decrease the load consumption; thus, minimizing the energy required to meet the industrial load [133]. In addition, when BESS is considered and the load is represented through a TV-ZIP (case 3), even though more energy is purchased than case 2, the total expenses are lower than the other cases because of the energy arbitrage done by the BESS.